2000:21

LULEÅ
UNIVERSITY
OF TECHNOLOGY

DOCTORAL THESIS

Influence of Fractures and Air Bubbles on the Pressure Distribution in Embankment Dams

MATS BILLSTEIN

Department of Environmental Engineering
Division of Water Resources Engineering

2000:21 • ISSN: 1402 - 1544 • ISRN: LTU - DT - - 00/21 - - SE

LULEÅ
UNIVERSITY
OF TECHNOLOGY

Influence of Fractures and Air Bubbles on the Pressure Distribution in Embankment Dams

Mats Billstein

Division of Water Resources Engineering
Luleå University of Technology
S-971 87 Luleå, Sweden
Phone +46 920 72307
Fax +46 920 91697
E-mail Mats.Billstein@sb.luth.se

Akademisk avhandling som med vederbörligt tillstånd av tekniska fakultetsnämnden vid Luleå tekniska universitet kommer att presenteras i sal A109 tisdagen den 20 juni 2000 kl. 10.30. Opponent är professor Kaare Höeg, Institutt for Geologi, Universitetet i Oslo, Norge.

Academic thesis which with the permission of the Faculty of Engineering at Luleå University of Technology will be presented in room A109 on Tuesday the 20th of June at 10.30. Opponent is Professor Kaare Höeg, Department of Geology, Oslo University, Norway.

2000:21 •ISSN:1402 – 1544 • ISRN: LTU – DT - - 00/21 - - SE

Influence of Fractures and Air Bubbles on the Pressure Distribution in Embankment Dams

by

Mats Billstein

Department of Environmental Engineering
Division of Water Resources Engineering
Luleå University of Technology
SE-971 87 Luleå
Sweden

April 2000

On the cover: WAC Bennett Dam Canada. Photograph by M. Billstein.

PREFACE

This thesis is presented as a partial fulfilment of the requirements for the degree of Doctor of Philosophy (Ph. D.). The research was carried out at the Division of Water Resources Engineering, Luleå University of Technology. Partial funding was provided by Vattenfall AB and ELFORSK AB. Mr. Urban Norstedt and Mr. Gunnar Sjödin, SwedCOLD, provided me with invaluable contacts in Sweden as well as abroad. Mr. Nils Johansson initiated the two issues that this thesis is founded upon; the influence of fractures and air bubbles on the pressure distribution in embankment dams. He also supervised the laboratory experiments concerning the Hele-Shaw cell conducted at Vattenfall Utveckling AB.

The thesis consists of a summary of collected journal articles and conference papers:

1. Billstein M., Svensson U., and Johansson N.: 1999, Development and validation of a numerical model of flow through embankment dams - comparisons with experimental data and analytical solutions, *Transport in Porous Media,* **35**, 395 - 406.
2. Billstein M., Svensson U., and Johansson N.: 1999, Application and validation of a numerical model of flow through embankment dams with fractures - comparisons with experimental data, *Canadian Geotechnical Journal*, **36**, 651 - 659.
3. Billstein M., and Svensson U.: A numerical evaluation of air bubbles as a potential explanation to the higher than expected pore pressures in the core of WAC Bennett Dam, (Submitted to *Journal of Hydraulic Research*).
4. Billstein M., and Svensson U.: 2000, Air bubbles - a potential explanation of the unusual pressure behaviour of the core at WAC Bennett Dam, In: *Proc. ICOLD's 20th Congress*, Beijing, Q.78-R.26, 369 - 384.
5. Billstein M.: 1998, Experimental study of flow through a bed of packed glass beads, In: *Proc. International symposium on new trends and guidelines on dam safety*, Barcelona, **2**, 833 - 840.

The abstracts in Papers 2, 3, and 4 have been translated to French by Mr. Christian Maurice.

Prof. Urban Svensson has supervised me in the development of the numerical models, the experimental design, the writing of the papers and the thesis. Prof. Anders Sellgren has assisted in the writing of the thesis.

Luleå, April 2000

Mats Billstein

ABSTRACT

In some large embankment dams unexpected pore pressure distributions within the core have been observed. As an example, the piezometer pressures in WAC Bennett Dam, Canada, which rose for about four years after the reservoir was filled, were steady for two years and subsequently declined. One peak pressure head was as much as 60 m higher than the expected steady state pressure head of 40 m. However, the pressure head had dropped 55 m from the peak value 25 years later. Four hypotheses have already been proposed to explain the anomalous pore pressures within embankment dams. The objective of this study is to examine two of them, inhomogenities (e.g. fractures) in the core and trapped air bubbles, which can both be examined from a fluid mechanical point of view. The other two mechanisms, settlements and bleeding of fine material, must also be examined from a geotechnical aspect.

This examination, based on results from two numerical models, is mainly theoretical. Results from numerical simulations of simplified homogeneous and inhomogeneous embankment dams are compared with analytical solutions and basic experiments. Results from numerical simulations, including the influence of air bubbles, are evaluated using a plug flow analysis and field measurements.

A Hele-Shaw cell and a bed of packed glass beads, both a homogeneous and an inhomogeneous experimental set up, were used in the examination of how inhomogenities influence the pressure distribution. In the inhomogeneous case, a horizontal fracture extended from the upstream boundary to a point within the embankment. The fracture was shown to have a significant influence on the pressure distribution, discharge, seepage level, and free surface profile. The numerical model is based on a direct solution of the conservation equations (mass and momentum). In the numerical simulations, the flow resistance is determined from a laminar velocity profile in a slot with smooth walls (Hele-Shaw cell) and from the Forchheimer equation (bed of packed glass beads). The problem is considered to be two-dimensional.

Since air bubbles are always initially present in the voids, that air is compressible, and that the amount of air that can go into solution increases with pressure, a mechanism that generates hydraulic blockage in the downstream part of the core can be anticipated. The blockage decreases the hydraulic conductivity in the flow direction resulting in a pressure increase. The numerical model for this case is based on a direct solution of the conservation equations (mass and momentum) and Darcy's, Boyle's, and Henry's law. It is a two-phase problem treated as one-dimensional.

The main result of the study is the development of numerical models to simulate how inhomogenities and trapped air bubbles influence the pressure distribution. These models have a solid foundation, i.e. are based on conservation principles, physical laws, and the best available empirical relationships. The models have been validated through comparisons with analytical solutions, basic experiments, and field measurements and thus provide a good starting point in the development of tools that can be used in dam engineering.

ABSTRACT (Swedish)

I ett antal höga jordfyllningsdammar har man uppmätt oväntade portrycksfördelningar i tätkärnan. Som ett exempel kan nämnas att när reservoaren i WAC Bennett Dam, Kanada, blivit fylld så fortsatte portrycken att stiga i ungefär fyra år, var sedan stabila i två år för att därefter sjunka. Vid ett tillfälle var det uppmätta portrycket 60 m (vattenpelare) högre än det förväntade stationära portrycket på 40 m. Det maximala portrycket har därefter sjunkit 55 m under 25 år. Fyra hypoteser har föreslagits för att förklara de oväntade portrycksfördelningarna. Syftet med detta arbete är att undersöka två av hypoteserna, inhomogeniteter (sprickor) och luftbubblor i tätkärnan. Båda dessa hypoteser kan undersökas utifrån ett strömningstekniskt perspektiv medan de två andra hypoteserna, sättningar och inre materialtransport, även inkluderar ett geotekniskt perspektiv.

Avhandlingen är i huvudsak en teoretisk utvärdering som baseras på resultat från två numeriska modeller. Resultat från numeriska simuleringar av förenklade jordfyllningsdammar (homogena och inhomogena) jämförs med analytiska lösningar och renodlade experiment. Resultat från numeriska simuleringar där luftbubblor i tätkärnan har inkluderats jämförs med en pluggflödesanalys och fältmätningar.

För att undersöka hur inhomogeniteter påverkar tryckfördelningen i en tätkärna användes dels en Hele-Shaw cell, dels en försöksuppställning med packade glaskulor. Tätkärnorna var både homogena och inhomogena. I det inhomogena fallet utbredde sig en horisontell spricka från uppströms kant till en bit in i dammen. Sprickan visade sig ha en signifikant inverkan på tryckfördelningen, vattenflödet genom dammen, vattenyteprofilen samt källsprångets läge. Den numeriska modellen är tvådimensionell och baseras på en direkt lösning av massbalans- och rörelsemängdsekvationerna. Friktionskraften uttrycks med hjälp av antingen en laminär hastighetsprofil i en spalt med släta väggar (Hele-Shaw cell) eller med Forchheimers ekvation (packade glaskulor).

Om det initialt finns luftbubblor i dammen finns förutsättning för bildandet av en hydraulisk barriär i tätkärnans nedströmsdel. Detta som en effekt av att luften är kompressibel och att mängden luft som kan lösas i vattnet ökar med ökat vattentryck. Barriären minskar den hydrauliska konduktiviteten i flödesriktningen med en tryckökning som följd. Den numeriska modellen för detta fall är endimensionell, inkluderar tvåfasströmning och baseras på en direkt lösning av massbalans- och rörelsemängdsekvationerna samt Darcy's, Boyle's och Henry's lag.

Arbetet har resulterat i att numeriska modeller har utvecklats som kan simulera hur inhomogeniteter (sprickor) och luftbubblor påverkar tryckfördelningen. Modellerna baseras på massbalans- och rörelsemängdsekvationerna, fysikaliska samband och bästa tillgängliga empiriska samband. Vidare är modellerna validerade genom jämförelser med analytiska lösningar, renodlade experiment och fältmätningar och utgör således en bra plattform för utveckling av användbara verktyg inom dammindustrin.

CONTENTS

PREFACE i

ABSTRACT ii

ABSTRACT (Swedish) iii

CONTENTS iv

1. INTRODUCTION 1
- 1.1 Embankment dams 1
- 1.2 Dam safety in Sweden 2
- 1.3 Surveillance of embankment dams 3
- 1.4 Anomalous pore pressures 4
- 1.5 Objective 5

2. INHOMOGENITIES IN THE CORE 7
- 2.1 Analytical solution 7
- 2.2 Experiments 7
  - 2.2.1 Homogeneous Hele-Shaw cell and bed of packed glass beads 8
  - 2.2.2 Inhomogeneous Hele-Shaw cell and bed of packed glass beads 8
- 2.3 Mathematical formulation 9
- 2.4 Results 11
  - 2.4.1 Homogeneous Hele-Shaw cell and bed of packed glass beads 11
  - 2.4.2 Inhomogeneous Hele-Shaw cell and bed of packed glass beads 11
- 2.5 Discussion 14
- 2.6 Conclusions 20

3. AIR HYPOTHESIS 21
- 3.1 The situations considered 22
  - 3.1.1 Hypothetical core 22
  - 3.1.2 WAC Bennett Dam 22
- 3.2 Mathematical formulation 23
- 3.3 Results 26
  - 3.3.1 Hypothetical core 26
  - 3.3.2 WAC Bennett Dam 26
- 3.4 Discussion 27
- 3.5 Conclusions 29

4. GENERAL DISCUSSION 31

5. CONCLUSION 33

6. REFERENCES 35

APPENDICES

Paper 1
Paper 2
Paper 3
Paper 4
Paper 5

1. INTRODUCTION

1.1 Embankment dams

Mankind has retained water for a very long time. One of the earliest dams recorded was that at Sadd-El-Katara in Egypt, built approximately 4800 years ago. The dam was 12 m high and consisted of two rubble walls 36 m apart and 24 m thick at the base. The intermediate space was filled with random material and the first zoned embankment dam of significance was built (Singh and Varshney, 1995; Jackson, 1995). The dam breached, probably as a consequence of flood overtopping, after a relatively short period of service.

Statistics to establish the total number of dams in service worldwide are not available. Accurate statistical data are confined to "large dams", i.e. dams higher than 15 m, which are entered under national listings in the World register of dams, published by the International Commission on Large Dams, (ICOLD, 1998). ICOLD identifies 46000 dams. The dams are of various types; embankment, gravity, buttress, and arch dams (Novak et al., 1990), though 70 percent of the large dams are embankment dams. Sweden has 190 dams classified as large with 130 of them being embankment dams. Presently, the highest dam of any type in the world is the 335 m high Rogun dam in Tadjikistan, an earthfill/ rockfill dam; the highest dam in Sweden is the 125 m high Trängslet dam, a rockfill dam.

The embankment dam shown in Figure 1 is a common type used by the hydropower industry in Sweden (Vattenfall, 1988). A central core of moraine provides the sealing while the filter material upstream and downstream protect the dam against erosion. A transition layer made of slightly coarser material is placed outside the filters and a rock fill is finally provided for protection and stability. The seepage through an embankment dam is between 10 - 20 l/s over a length of several hundred meters.

To prevent increased seepage rates and abrupt failures of embankment dams which may lead to tremendous damages and loss of human lives, the dams are designed and constructed with three different defence lines:

- In an intact dam, the downstream filter prevents the core material to be flushed away.
- If the upstream part of the core is damaged (e.g. a fracture appears), the upstream filter penetrates the core and fills up the free paths. This redistribution of material from the upstream filter into the damaged core results in a sink hole at the upstream dam crest.

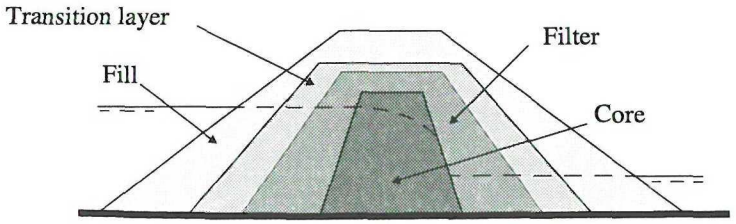

Figure 1. Schematic figure showing a vertical section through an embankment dam.

- The fill material alone (with no core, filter, or transition layer present) is dimensioned to sustain the hydrostatic pressure and seepage without losing its stability.

In spite of these precautions, there are problems and incidents with embankment dams. Data from 111 failures identifies three main reasons (ICOLD, 1995):

- Overtopping at high flood discharge (about 30 percent of the failures reported).
- Internal erosion and seepage problems in the embankment (about 20 percent).
- Internal erosion and seepage problems in the foundation (about 15 percent).

Hence, internal erosion and seepage are major problems in embankment dams. The seepage rate is influenced by the hydraulic conductivity of the core which is strongly influenced by the core material and the way the material is compacted. In practice, it is impossible to construct a dam without inhomogenities as dams are always more or less stratified horizontally from being constructed in horizontal layers. An increased seepage rate increases the rate of material transport which may lead to erosive leakage. Most cases of erosive leakage or excessive seepage in embankment dams have been interpreted in terms of internal erosion, hydraulic fracturing, or piping (Sherard, 1986; Löfquist, 1992). However, these interpretations describe only what can be suspected or seen at the dam after the process has been going on for some time. The real origin of the leak is usually difficult to discover or to explain.

1.2 Dam safety in Sweden

To date, no major dam accidents have occurred in Sweden, although there have been some failures of small dams. The best known is the overtopping of the Noppikoski dam in 1985. After that failure, dam safety work in Sweden accelerated. A task committee was appointed by the Swedish Meteorological and Hydrological Institute (SMHI) and the hydro power industry. Its task was to re-evaluate the guidelines for Swedish design floods, a work that was reported in Flödeskommittén (1990). The new design floods are in some cases 30 percent higher than the old ones. In Statens offentliga utredningar (1987, 1995) results from two governmental investigations were presented which concluded that dam safety in Sweden can be considered good. The present dam safety work and research in Sweden can be divided into six main topics:

- Hydrology.
- Stability.
- Surveillance.
- Spillway capacity.
- Operation of reservoirs and rivers.
- Risk analysis.

The objectives of the topics are: *Hydrology* - develop accurate prognoses for precipitation, runoff and snowmelt, i.e. how much water the reservoir can expect at a certain time. *Stability* - examine the stability of the dam for an increased seepage rate or overtopping. *Surveillance* - determine the status of the dam and core, e.g. defects in the core. *Spillway capacity* - is the capacity enough and how can it be guaranteed in critical situations, e.g. lots of debris, out of electricity, etc. *Operation of reservoirs and rivers* - the main river with all its minor river branches is now considered as one unit which renders the possibility of flood dampening. *Risk analysis* - a methodology of probabilistic risk assessment for evaluating the risk of dam failures.

1.3 Surveillance of embankment dams

To guarantee dam safety, the dams are surveyed by inspections and measurements. The inspections take place at the dam site; high hazard dams are inspected more frequently than low hazard dams. The measurements are often continuous with the most common measurements/methods being:

- Pore pressure.
- Inclination and settlement.
- Temperature.
- Resistivity.
- Self-potential.
- Seepage rate.
- Turbidity of the seepage water.
- Ground penetration radar.
- Bore hole tomography.

The objectives of the measurements/methods are: *Pore pressure* - indicates changes in the core, e.g. fractures or blockage. *Inclination and settlement* - detect movements in the dam body and the foundation. *Temperature, resistivity, and self-potential* - detect flow anomalies (Johansson, 1997). *Seepage rate* - an increased seepage rate may indicate de-

fects of the core. *Turbidity of the seepage water* - if there is an increased turbidity of the seepage water, it may be due to a material transport from the core, i.e. poor filter at the downstream side. *Ground penetration radar and bore hole tomography* - detect changes in the water content of the core material. Some of the above mentioned measurements give similar information, but it is always advantageous to have an extensive instrumentation as some measurements work better than others under severe field conditions.

1.4 Anomalous pore pressures

When measuring pore pressures within the core, one of the most common techniques in embankment dams surveillance, anomalous pore pressures have been observed (Schober, 1967; Stewart et al., 1990; Stewart and Imrie, 1993; Verma et al., 1985). At WAC Bennett Dam in Canada, for example, the piezometer pressures continued to rise for about four years after the reservoir was filled, were steady for two years, and declined after that. One peak pressure head was as much as 60 m higher than the expected steady state pressure head of 40 m; however, 25 years later, the pressure head within the core had dropped 55 m from the peak value. Because some pore pressures were almost three times higher than the expected, creating a load that was three times greater than the design load, dam safety was jeopardized. Even though the phenomenon with higher than expected pore pressures has been addressed by many specialists in dam engineering, it is not yet fully understood. It may be a single condition/process, or a combination of conditions/processes. If it is a combination, it is unclear between which conditions/processes. St-Arnaud (1995) made a review of the proposed hypotheses to explain the high pore pressures, (1) to (4), but emphasised (4):

1. Settlements and deformations in the core and filter.
2. Bleeding of fine material from the core to the filter, forming a filter blockage.
3. Inhomogenities (e.g. fractures) in the core.
4. Trapped air bubbles in the embankment during the first reservoir filling.

It is important to be able to determine what condition/process is responsible for the anomalous pore pressures. Some conditions/processes are due to poor construction, e.g. (1) and (2), whereas some are a consequence of the physical properties of the phases involved, e.g. (4), and have nothing to do with poor construction. As every embankment dam is unique with respect to site, geometry and material properties, and because the pressure behaviour is probably due to a combination of mechanisms, it is difficult to give general explanations to particular problems. Still, there are always some conditions that have to be considered:

- Inhomogenities in the core as a result of being constructed in horizontal layers.
- Initially, air is always present in the voids (Sherard et al., 1963).

Since air is compressible and the amount of air that can go into solution increases with pressure, the last condition has been designated the Air Hypothesis. Thus, inhomogenities and air in voids should always be considered in the interpretation of pore pressure measurements.

1.5 Objective

The objective of this work is to examine how: (a) inhomogenities in the core and (b) trapped air bubbles influence the pressure distribution in an embankment dam.

In order to meet objective (a), a numerical model of flow through a homogeneous embankment dams was developed, Papers 1 and 5, followed by an extension to incorporate inhomogenities, Paper 2. This work is described in Section 2. Objective (b) was met by developing a one-dimensional numerical model based on relevant conservation principles and physical laws (Darcy's, Boyle's, and Henry's law), Papers 3 and 4, which are described in Section 3.

2. INHOMOGENITIES IN THE CORE

To examine the influence of inhomogenities in the core, a numerical model was developed. An accurate simulation of the flow in an embankment dam requires that the model describes both laminar and turbulent flow conditions as well as homogeneous and inhomogeneous hydraulic conductivity conditions. The flow is a reflection of the pore pressure distribution within the dam and any change in the flow conditions will result in a modified pressure distribution. An inhomogeneity may be a fracture or an impervious layer. A demonstration to simulate the hydraulics of a dam in a satisfactory way is required. The validation of the model was conducted in five steps. The first step, the most fundamental case, was a comparison with an analytical solution, whereas steps two to five were based on comparisons with experiments that became more and more complex with respect to the porous media.

2.1 Analytical solution

If the dam has a rectangular cross-section, a constant hydraulic conductivity, a steady flow, is laminar, and essentially two-dimensional, an analytical solution will give the free surface profile and seepage level, h_0, as functions of the height of the upstream reservoir, H, the height of the downstream reservoir, h, and the length of the dam, L, Figure 2 (Polubarinova-Kochina, 1962; Crank, 1984). Further details are given in Paper 1, pp. 398-399.

2.2 Experiments

Two series of experiments with the same conditions as in the analytical solution were conducted, i.e. the numerical solutions could be compared with both an analytical solution and experimental results. Also, two series of experiments, which include a fracture and where no analytical solutions are available, were conducted, i.e. the numerical solutions could only be compared with experimental results. All the experiments were designed to minimize as many uncertainties as possible regarding the embankment geometry, flow resistance, and fracture geometry.

One experimental set up included a Hele-Shaw cell, the other included a bed of packed glass beads. In all experiments the surface levels upstream and downstream were held constant and the steady flow in between the domain was studied. The walls of the dam were made of clear acrylic. Once the discharge was steady, the pressure distribution, discharge, free surface profile, and seepage level were measured.

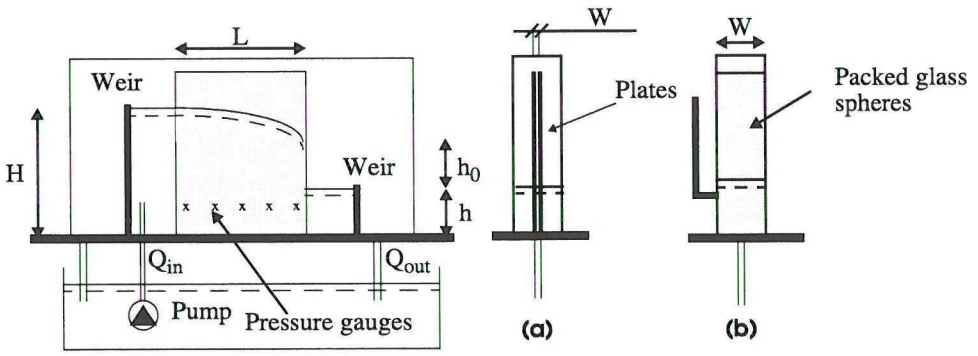

Figure 2. Schematic view of the simplified embankment dam in the experimental set up: section (a) for the Hele-Shaw cell and section (b) for bed of packed glass spheres.

2.2.1 Homogeneous Hele-Shaw cell and bed of packed glass beads

The second step was to compare numerical results with results from the most idealized experiment, the Hele-Shaw cell, Figure 2 (a). The Hele-Shaw cell is based on the analogy between a creeping flow and flow through a porous media and is valid if inertia terms are negligible (Batchelor, 1967). The advantage of the Hele-Shaw cell is that one does not need to create a porous matrix. Glycerine was used as fluid to enable a spacing between the plates in the range one to 20 mm.

Step three involved a porous matrix and water as fluid. Glass beads of uniform diameter were randomly packed between two parallel plates, Figure 2 (b). A thin net, with negligible flow resistance, kept the beads in place. Two different bead diameters, 0.002 m and 0.025 m, were used so as to vary the Reynolds number, *Re*, between four and 1500.

2.2.2 Inhomogeneous Hele-Shaw cell and bed of packed glass beads

Steps four and five incorporated a fracture in the Hele-Shaw cell as well as in the experiment with the bed of packed glass beads, Figure 3. A horizontal fracture extended from the upstream boundary to a point within the embankment. The fracture in the Hele-Shaw cell was created by a local increase in the space between the two parallel plates at a certain level over a certain length. In the porous media experiment, the fracture was made out of two parallel plates, spaced apart and perforated to allow the water to enter from all directions. A thin net kept the fracture free from the beads. The width of the fracture was equal to the spacing between the walls. A range of fracture lengths, fracture locations, and boundary conditions were examined. To obtain additional information about the flow in the vicinity of the fracture, a tracer was introduced at the upstream boundary in some of the tests.

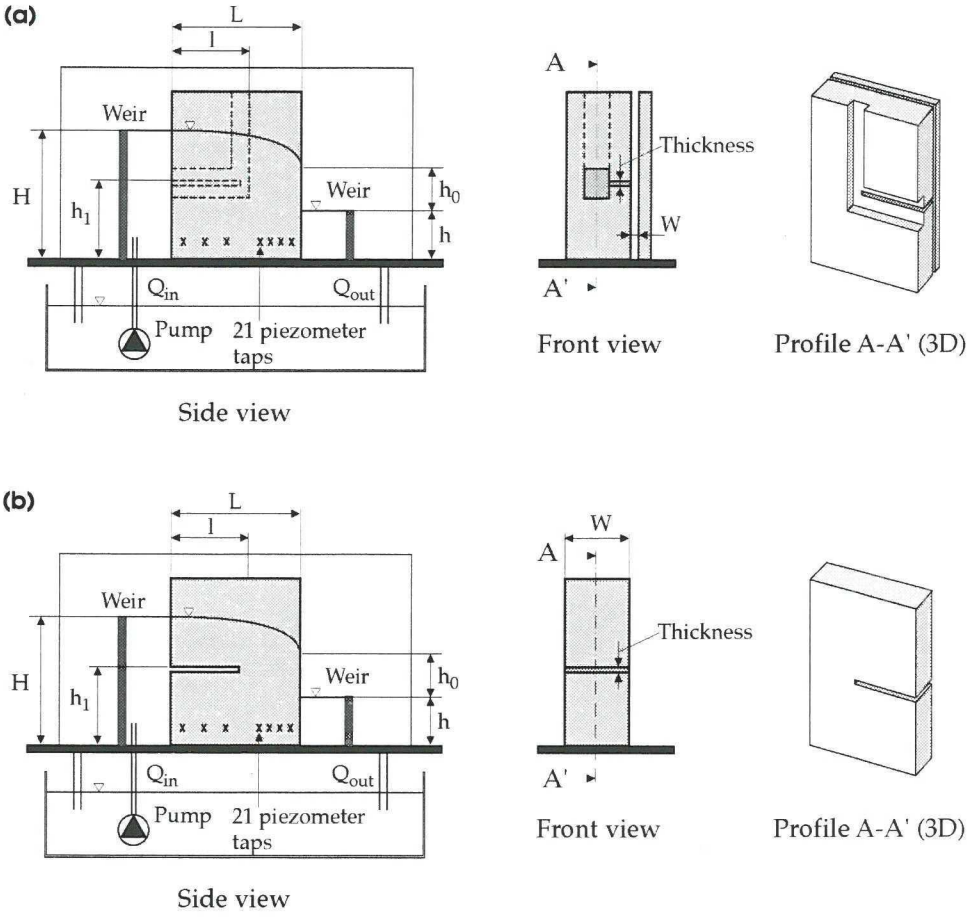

Figure 3. Schematic view of the simplified embankment dam with a fracture in the experimental set up: section (a) for the Hele-Shaw cell and section (b) for bed of packed glass spheres.

2.3 Mathematical formulation

The numerical simulation model is based on a direct solution of the relevant conservation equations. For an incompressible fluid, these equations are given as

$$\nabla(\rho \boldsymbol{u}) = 0 \tag{1}$$

for conservation of mass, and

$$-\nabla p + \rho \boldsymbol{g} + \boldsymbol{F} = 0 \tag{2}$$

for conservation of momentum, where $\boldsymbol{u}$ is the velocity vector, ρ density, p pressure, $\boldsymbol{g}$ gravitational vector, and $\boldsymbol{F}$ is a vector representing the frictional forces. ∇ is the vector operator $\frac{\partial}{\partial x}, \frac{\partial}{\partial y}$.

The frictional forces in the Hele-Shaw cell are determined from the laminar velocity profile in a slot with smooth walls (Bear, 1972):

$$F = \left(-\frac{12\mu}{W^2}u, -\frac{12\mu}{W^2}v\right) \tag{3}$$

in which u is the x-component mean velocity, v y-component mean velocity, W width of the slot, and μ is the dynamic viscosity of the fluid.

In the experiments with the packed glass beads, the flow is categorized as "Forchheimer" or "Turbulent", i.e. inertia forces and turbulence are significant (Fand et al., 1987; Kececioglu and Jiang, 1994). A non-linear resistance formula is required; therefore, the Forchheimer equation (Forchheimer, 1901), with constants according to Ergun (1952), was used in the simulations:

$$F = \left(-A\frac{(1-n)^2}{n^3}\frac{\mu}{d^2}u - B\frac{(1-n)}{n^3}\frac{\rho}{d}u^2, -A\frac{(1-n)^2}{n^3}\frac{\mu}{d^2}v - B\frac{(1-n)}{n^3}\frac{\rho}{d}v^2\right) \tag{4}$$

in which u is the x-component Darcy velocity, v y-component Darcy velocity, A and B empirical constants, n porosity, and d is the sphere diameter. The empirical constant A was chosen as 200, B as 1.8, in all simulations (Macdonald et al., 1979; Du Plessis, 1994). The porosity in Erguns equation was chosen as 0.34 for the small beads, 0.41 for the large beads (Graton and Fraser, 1935; Kunii and Levenspiel, 1969; Crawford and Plumb, 1986). The difference being due to a wall effect (Dudgeon, 1967; Hansen, 1992).

A hydrostatic pressure distribution was specified at the upstream and downstream boundaries whereas the pressure above the free surface is atmospheric.

The fracture in the Hele-Shaw cell was simulated by defining the pressure along the fracture. At the fracture entrance, the upstream pressure at the fracture level was prescribed; along the fracture, a pressure drop of 10 to 40 Pa was specified. In the glass beads experiment, a zone of low flow resistance was defined. At the boundary between the fracture and the surrounding porous matrix, a skin resistance, due to the net around the fracture, was specified.

2.4 Results

2.4.1 Homogeneous Hele-Shaw cell and bed of packed glass beads

In Tables 1 and 2, results from the two homogeneous experiments are compared with the corresponding numerical and analytical solutions with respect to seepage levels and discharges (only the porous media experiment). In Figure 4 the surface profiles are shown, Figure 5 shows the pressure profiles. The analytical and numerical solutions give remarkably similar results whereas the predicted seepage levels are systematically lower than the experimental results in the Hele-Shaw cell. The good agreement between the numerical and analytical solution indicate that the numerical model provides a correct solution of the governing equations. The higher seepage levels in the experiments must therefore be due to some effect not included in the theory. Inertia effects can be ruled out, as the disagreement is found for the whole range of Reynolds numbers investigated. In the porous media experiment, the measured pressure profiles, seepage levels, surface profiles, and discharges corresponded well with the calculations.

2.4.2 Inhomogeneous Hele-Shaw cell and bed of packed glass beads

Results from the two experiments are compared with the corresponding numerical solution and the numerical solution for the homogeneous case, called the reference case. Tables 3 and 4 contain all seepage levels and discharges for the two experiments; Table 3 relates to the Hele-Shaw cell and Table 4 to the bed of packed glass beads. Figures 6 to 8 show the free surface profiles and the pressure profiles.

Table 3 and Figure 6 show that a fracture has a significant influence on the discharge, seepage level, and the free surface profile in the Hele-Shaw cell. The discharge increases by 60-70 percent with a long fracture (0.2 m) present, but only by 10-30 percent with a short fracture (0.1 m) present. Based on the results from some of the tests and the numerical simulations, it is shown that the discharges increase more with a fracture located far from the free surface profile than with a fracture located close to the surface profile. The seepage level is strongly dependent upon the length of the fracture. Also, in the porous media experiment, the fracture has a significant influence on the pressure distribution, discharge, seepage level, and water surface profile, Table 4 and Figures 7 and 8.

Table 1. Comparison of seepage levels as given by Hele-Shaw experiment, the analytical solution, and the numerical simulation.

L (m)	W (m)	H (m)	h (m)	Re	$h_{0\ exp}$ (m)	$h_{0\ analy}$ (m)	$h_{0\ numer}$ (m)
0.300	0.002	0.288	0.144	0.004	0.02	0.009	0.006
	0.004	0.288	0.144	0.03	0.02	0.009	0.006
	0.008	0.287	0.145	0.2	0.02	0.009	0.006
	0.016	0.136	0.000	1.4	0.043	0.022	0.021
	0.016	0.184	0.013	1.8	0.052	0.030	0.030

Note: Subscripts: exp, experimentally; analy, analytically; numer, numerically.

Table 2. Comparison of flow and seepage levels as given by porous media experiment, the analytical solution, and the numerical simulation.

diameter (m)	W (m)	n (%)	L (m)	H (m)	h (m)	Re	$h_{0\ exp}$ (m)	$h_{0\ analy}$ (m)	$h_{0\ numer}$ (m)	Q_{exp} (l/s)	Q_{numer} (l/s)
0.002	0.132	34	0.205	0.518	0.388	11	0.01	0.016	0.015	0.45	0.44
				0.521	0.104	23	0.28	0.268	0.263	0.82	0.85
				0.522	0.015	25	0.35	0.357	0.353	0.85	0.88
			0.505	0.368	0.258	4	0.00	0.005	0.000	0.11	0.11
				0.367	0.096	10	0.04	0.030	0.029	0.19	0.19
				0.367	0.015	12	0.09	0.084	0.087	0.20	0.21
0.025	0.301	41	0.500	0.285	0.262	500	0.00	-	0.000	2.05	2.02
				0.279	0.200	900	0.01	-	0.000	3.42	3.40
				0.292	0.118	1100	0.01	-	0.008	4.42	4.56
				0.434	0.292	1200	0.01	-	0.002	6.91	7.08
				0.292	0.042	1400	0.07	-	0.052	4.66	4.78
				0.429	0.140	1500	0.08	-	0.050	8.23	8.42

Note: Q, discharge; n, porosity. Subscripts: exp, experimentally; analy, analytically; numer, numerically.

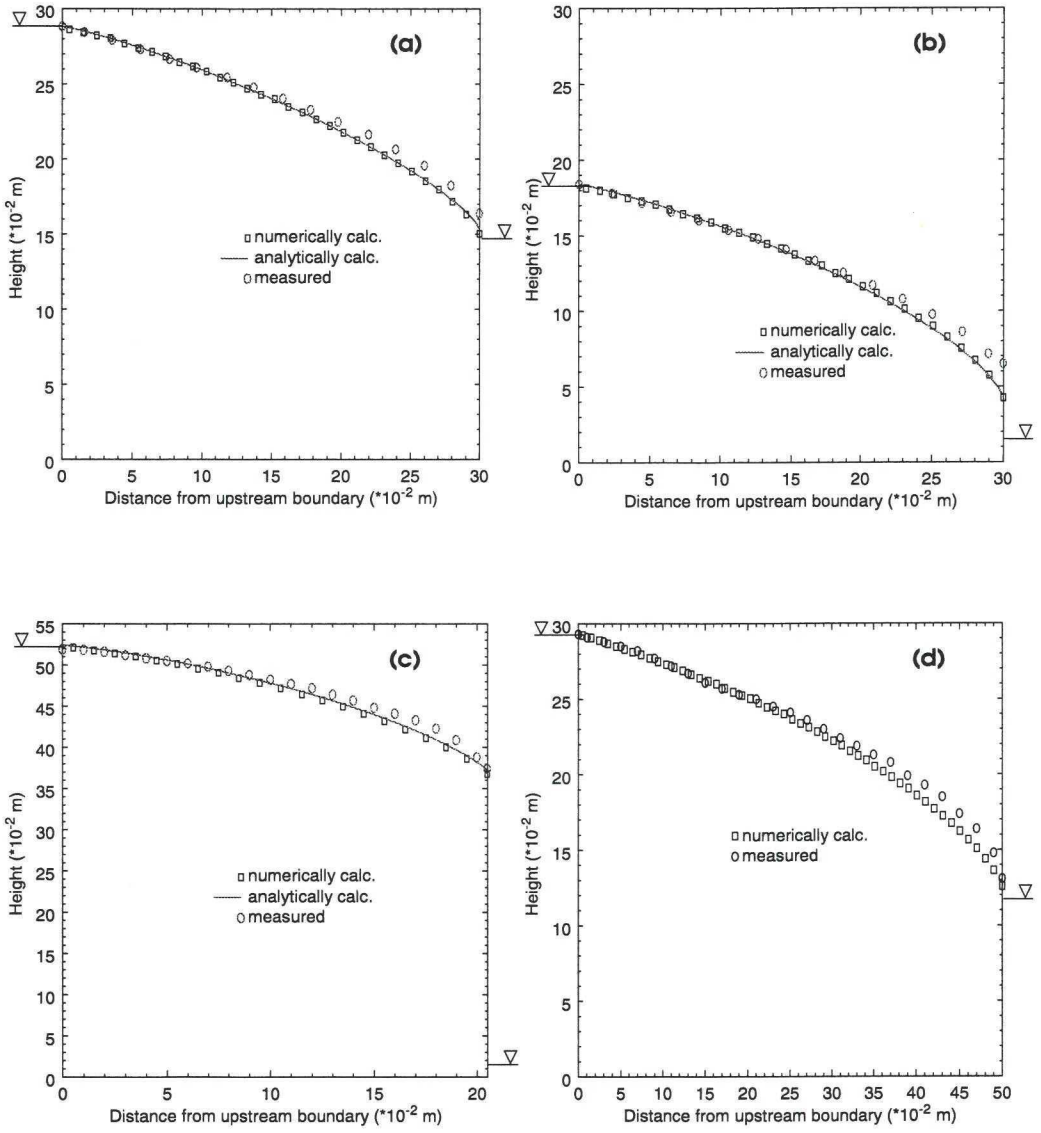

Figure 4. Surface profiles for the Hele-Shaw experiment (a) and (b), and the porous media experiment (c) and (d).
(a) W = 2 mm, H = 0.288 m, h = 0.144 m, Re = 0.004.
(b) W = 16 mm, H = 0.184 m, h = 0.013 m, Re = 1.8.
(c) sphere diameter 0.002 m, H = 0.522 m, h = 0.015 m, Re = 25.
(d) sphere diameter 0.025 m, H = 0.292 m, h = 0.118 m, Re = 1100.

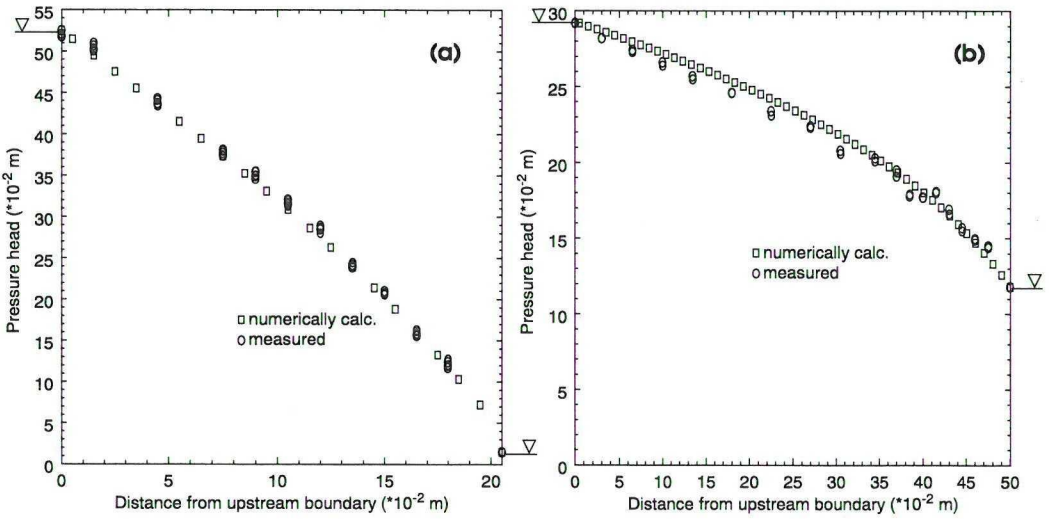

Figure 5. Pressure profiles for the porous media experiment.
(a) sphere diameter 0.002 m, H = 0.522 m, h = 0.015 m, Re = 25.
(b) sphere diameter 0.025 m, H = 0.292 m, h = 0.118 m, Re = 1100.

2.5 Discussion

The results demonstrate that the numerical model can simulate the flow through a simplified embankment dam and capture the influence of fractures. However, some minor differences can be found. The discrepancy in seepage level between the homogeneous Hele-Shaw cell and the calculations may be due to nonideal outflow conditions in the experimental set up. Glycerine is very adhesive and it was noted in the experiment that it stuck to the walls perpendicular to the outlet; this may have resulted in some additional friction at the outlet not considered in the numerical simulations.

It should also be emphasized that the resistance formula, Forchheimers equation, is empirical. To use Forchheimers equation, one must know the porosity of the porous medium. The simulations are sensitive to the porosity value. If the porosity is modified by two percent (34 $\pm$ 2 percent and 41 $\pm$ 2 percent), the discharge changes by approximately $\pm$ 20 percent for the small beads and $\pm$ 10 percent for the larger ones.

The predicted surface profiles are systematically between one and four percent higher than the experimental results in the Hele-Shaw cell with a fracture present, an effect enhanced by a long fracture. In the experiments with the tracer, it was shown that the streamlines leaving the fracture did not do so at right angles to the fracture. This finding indicates that the fracture is not an equipotential line, i.e., the potential is not constant along the fracture.

Table 3. Comparison of discharges and heights of the seepage faces as given by Hele-Shaw experiment and the numerical simulation.

L (m)	W (m)	H (m)	h (m)	T (°C)	l (m)	h_1 (m)	$h_{0\,exp}$ (m)	$h_{0\,numer}$ (m)	Q_{exp} (ml/s)	Q_{numer} (ml/s)	$h_{0\,numer}$ (m)	Q_{numer} (ml/s)
					With fracture						Without fracture	
0.300	0.0044	0.304	0.000	21.7	0.20	0.20	0.179	0.181	59.7	58.2	0.103	37.0
0.300	0.0043	0.303	0.000	22.2	0.20	0.10	0.169	0.163	55.5	62.0	0.103	37.0
0.300	0.0044	0.303	0.000	22.3	0.10	0.20	0.129	0.121	38.3	42.0	0.103	37.0
0.300	0.0045	0.304	0.000	21.7	0.10	0.10	0.127	0.122	41.5	46.7	0.103	37.0
0.300	0.0044	0.304	0.152	22.5	0.20	0.20	0.042	0.042	49.0	46.2	0.012	28.0
0.300	0.0044	0.303	0.151	22.7	0.20	0.10	0.036	0.031	44.8	47.1	0.012	28.0
0.300	0.0044	0.303	0.151	22.0	0.10	0.20	0.020	0.014	29.3	31.9	0.012	28.0
0.300	0.0045	0.303	0.151	22.1	0.10	0.10	0.017	0.013	33.9	34.8	0.012	28.0

Note: Q, discharge. Subscripts: exp, experimentally; numer, numerically.

Table 4. Comparison of discharges and heights of the seepage faces as given by porous media experiment and the numerical simulation.

diameter (m)	W (m)	n (%)	L (m)	H (m)	h (m)	Re	l (m)	h_1 (m)	$h_{0\,exp}$ (m)	$h_{0\,numer}$ (m)	Q_{exp} (l/s)	Q_{numer} (l/s)	$h_{0\,numer}$ (m)	Q_{numer} (l/s)
							With fracture						Without fracture	
0.002	0.132	34	0.505	0.381	0.015	12	0.25	0.27	0.17	0.13	0.28	0.27	0.10	0.22
0.002	0.132	34	0.505	0.380	0.015	12	0.25	0.10	0.14	0.12	0.28	0.28	0.10	0.22
0.002	0.132	34	0.505	0.380	0.097	10	0.25	0.27	0.09	0.06	0.27	0.26	0.03	0.20
0.002	0.132	34	0.505	0.381	0.097	10	0.25	0.10	0.08	0.06	0.27	0.27	0.03	0.20
0.002	0.132	34	0.505	0.380	0.262	4	0.25	0.27	0.00	0.00	0.16	0.16	0.00	0.12
0.002	0.132	34	0.505	0.380	0.262	4	0.25	0.10	0.00	0.00	0.16	0.16	0.00	0.12
0.025	0.301	41	0.500	0.290	0.042	1400	0.25	0.21	0.08	0.07	5.10	5.20	0.05	4.78
0.025	0.301	41	0.500	0.290	0.042	1400	0.25	0.13	0.09	0.07	5.20	5.28	0.05	4.78
0.025	0.301	41	0.500	0.288	0.121	1100	0.25	0.21	0.02	0.01	4.85	4.90	0.01	4.56
0.025	0.301	41	0.500	0.289	0.122	1100	0.25	0.13	0.03	0.01	4.89	4.96	0.01	4.56
0.025	0.301	41	0.500	0.288	0.264	500	0.25	0.21	0.00	0.00	2.30	2.31	0.00	2.02
0.025	0.301	41	0.500	0.290	0.265	500	0.25	0.13	0.00	0.00	2.30	2.31	0.00	2.02

Note: Q, discharge; n, porosity. Subscripts: exp, experimentally; numer, numerically.

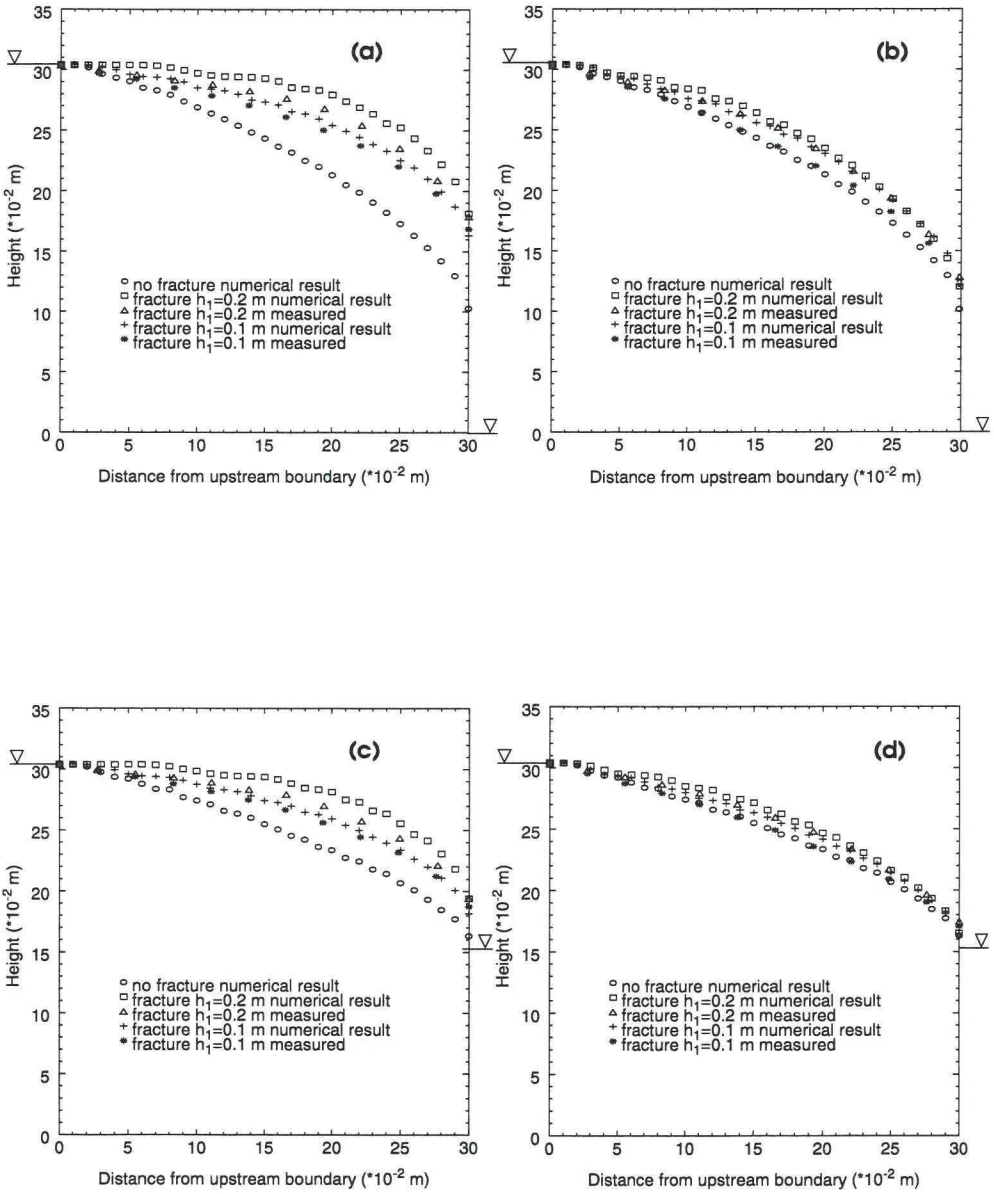

Figure 6. Free surface profiles in the Hele-Shaw experiment for different fracture lengths and fracture levels (see Figure 3).
(a) H=0.304 m, h=0.0 m and l=0.20 m.
(b) H=0.304 m, h=0.0 m and l=0.10 m.
(c) H=0.304 m, h=0.151 m and l=0.20 m.
(d) H=0.304 m, h=0.151 m and l=0.10 m.

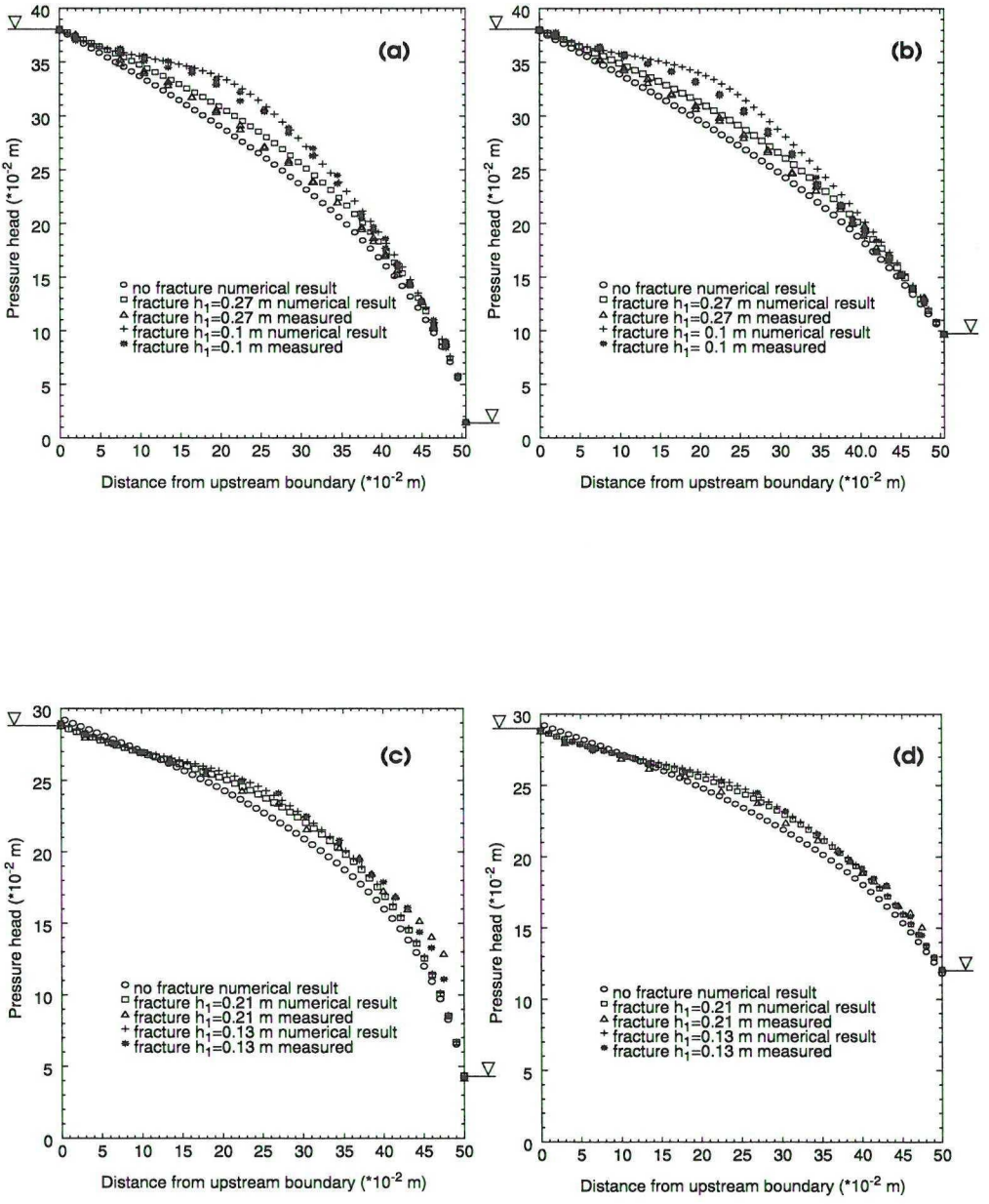

Figure 7. Pressure profiles in the porous media experiment for different fracture levels.
(a) sphere diameter 0.002 m, H=0.380 m, h=0.015 m and l=0.25 m.
(b) sphere diameter 0.002 m, H=0.380 m, h=0.097 m and l=0.25 m.
(c) sphere diameter 0.025 m, H=0.290 m, h=0.042 m and l=0.25 m.
(d) sphere diameter 0.025 m, H=0.289 m, h=0.121 m and l=0.25 m.

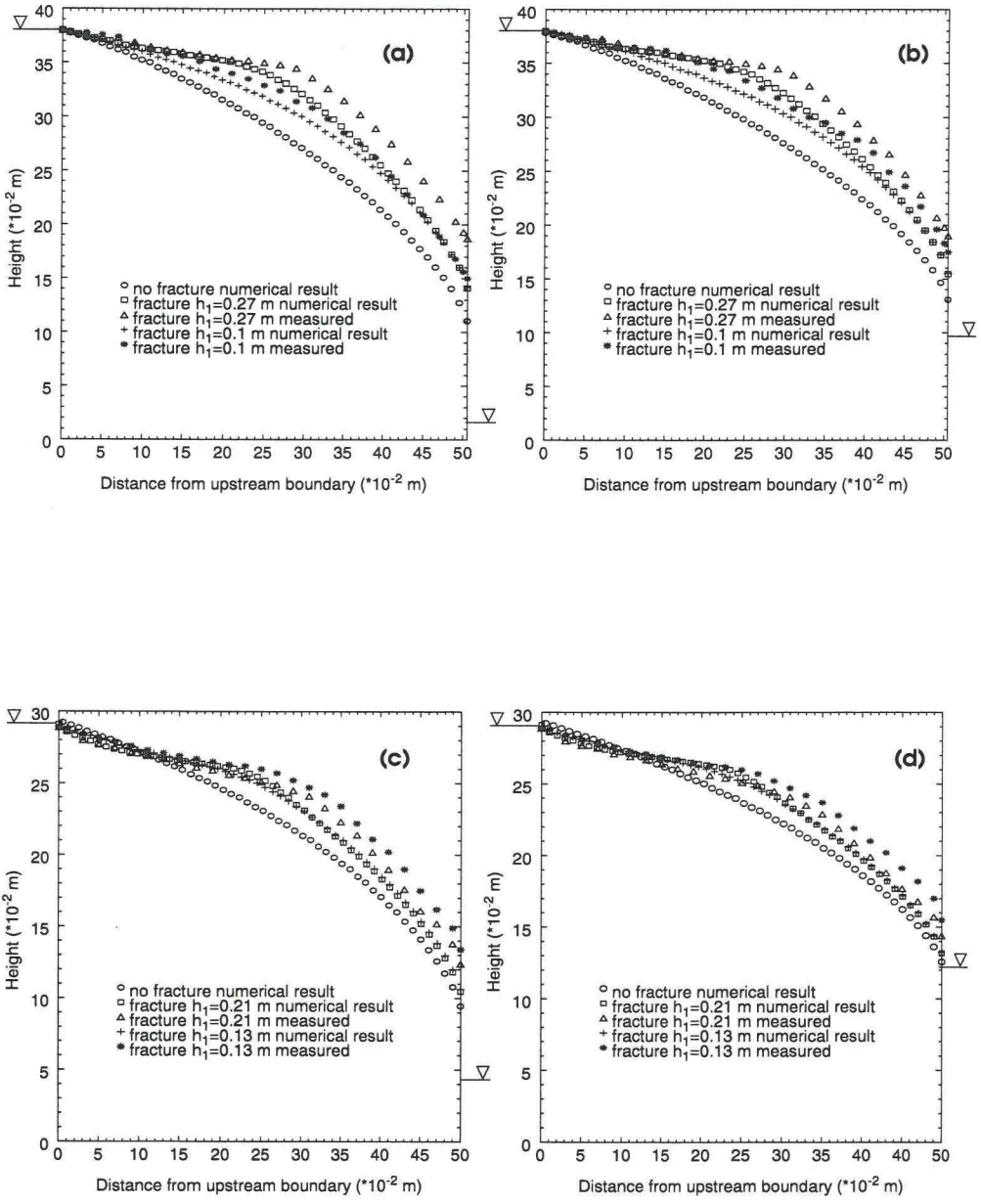

Figure 8. Water surface profiles in the porous media experiment for different fracture levels.
(a) sphere diameter 0.002 m, H=0.380 m, h=0.015 m and l=0.25 m.
(b) sphere diameter 0.002 m, H=0.380 m, h=0.097 m and l=0.25 m.
(c) sphere diameter 0.025 m, H=0.290 m, h=0.042 m and l=0.25 m.
(d) sphere diameter 0.025 m, H=0.289 m, h=0.121 m and l=0.25 m.

A pressure drop of 10 to 40 Pa was specified along the fracture in the numerical model. However, because the numerically calculated free surface profiles are systematically higher than the measured ones, it is possible that the actual pressure drop was somewhat higher than indicated above. Uncertainty about the pressure drop along the fracture may thus explain the higher calculated free surface profile.

The viscosity of glycerine, used in the Hele-Shaw experiment, is strongly dependent upon temperature and water content (Rehbinder, 1990). A change of water content by one percent causes a change in viscosity by 100 percent. A pump recirculated the glycerine and increased its temperature, thereby decreasing the viscosity. When glycerine is exposed to air, it absorbs water, thereby increasing the water content and reducing the viscosity. A change in viscosity does not influence the free surface profile or the seepage level, but it does influence the discharge which is linearly dependent upon the viscosity.

With packed glass beads and a fracture present, the predicted surface profiles are systematically one to seven percent lower than the experimental results. A possible explanation is that the resistance due to the net around the fracture is higher than estimated. The resistance coefficient was determined in a flume experiment with no glass beads. However, the coefficient may be larger with the glass beads present on one side of the net.

2.6 Conclusions

Four new series of experiments for analysing steady flow through simplified embankments are presented, two with a Hele-Shaw cell and two with a bed of packed glass beads. Both a homogeneous and an inhomogeneous experimental set up have been used. In the inhomogeneous set up, a horizontal fracture extended from the upstream boundary to a point within the embankment. The fracture was shown to have a significant influence on the pressure distribution, discharge, seepage level, and the free surface profile.

From the experiments it can be concluded that: (1) the discharge increases with a fracture present; (2) a fracture far from the free surface profile increases the discharge more than a fracture close to the free surface profile; (3) the height of the seepage face is strongly dependent upon the length of the fracture; (4) with a fracture close to the free surface profile, the influence on the free surface profile is higher than with a fracture far from the free surface profile.

Analytical and numerical solutions give nearly identical results. The numerical model can predict the pressure distribution, the seepage level, the free surface profile, and the discharge in a homogeneous as well as in an inhomogeneous embankment dam. All of the above listed effects of a fracture were also found in the numerical simulations; in most case a good quantitative agreement was achieved.

3. AIR HYPOTHESIS

The key feature of the Air Hypothesis is that *trapped air bubbles in the embankment dam cause a blockage that decreases the hydraulic conductivity and results in a pressure increase.* To examine how trapped air bubbles influence the pressure distribution, relevant conservation principles and physical laws (Darcy's, Boyle's, and Henry's law) have been implemented in a one-dimensional numerical model. The basic idea is as follows (Figure 9):

- When the dam is completed, the voids are filled with both water and air; the air presumably in the form of bubbles.
- As the filling of the reservoir starts, the pressure on the upstream side, as well as progressively inside the core, increases.
- Two effects can be expected as the pressure increases:
  1. The bubbles will be compressed and hence the volume will be reduced (a water pressure head of 100 m will cause a reduction in the volume of air by a factor of 10).
  2. The air in the upstream part of the core will go into solution, be transported by the water, and evolve again in the downstream part of the core due to a lower ambient pressure.
- The air bubbles in the downstream part of the core cause a blockage for the water and, therefore, a decreasing hydraulic conductivity in the flow direction.
- Eventually, all air bubbles will be dissolved by the water and a fully saturated core will be the final steady state condition.

A full account of the Air Hypothesis can be found in St-Arnaud (1995) and in LeBihan and Leroueill (1999).

The numerical model was applied to both a hypothetical core and the core of WAC Bennett Dam. The hypothetical case was used to discuss in detail the transport mechanisms of the air and for a comparison with a plug flow analysis. Results from pore pressure measurements in the core of WAC Bennett Dam were used for comparisons with simulated pressure development.

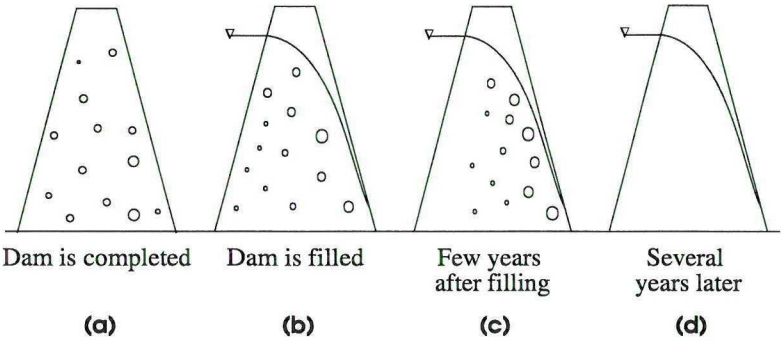

Figure 9. Schematic outline of the Air Hypothesis. (a) when the dam is completed the voids are filled with both water and air. (b) an increased pressure will compress the air and increase the amount of air that can go into solution. (c) at the downstream part of the core the pressure decreases, the air will be decompressed, and air bubbles will evolve again. (d) eventually, all air bubbles will be dissolved by the water.

3.1 The situations considered

3.1.1 Hypothetical core

The hypothetical core is 100 m long with the same material properties and initial conditions as the core of WAC Bennett Dam. At the upstream boundary the pressure head is 100 m while atmospheric pressure prevails at the downstream boundary. The upstream pressure head is applied instantaneously and held constant throughout the calculations.

Two situations are considered: one where there is no Darcian flow of air and one where there is a flow of air.

3.1.2 WAC Bennett Dam

The core of WAC Bennett Dam and the impoundment are outlined in Figure 10 (Stewart et al., 1990; Stewart and Imrie, 1993). The core consists of well graded, non-plastic, silty sand and gravel. The core had a mean water saturation of about 0.64 as placed in the core and a hydraulic conductivity of $6*10^{-7}$ m/s. A core like this is likely to have a void ratio of 0.23 to 0.35, equivalent to a porosity of 0.22, a value that was used in the simulations (Bernell, 1957). Peck (1990) stated that it was probably not atmospheric conditions at the downstream boundary of the core; therefore, a downstream pressure head of 10 m was assumed. The average temperature was set to 4 ^{o}C. The water entering the core was assumed to be saturated with air at atmospheric pressure. The reservoir was filled at a rate of 14 m/month over the first eight months; thereafter at a rate of 1.3 m/month until the reservoir was full after three years. In the numerical simulations, it was assumed that the pore pressure head at the upstream boundary of the core was equal to the reservoir level.

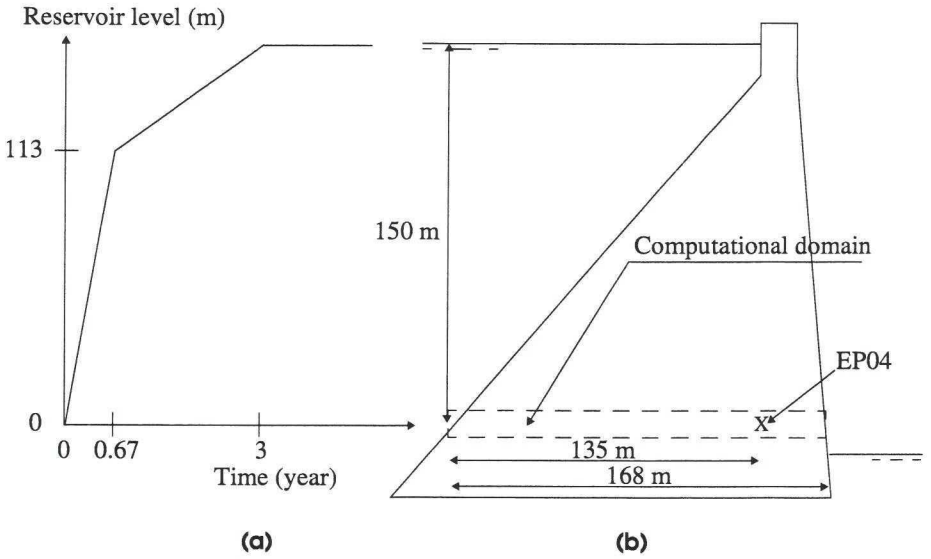

Figure 10. The core of WAC Bennett Dam: (a) reservoir level versus time with reference to the level where piezometer EP04 is located; (b) geometry of the core and the position of piezometer EP04.

Piezometer EP04 is located 150 m below the reservoir level and 135 m downstream from the upstream boundary. The length of the core where EP04 is located is 168 m. 25 years of pressure records have been used for comparisons with simulated pressure development.

3.2 Mathematical formulation

When the dam is completed and the impoundment starts, the flow through the dam is unsaturated whereas it is saturated when all air is dissolved. To describe fluid flow in both unsaturated and saturated soil, the relationship between the air and water conductivity and the water saturation level must be determined. A review of existing relationships is summarised in Figure 11, indicating that all cited relationships are in fair agreement.

Boyle's law describes the pressure/volume relationship for a perfect gas:

$$p_1 V_1 = p_2 V_2 \tag{5}$$

in which p is pressure in atm, V volume, and index *1* and *2* represent two states.

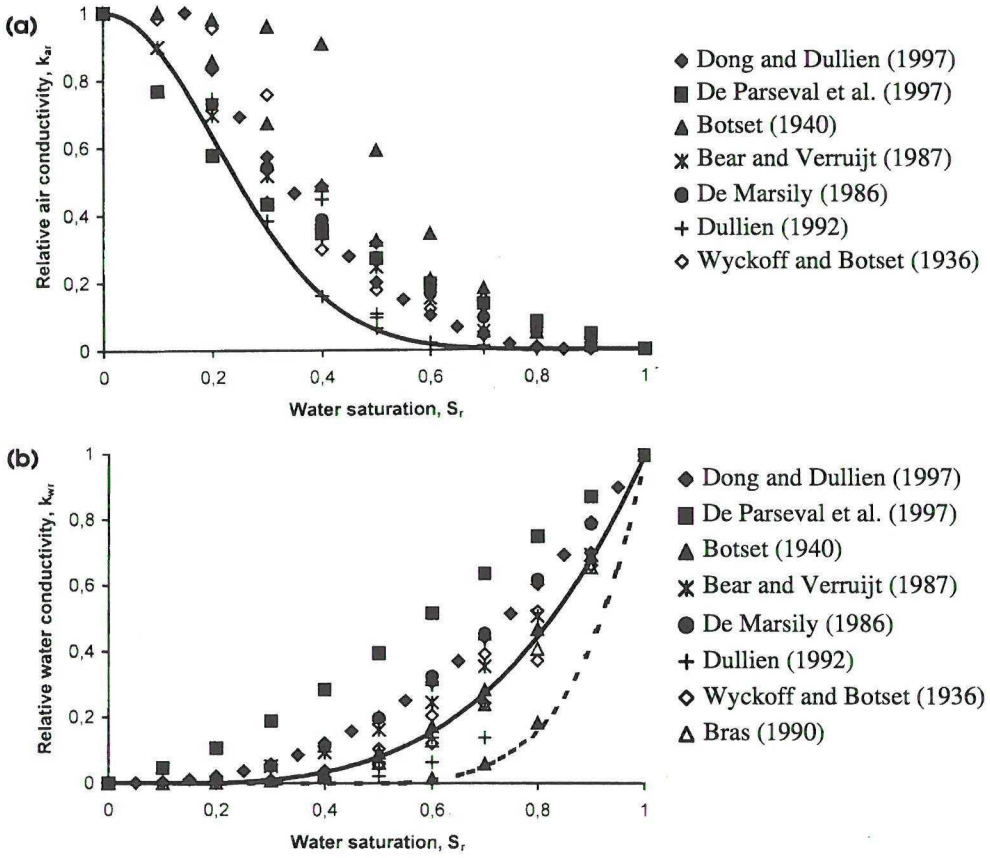

Figure 11. (a) relationship between relative air conductivity and water saturation level. ——— is the relationship used in this work. (b) relationship between relative water conductivity and water saturation level. ——— is the best fit relationship and - - - - is an alternative relationship used in the application to WAC Bennett Dam.

Henry's law, given as

$$C_s = Hp \tag{6}$$

states the amount of air that can be dissolved at a given pressure. In (6), C_s is the saturation concentration of air in the water and H is Henry's constant (numerical values can be found in Fredlund and Rahardjo, 1993).

The dissolution of air bubbles into the water is a diffusion process:

$$\dot{m} = -K(C_s - C_l) \tag{7}$$

in which $\dot{m}$ is the rate of mass flow, K overall mass transfer coefficient (numerical values can be found in American water works association, 1990), and C_l is the current concentration of air in the water.

All the physical mechanisms described above are combined with relevant conservation laws expressed in a set of differential equations. In the numerical simulations, the problem is considered to be one-dimensional and transient, the air is assumed to be compressible, and the water is treated as incompressible. It is thus a two-phase problem.

The momentum equations given as

$$0 = -r_l \frac{\partial p}{\partial x} - r_l \rho_l \phi_l u_l \tag{8}$$

$$0 = -r_g \frac{\partial p}{\partial x} - r_g \rho_g \phi_g u_g \tag{9}$$

are a balance between a pressure gradient and a linear resistance term, i.e. Darcy's law. r is the volume fraction, ϕ resistance factor, and u is the Darcy velocity. Index l denotes liquid and g gas.

The resistance factor is defined as:

$$\phi = \frac{g}{k} \tag{10}$$

in which g is the gravitational constant and k the air or water conductivity, see Figure 11.

The volume change of the two phases, water and air, are calculated with the following volume fraction equations:

$$\frac{\partial}{\partial t} r_l \rho_l + \frac{\partial}{\partial x} r_l \rho_l u_l = \dot{m} \tag{11}$$

$$\frac{\partial}{\partial t} r_g \rho_g + \frac{\partial}{\partial x} r_g \rho_g u_g = \dot{m} \tag{12}$$

An obvious constraint is that the two phases should fill the whole void space, that is $r_l + r_g = 1$.

The change of current air concentration in water can be determined using the liquid phase saturation equation:

$$\frac{\partial}{\partial t} c_l r_l \rho_l + \frac{\partial}{\partial x} c_l r_l \rho_l u_l = \dot{m} \tag{13}$$

3.3 Results

3.3.1 Hypothetical core

Figure 12 shows the time required to remove air from the first seven cells of the core (the core is divided into 10 cells). The computational conditions in this case are: there is no Darcian flow of air and the hydraulic conductivity is constant, i.e. not a function of saturation.

When a pressure head of 100 m is applied at the upstream boundary, it takes about 2000 hours to obtain a linear pressure distribution within the core. After 2000 hours, all the air in cells 1 and 2 have been dissolved whereas in cells 3 to 7, 0.80, 0.82, 0.84, 0.86, and 0.88 kg of air remain. The pressure in cells 3 to 7 is 8.26, 7.29, 6.32, 5.36, and 4.39 atm. When the water enters cell 3, saturated with air at atmospheric pressure, some air is dissolved to saturate the water at 8.26 atm. When the water leaves cell 3, it is saturated. In cell 4, the pressure is 7.29 atm with some air evolving so that the water becomes saturated at the current pressure. The process is repeated in the following cells; oversaturated water enters the cells with some air evolving so that the water becomes saturated at current pressures. The same amount of air will evolve in each cell due to the linear pressure distribution. After 4800 hours, the 0.80 kg air from cell 3 is removed and evenly distributed in cells 4 to 10 with 0.11 kg in each. Hence, after 4800 hours, the amount of air in cells 4 to 7 has increased to 0.93, 0.95, 0.97, and 0.99 kg. When there is no air left in cell 3, the same process will be repeated in cell 4 and so on.

From a plug flow analysis (for details, see Paper 3), it is estimated that the time required to remove the air from cell 3 is 4500 hours. This is in accordance with the numerical results.

3.3.2 WAC Bennett Dam

Figure 13 shows the measured and numerically calculated pressure evolution in the core of WAC Bennett Dam. The numerical result in Figure 13 (a) is based on a Darcian flow of air and conductivities that are a function of saturation. The calculated pressures continue to rise for about five years after the filling and decline after that, a behaviour similar to what was found in WAC Bennett Dam. The measured peak pressure head is 98 m after nine years and the simulated is 65 m after seven years. The measurements indicate a pressure residual of 35 to 40 m after 25 to 30 years whereas the calculated pressure residual is 38 m after 12 years, i.e. when all air bubbles are dissolved and steady state conditions are approached.

The result in Figure 13 (b) is based on the same computational conditions as the simulation shown in Figure 13 (a), except for the relationship hydraulic conductivity - water saturation level. In this case the alternative relationship, see Figure 11, is chosen. The alternative relationship resulted in an increased peak pressure head, 90 m after eight years, and all air bubbles dissolved after 13 years.

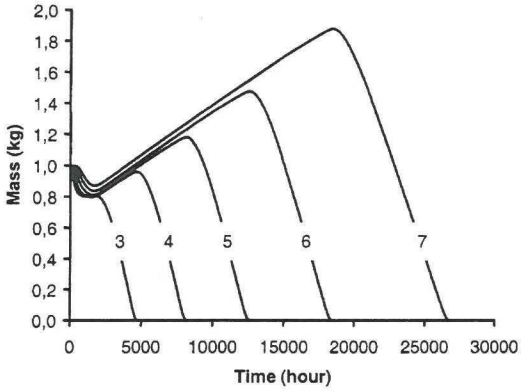

Figure 12. The distribution of air in cells 3 to 7 as function of time for the hypothetical core with no Darcian flow of air and a constant hydraulic conductivity, i.e. not a function of saturation. The upstream and downstream pressure head is 100 m and 0 m, respectively. The numbers in the figure are referring to cell numbers.

Figure 13 (c) is based on the same situation as in Figure 13 (b), but with no Darcian flow of air. In this case, the peak pressure head is 104 m after 12 years and steady state conditions are obtained after 14 years. The two pressure distributions are too similar to evaluate whether Darcian flow of air is significant or not.

3.4 Discussion

The results indicate that the mathematical model presented can simulate the effect of air bubbles on the pressure distribution in an embankment dam. The model is based on relevant conservation principles and physical laws (Darcy's, Boyle's, and Henry's law), but less fundamental assumptions are still needed. In order to put the simulation in perspective, the more important of these will now be listed and discussed:

- One-dimensional simulation:

  A vertical transport of air bubbles due to buoyancy can be expected. However, the one-dimensional assumption is still reasonable because the amount of air bubbles entering and leaving the core remains the same even though the bubbles leave the core a little bit downstream from the entering point, i.e. there is no net flow of air in the vertical direction. However, to be able to consider a realistic cross section and the water surface profile, two dimensions are necessary.

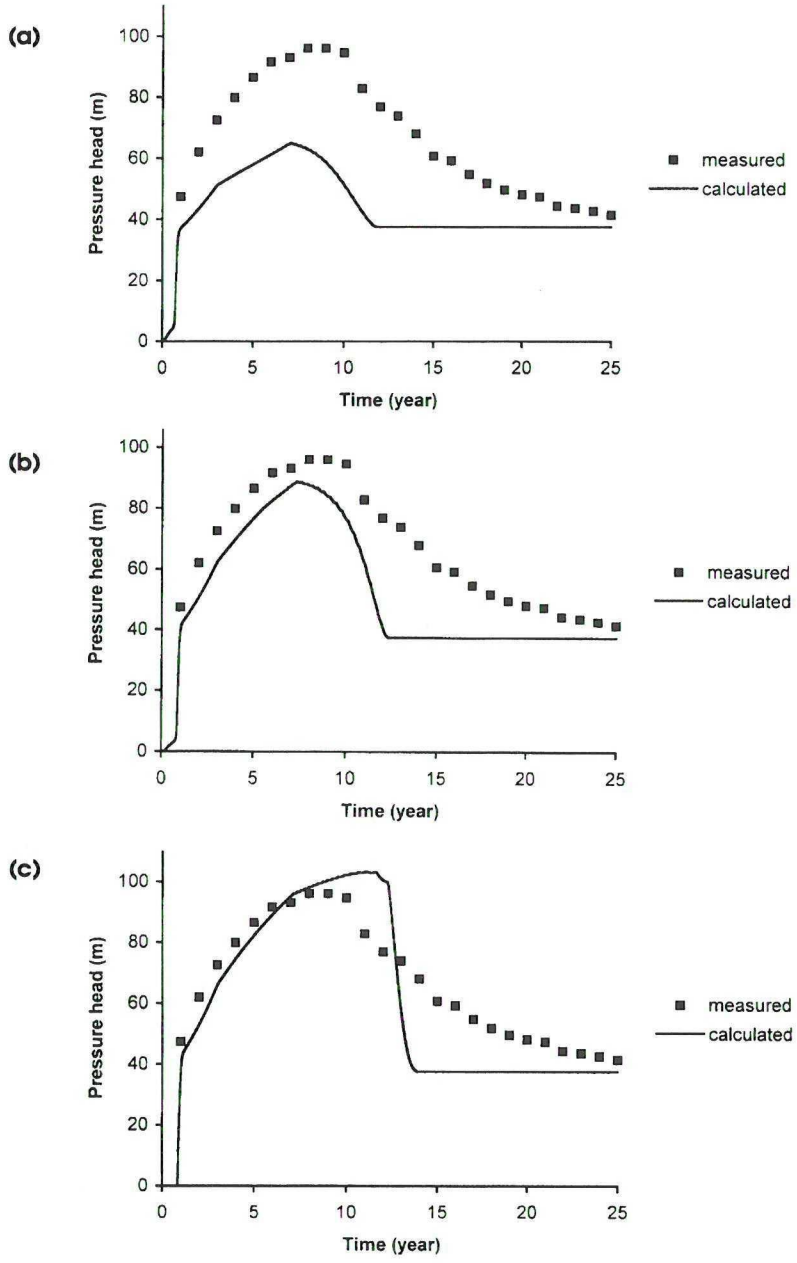

Figure 13. Piezometer EP04 (see Figure 10): (a) measured and calculated pressure evolution; (b) measured and calculated pressure evolution where the alternative relationship hydraulic conductivity - water saturation level is used, see Figure 11; (c) measured and calculated pressure evolution where the alternative relationship hydraulic conductivity - water saturation level is used and Darcian flow of air is neglected.

- Hydraulic conductivity - water saturation level relationships:

  The relationship between the relative water conductivity and water saturation level is uncertain; the sensitivity is demonstrated in Figures 13 (b) and (c). The relationship between the relative air conductivity and water saturation level used in this work is in fair agreement with a number of experimental results. However, the relationship must still be regarded as uncertain. In the further development of the model, an increased knowledge concerning the conductivity data is certainly one of the key elements.

- The overall mass transfer coefficient, K:

  The value of K used in the simulation is somewhat uncertain, but this not crucial as the dissolution process is fast in comparison with the time scale of the problem considered. There is hence always time for an equilibrium to be established.

It should also be pointed out that the input data for the WAC Bennett Dam simulation are incomplete. The porosity, temperature, level of air saturation of the water entering the core, and the pressure conditions on the upstream and downstream boundary are not known, but only assumed.

3.5 Conclusions

From the comparisons between the measured and simulated pressure evolution, it can be concluded that the Air Hypothesis is a potential explanation to the unexpected behaviour of the core at WAC Bennett Dam.

The numerical model is able to predict the pressure evolution in both a qualitative and quantitative way. From the simulations, it cannot be stated whether the Darcian flow of air is significant or not.

4. GENERAL DISCUSSION

There are four hypotheses already proposed to explain the anomalous pore pressures within embankment dams. This study examines two of them, inhomogenities in the core and trapped air bubbles, which can both be examined from a fluid mechanical point of view. The other two mechanisms, settlements and bleeding of fine material, must be examined also from a geotechnical aspect.

It is the objective of this work to examine the importance of fractures and trapped air bubbles when analysing the pressure distributions in embankment dams. In this section, what has been achieved and what is further required before a realistic analysis of a real dam can be performed will be discussed.

What differences from the homogeneous core, with respect to the pressure distribution, can be expected with either a fracture or trapped air bubbles present? Results from the numerical simulations and the idealized experiments indicate that with a fracture present, i.e. the specific fractures used in these experiments, the pressure increases by roughly 20 percent. With trapped air bubbles taken into consideration, the pressure increase was found to be between 70 and 170 percent, based on numerical simulations. If these values are transferable to a real dam, one should then be able to detect the effect of fractures or air bubbles.

This examination, based on results from two numerical models, is mainly theoretical. Numerical results from the homogeneous and inhomogeneous embankment dam are compared with analytical solutions and fundamental experiments whereas numerical results from the Air Hypothesis are compared with a plug flow analysis and field measurements. Thus, the models are well validated and can be used as tools in the examination of pressure distributions for the idealized cases treated in this work. It is argued that the models also provide a well-founded platform for the development of more site-specific models.

No attempts have, however, been made to simulate the hydraulics of a "real world" dam. Applying the model to a real dam is a major undertaking, with respect to the specification of the porous media, even though this work shows that the computational technique for such an application is available. Further work with the model will require an extension to three dimensions and specification of a realistic porous media. The model with the Air Hypothesis is one-dimensional; to be able to consider a realistic cross section and the water surface profile, at least two dimensions are necessary. To get a more solid foundation for the Air Hypothesis, a suitable one-dimensional laboratory experiment is required for detailed verification of the simulations.

5. CONCLUSION

The main result of the study is the development of numerical models to simulate how inhomogenities and trapped air bubbles influence the pressure distribution. These models have a solid foundation, i.e. are based on conservation principles, physical laws, and the best available empirical relationships. The models have been validated through comparisons with analytical solutions, basic experiments, and field measurements and thus provide a good starting point in the development of tools that can be used in dam engineering.

The study also provides new data from basic laboratory experiments, suitable for verification of numerical models.

6. REFERENCES

American water works association: 1990, *Water quality and treatment: a handbook of community water supplies*, McGraw-Hill, New York.

Batchelor, G.K.: 1967, *An introduction to fluid dynamics*, Cambridge University Press, Cambridge.

Bear, J.: 1972, *Dynamics of fluid in porous media*, American Elsevier Publishing Company, New York.

Bear, J., and Verruijt, A.: 1987, *Modeling groundwater flow and pollution*, D. Reidel Publishing Company, Dordrecht.

Bernell, L.: 1957, The properties of moraines, In *Proc. 4th International Conference on Soil Mechanics and Foundation Engineering,* London, **2**, 286-290.

Botset, H.G.: 1940, Flow of gas-liquid mixtures through consolidated sand, *Trans. AIME,* **186**, 91-108.

Bras, R.L.: 1990, *Hydrology - an introduction to hydrologic science*, Addison-Wesley Publishing Company, Massachusetts.

Crank, J.: 1984, *Free and moving boundary problems*, Oxford University Press, Oxford.

Crawford, C.W., and Plumb, O.A.: 1986, The influence of surface roughness on resistance to flow through packed beds, *Journal of Fluids Engineering*, **108**, 343-347.

De Marsily, G.: 1986, *Quantitative hydrogeology - groundwater hydrology for engineers*, Academic Press, San Diego.

De Parseval, Y., Pillai, K.M., and Advani, S.G.: 1997, A simple model for the variation of the permeability due to partial saturation in dual scale porous media, *Transport in Porous Media*, **27**, 243-264.

Dong, M., and Dullien, F.A.L.: 1997, A new model for immiscible displacement in porous media, *Transport in Porous Media*, **27**, 185-204.

Dudgeon, C.R.: 1967, Wall effects in permeameters, *Journal of the Hydraulics Division, ASCE,* **93**, 137-148.

Dullien, F.A.L.: 1992, *Porous media - fluid transport and pore structure*, Academic Press, San Diego.

Du Plessis, J.P.: 1994, Analytical quantification of coefficients in the Ergun equation for fluid friction in a packed bed, *Transport in Porous Media*, **16**(2), 189-207.

Ergun, S.: 1952, Fluid flow through packed columns, *Chemical Engineering Progress*, **48**(2), 89-94.

Fand, R.M., Kim, B.Y.K., Lam, A.C.C., and Phan, R.T.: 1987, Resistance to flow of fluids through simple and complex porous media whose matrices are composed of randomly packed spheres, *Journal of Fluids Engineering*, 109, 268-274.

Flödeskommittén: 1990, *Riktlinjer för bestämning av dimensionerande flöden för dammanläggningar (Guidelines for determination of design floods in hydro power,* in Swedish*)*, Norrköping.

Forchheimer, P.: 1901, Wasserbeweguing durch Boden, *Zeischrift, Verein Deutscher Ingenieure*, **45**, 1782-1788.

Fredlund, D.G., and Rahardjo, H.: 1993, *Soil mechanics for unsaturated soils*, John Wiley & Sons, New York.

Graton, L.C., and Fraser, H.J.: 1935, Systematic packing of spheres with particular relation to porosity and permeability, *Journal of Geology*, **43**, 785-909.

Hansen, D.: 1992, *The behaviour of flowthrough rockfill dams*, Doctoral thesis, University of Ottawa, Ottawa.

ICOLD: 1995, *Dam failures statistical analysis*, Bulletin 99.

ICOLD: 1998, *World register of dams.*

Jackson, D.C.: 1995, *Building the ultimate dam*, University Press of Kansas, Kansas.

Johansson, S.: 1997, *Seepage monitoring in embankment dams*, Doctoral thesis, Royal Institute of Technology, Stockholm.

Kececioglu, J., and Jiang, Y.: 1994, Flow through porous media of packed spheres saturated with water, *Journal of Fluids Engineering, Transactions of the ASME*, **116**, 164-170.

Kunii, D., and Levenspiel, O.: 1969, *Fluidization engineering*, John Wiley & Sons, New York.

LeBihan, J.P., and Leroueil, S.: 1999, Transient water flow through unsaturated soils: implications for earth dams, In *Proc. 52nd Canadian Geotechnical Conference*, Regina.

Löfquist, B.: 1992, Hydraulic penetration in embankment dams, *Ground Engineering*, **6**: 40-43.

Macdonald, I.E., El-Sayed, M.S., Mow, K., and Dullien, F.A.L.: 1979, Flow through porous media - the Ergun equation revisited, *Industrial and Engineering Chemistry Fundamentals*, **18**(3), 199-208.

Novak, P., Moffat, A.I.B., Nalluri, C., and Narayanan, R.: 1990, *Hydraulic structures*, Unwin Hyman, London.

Peck, R.B.: 1990, Interface between core and downstream filter, In *Proc. H. Bolton Seed Memorial Symposium*, San Francisco, **2**, 237-251.

Polubarinova-Kochina, P.Ya.: 1962, *Theory of ground water movement*, Princeton University Press, Princeton, New Jersey.

Rehbinder, G.: 1990, *Strömning genom en damm med läckvägar. Teori och experiment, etapp 1 (Flow through an embankment dam with fractures. Theory and experiment, part 1,* in Swedish*)*. Report No. 47, Royal Institute of Technology, Stockholm.

Schober, W.: 1967, Behaviour of the Gepatsch rockfill dam, In *Proc. ICOLD's 9th Congress*, Istanbul.

Sherard, J.L.: 1986, Hydraulic fracturing in embankment dams, *Journal of Geotechnical Engineering, ASCE*, **112**(10): 905-927.

Sherard, J.L., Woodward, R.J., Gizienski, S.F., and Clevenger, W.A.: 1963, *Earth and earth-rock dams*, John Wiley & Sons, New York.

Singh, B., and Varshney, R.S.: 1995, *Engineering for embankment dams*, A.A. Balkema, Rotterdam.

St-Arnaud, G.: 1995, The high pore pressures within embankment dams: an unsaturated soil approach, *Canadian Geotechnical Journa*l, **32**(5), 892-898.

Statens offentliga utredningar: 1987, *SOU 1987:64 Betänkande av Dammsäkerhet och skydd mot översvämningar (Dam safety and overtopping,* in Swedish*)*, Stockholm.

Statens offentliga utredningar: 1995, *SOU 1995:40 Betänkande av Utredningen om dammsäkerhet och höga flöden (Dam safety and floods,* in Swedish*),* Stockholm.

Stewart, R.A., and Imrie, A.S.: 1993, A new perspective based on the 25 year performance of WAC Bennett Dam, In *Proc. International Workshop on Dam Safety Evaluation*, Grindelwald, 53-69.

Stewart, R.A., Imrie, A.S., and Hawson, H.H.: 1990, Unusual behaviour of the core at WAC Bennett Dam, In *Proc. 43rd Canadian Geotechnical Conference*, Quebec, **2**, 549-558.

Vattenfall: 1988, *Jord- och stenfyllningsdammar* (*Earth and earth-rock dams*, in Swedish), Stockholm.

Verma, N.S., Pare, J.J., Boncompain, B., Garneau, R., and Rattue, A.: 1985, Behaviour of the LG 4 main dam, In *Proc. 11th International Conference on Soil Mechanics and Foundation Engineering*, San Francisco, 2049-2054.

Wyckoff, R.D., and Botset, H.G.: 1936, The flow of gas-liquid mixtures through unconsolidated sands, *Physics*, **7**, 325-345.

Paper 1

Billstein M., Svensson U., and Johansson N.: 1999, Development and validation of a numerical model of flow through embankment dams - comparisons with experimental data and analytical solutions, *Transport in Porous Media,* **35**, 395 - 406.

Transport in Porous Media **35:** 395–406, 1999.

Development and Validation of a Numerical Model of Flow Through Embankment Dams – Comparisons with Experimental Data and Analytical Solutions

MATS BILLSTEIN[1], URBAN SVENSSON[2] and NILS JOHANSSON[3]
[1]*Division of Water Resources Engineering, Luleå University of Technology, Sweden*
[2]*Computer-Aided Fluid Engineering AB, Norrköping, Sweden*
[3]*Vattenfall Utveckling AB, Älvkarleby, Sweden*

(Received: 4 December 1997; in final form: 19 June 1998)

Abstract. The development and validation of a numerical simulation model of the flow through embankment dams is described. The paper focuses on basic verification studies, that is, comparisons with analytical solutions and data from laboratory experiments. Two experimental studies, one dealing with the flow in a Hele–Shaw cell and the other with the flow through a bed of packed glass beads, are also described. Comparisons are carried out with respect to the phreatic surfaces, pressure profiles, seepage levels and discharges. It is concluded that the agreement between experimental, analytical and numerical results is generally satisfactory.

Key words: numerical model, embankment dam, experimental data.

1. Introduction

The embankment dam shown in Figure 1 is a common type of structure used by the hydropower industry to retain water. A core of moraine provides the sealing, and the filter material upstream and downstream protect the dam against erosion. A transition layer made of slightly coarser materials is placed outside the filters, and finally a rock fill is provided for protection and stability. For safety reasons, the dams need to be inspected regularly. Dams are inspected in different ways, for example pore pressure measurements, discharge measurements, temperature/resistivity measurements, radar measurements (Johansson, 1997) and self-potential measurements (Triumf and Thunehed, 1996).

As in most other engineering branches, numerical simulation models can be useful complements to existing techniques. With them, pressure distributions, water surface profiles, seepage levels, velocity distributions and discharges can be studied for different flow conditions – both stationary and transient. However, before an extensive use of numerical models, a demonstration that the models can simulate the hydraulics of the dams in a satisfactory way is required.

The objective of the work described in this paper was to develop a well verified numerical model of embankment dams. A first step in this work is to compare

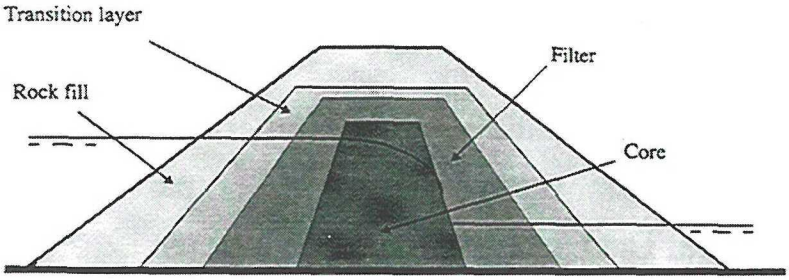

Figure 1. Schematic figure showing a vertical section through an embankment dam.

results from the numerical model with analytical solutions and data from laboratory experiments; this paper presents that first step.

Some numerical simulations of the flow and pressure distributions in earth dams have already been carried out (Mitchell and Hunt, 1985; Goodwill and Kalliontzis, 1988; Hansen, 1992; Greenly and Joy, 1996; Koo and Leap, 1998) but suitable laboratory experiments are needed. Therefore the project includes an experimental part, primarily to provide data for verification of the numerical model.

The outline of the paper is as follows: in the next section experimental studies are described and thereafter an analytical solution is outlined. The numerical model and a review of friction formulae are the subjects of the following section. All results, from experiments, analytical and numerical solutions, are given in the result section. Finally some conclusions are formulated.

2. Experimental Studies

Two types of experiments were conducted (Figure 2). In both experiments the water levels upstream and downstream were held constant and the steady flow in the domain in between was studied. One experiment used a Hele–Shaw cell, that is the creeping

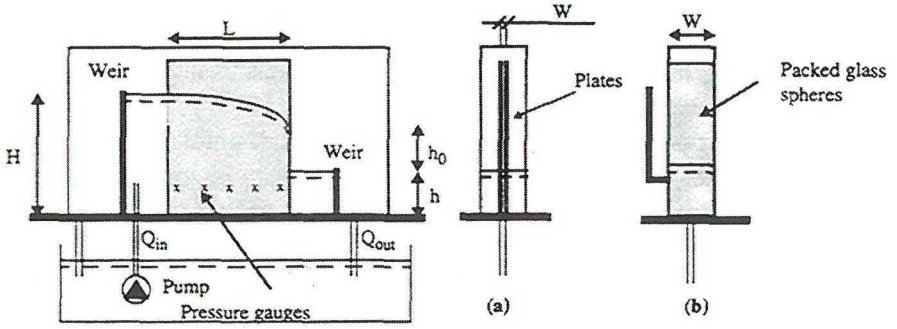

Figure 2. Experimental set up: section (a) for the Hele–Shaw experiment, and section (b) for bed of packed glass spheres.

flow between two parallel plates was studied; in the other experiment a bed of packed glass beads provided the flow resistance.

The Hele–Shaw method is based on the analogy between a creeping flow and flow through a porous media. This analogy is valid if inertia terms are negligible (Batchelor, 1967). The advantage of the method is that one does not need to create a porous matrix. The establishment of creeping flow requires the use of very small distances between the parallel plates, Figure 2(a), and hence introduce an uncertainty in the experimental conditions. However, if glycerine is used as fluid (glycerine has a viscosity about 1000 times higher than that for water) the spacing between the plates can be in the range 1–20 mm, and hence such a spacing is easy to manufacture and control. The objective of these experiments is to obtain the free surface profile and seepage level at the point of outflow (h_0 in Figure 2).

The second experiment did involve a porous matrix. Glass beads of uniform diameter were randomly packed between two parallel plates (Figure 2(b)). A thin net, with negligible flow resistance, at the upstream and downstream boundaries kept the beads in place. Two quite different bead diameters, 0.002 and 0.025 m, were used so as to vary the Reynolds number significantly. Once the discharge had become steady, the discharge, pressure distribution, free surface profile and seepage level were measured.

The experimental conditions are summarised in Table I. The temperature was recorded in each experimental run because the viscosity is a function of the temperature. In the Hele–Shaw experiment, the surface profile and the seepage level were determined from photographs. In the experiment with a porous matrix, the discharge was measured with a triangular weir and the pressures by a piezometer. The points where the pressure was measured were located 0.04 m above the bottom of the flume. The free water surface was measured from direct observations, taking the capillary rise into account. Also the seepage level was measured from direct observations.

Table I. Experimental conditions

Experiment	L (m)	W (m)	Bead diameter (m)
Hele–Shaw	0.30	0.002	–
		0.004	–
		0.008	–
		0.016	–
Porous medium	0.205	0.132	0.002
	0.505	0.132	0.002
	0.50	0.301	0.025

3. Analytical Solutions

An analytical prediction of this type of flow can be made if the following conditions are fulfilled:

- The flow is steady and laminar.
- The dam has rectangular cross-section and a constant hydraulic conductivity.
- The flow is essentially two-dimensional.

For these conditions Polubarinova-Kochina (1962) obtained a solution that gives the discharge, surface profile and seepage level as functions of H, h, L and K, in which K is the hydraulic conductivity.

For calculation of the discharge through a dam, Bear (1972) has shown that the Dupuit–Forchheimer formula is valid:

$$q = K\left(\frac{H^2 - h^2}{2L}\right), \tag{1}$$

in which q is the discharge per unit width. To find the equations describing the free surface profile and the seepage level, one uses methods based on hodograph transformations and obtains the following set of equations (Crank, 1984):

$$H = C\int_0^{\pi/2} \frac{\boldsymbol{K}(\beta + (1-\beta)(\sin\Psi)^2}{\sqrt{[\beta - \alpha + (1-\beta)(\sin\Psi)^2]}}\,\mathrm{d}\Psi, \tag{2}$$

$$h = C\sqrt{\alpha}\int_0^{\pi/2} \frac{\boldsymbol{K}(\alpha(\sin\Psi)^2)\sin\Psi}{\sqrt{[1-\alpha(\sin\Psi)^2)(\beta - \alpha(\sin\Psi)^2]}}\,\mathrm{d}\Psi, \tag{3}$$

$$L = C\int_0^{\pi/2} \frac{\boldsymbol{K}(\alpha + (\beta-\alpha)(\sin\Psi)^2)}{\sqrt{[1-\alpha-(\beta-\alpha)(\sin\Psi)^2]}}\,\mathrm{d}\Psi, \tag{4}$$

in which C, α and β are parameters and $\boldsymbol{K}(\zeta)$ is a complete elliptic integral. α, β and C have no physical meaning but are intermediate values required in the Schwarz–Christoffel transformation used in the analyses. The quantities C, α and β are determined, for different ratios L/H and h/H, from the system of Equations (2)–(4). The quantities α and β must satisfy the condition $0 \leqslant \alpha \leqslant \beta \leqslant 1$. Once C, α and β have been determined, Equations (5)–(7) can be used to determine the seepage level, h_0, and free surface profile, $(x(\Psi), y(\Psi))$ in which $0 \leqslant \Psi \leqslant \pi/2$.

$$h_0 = C\int_0^{\pi/2} \frac{\boldsymbol{K}((\cos\Psi)^2)\sin\Psi\cos\Psi}{\sqrt{[1-(1-\alpha)(\sin\Psi)^2][1-(1-\beta)(\sin\Psi)^2]}}\,\mathrm{d}\Psi, \tag{5}$$

$$x = L - C\int_0^{\Psi} \frac{\boldsymbol{K}((\sin\Psi)^2)\sin\Psi}{\sqrt{[1-\alpha(\sin\Psi)^2][1-\beta(\sin\Psi)^2]}}\,\mathrm{d}\Psi, \tag{6}$$

$$y = h + h_0 + C \int_0^{\Psi} \frac{\boldsymbol{K}((\cos\Psi)^2)\sin\Psi}{\sqrt{[1-\alpha(\sin\Psi)^2][1-\beta(\sin\Psi)^2]}}\,\mathrm{d}\Psi. \tag{7}$$

Equations (5)–(7) have to be solved numerically. The method used in the present work is based on Newton–Cotes formula and Simpson's rule for numerical integration. The code MATLAB®* was employed in the calculations.

4. Numerical Simulation Model

The numerical simulation model is based on a direct solution of the conservation equations. For an incompressible fluid, these are as follows:

Conservation of mass:

$$\nabla \cdot (\rho \mathbf{u}) = 0. \tag{8}$$

Conservation of momentum:

$$-\nabla p + \rho \mathbf{g} + \mathbf{F} = 0, \tag{9}$$

in which $\mathbf{u}$ is the Darcy velocity vector, ρ density, p pressure, $\mathbf{g}$ gravitational vector and $\mathbf{F}$ a vector representing frictional forces.

The Darcy equation involves a resistance term that is linear which is valid for small Reynolds numbers. Fand *et al.* (1987) have identified four regimes for flow through a porous medium:

Pre-Darcy	$\mathrm{Re} < 10^{-5}$,
Darcy	$10^{-5} < \mathrm{Re} < 2.3$,
Forchheimer	$5 < \mathrm{Re} < 80$,
Turbulent	$\mathrm{Re} > 120$,

in which the Reynolds number is based on the Darcy velocity, the diameter of the sphere and the kinematic viscosity. Kececioglu and Jiang (1994) identified the same regimes, although they suggested somewhat different values of the Reynolds numbers for the transitions.

The flow regimes in the porous media experiment described herein would then be categorized as 'Forchheimer' and 'Turbulent'. For these regimes, inertia forces and turbulence are significant, and a non-linear resistance formula is required. The general practise is to use the Forchheimer Equation (Forchheimer, 1901) with the constants presented by Ergun (1952):

$$\mathbf{F} = \left(-A\left[\frac{(1-n)^2}{n^3}\frac{\mu}{d^2}\right]u - B\left[\frac{(1-n)}{n^3}\frac{\rho}{d}\right]u^2,\right.$$
$$\left. - A\left[\frac{(1-n)^2}{n^3}\frac{\mu}{d^2}\right]v - B\left[\frac{(1-n)}{n^3}\frac{\rho}{d}\right]v^2\right), \tag{10}$$

* MATLAB® is a registered trademark for the Math Works, Inc.

in which A and B are empirical constants, n porosity, μ dynamic viscosity and d sphere diameter. For the empirical constants, Ergun suggested $A = 150$ and $B = 1.75$. More recently, investigators have proposed somewhat higher values; Macdonald *et al.* (1979) recommend $A = 180$ and $B = 1.8$ and DuPlessis (1994), 207 and 1.88, respectively. Fand *et al.* (1987) give $A = 182$ and $B = 1.92$ for the Forchheimer regime and 225 and 1.61, respectively, for turbulent flows. With reference to these investigations, the values $A = 200$ and $B = 1.8$ were chosen for the simulations in this work. Preliminary tests also indicated that these values would ensure good agreement with the present experimental data. The simulations are, however, not very sensitive to a small change of the constants. If the constants are modified by $\pm 2\%$ the discharge is changed with $\pm 1\%$.

To use Equation (10), one must know the value of the porosity. Spheres can be packed with various arrangements. The loosest one is the cubic packing, porosity 0.4764, and the most dense is the rhombohedral packing, porosity 0.2595 (Graton, 1935). The porosity for randomly packed spheres is usually in the range 0.31–0.43 (Kunii and Levenspiel, 1969). Crawford and Plumb (1986) found the porosity to be 0.356 for smooth particles and Kececioglu and Jiang assumed a value of 0.40 as an average porosity in their experiments. Fand *et al.* (1987) found the porosity to be in the interval 0.357–0.360. The glass beads used in the present experiment have diameters 0.002 and 0.025 m with a standard deviation of about 1% of the diameter. Although this variation is small, it may lead to porosities that are somewhat smaller than those for uniform spheres. From these considerations a porosity of 0.34 for the smaller glass beads was chosen. For the larger ones, the wall effect has an effect because the ratio d/W (where W is defined in Figure 2) is large, about 0.1. Hansen (1992) and Dudgeon (1967) have summarised estimates of the wall effect. From that summary, the average porosity is found to be some 5–10% larger than if the wall effect is negligible. These indications lead to an estimate of 0.41 for the porosity of the larger beads. Determined from our own porosity measurements, the porosity for the two bead diameters were in the range $34 \pm 2\%$ and $41 \pm 2\%$, values that correspond well with the estimates in the literature.

The system of equations was solved by the general equation solver PHOENICS, (Spalding, 1981). PHOENICS is based on a finite-volume formulation of the basic equations and serves for a wide range of coordinate systems (cartesian, body-fitted, cylindrical, etc.) and numerical techniques (higher order schemes, solvers, etc.). Several free surface techniques are also available in the PHOENICS system. The present application is based on an algorithm called the Height-of-Liquid (HOL) algorithm, (Spalding and Jun, 1991). The basic idea in the HOL-algorithm is to determine the position of the free surface from an application of the mass conservation principle to a depth-integrated control volume. In the numerical simulations, the grid-spacing was 0.01 m in both directions. This spacing was found to be adequate for grid-independent solutions.

Table II. Comparison of seepage levels as given by Hele–Shaw experiment, analytical solution and numerical simulation

L (m)	W (m)	H (m)	h (m)	Re	$h_{0\,\mathrm{exp}}$ (m)	$h_{0\,\mathrm{anal}}$ (m)	$h_{0\,\mathrm{num}}$ (m)
0.300	0.002	0.288	0.144	0.004	0.02	0.009	0.006
	0.004	0.288	0.144	0.03	0.02	0.009	0.006
	0.008	0.287	0.145	0.2	0.02	0.009	0.006
	0.016	0.136	0.000	1.4	0.043	0.022	0.021
	0.016	0.184	0.013	1.8	0.052	0.030	0.030

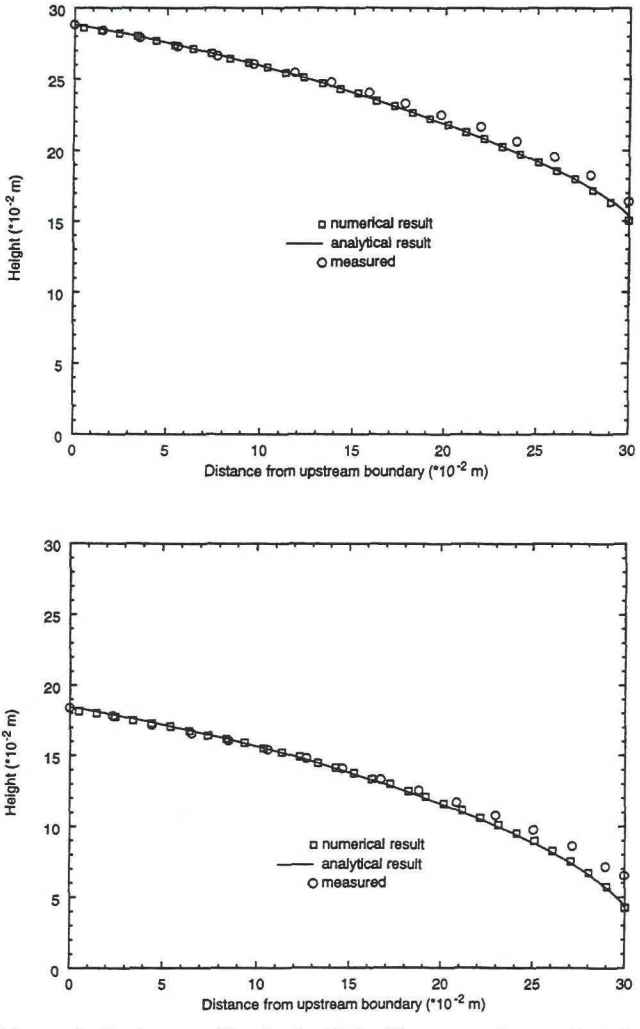

Figure 3. Surface profiles in the Hele–Shaw experiment. Top: $W = 2$ mm, $H = 0.288$ m, $h = 0.144$ m, Re $= 0.004$. Bottom: $W = 16$ mm, $H = 0.184$ m, $h = 0.013$ m, Re $= 1.8$.

5. Results

Results for the two basic situations used, the Hele–Shaw cell and the porous medium, can be compared if the analytical and numerical solutions are obtained for the same situations. This is the way results will be presented.

Seepage levels for the Hele–Shaw cell are summarised in Table II, and surface profiles are shown in Figure 3. The analytical and numerical solutions give remarkably similar results, whereas the predicted seepage levels are systematically lower than the experimental results. The good agreement between the numerical and analytical solution indicates that the numerical model provides a correct solution of the governing equations. The higher seepage levels in the experiment must therefore be due to some effect not included in the theory. Inertia effects can be ruled out as the disagreement is found for the whole range of Reynolds numbers investigated.

Next the results for the porous medium are presented and discussed. Table III contains a summary of the experimental, analytical and numerical results and the surface profiles and pressure distributions are shown in Figures 4 and 5. The calculated (analytically and numerically) discharges and seepage levels in Table III agree well with the measured ones. The seepage levels were calculated only analytically for the small glass beads because the analytical solution is based on a linear resistance term. Also the calculated surface profiles (Figure 4) and pressure profiles (Figure 5) correspond well with measured profiles.

Table III. Comparison of flow and seepage levels as given by porous medium experiment, analytical solution and numerical simulation

Diameter (m)	W (m)	n (%)	L (m)	H (m)	h (m)	Re	$h_{0\,\mathrm{exp}}$ (m)	$h_{0\,\mathrm{anal}}$ (m)	$h_{0\,\mathrm{num}}$ (m)	Q_{exp} (l/s)	Q_{num} (l/s)
0.002	0.132	34	0.205	0.518	0.388	11	0.01	0.016	0.015	0.45	0.44
				0.521	0.104	23	0.28	0.268	0.263	0.82	0.85
				0.522	0.015	25	0.35	0.357	0.353	0.85	0.88
			0.505	0.368	0.258	4	0.00	0.005	0.000	0.11	0.11
				0.367	0.096	10	0.04	0.030	0.029	0.19	0.19
				0.367	0.015	12	0.09	0.084	0.087	0.20	0.21
0.025	0.301	41	0.500	0.285	0.262	500	0.00	–	0.000	2.05	2.02
				0.279	0.200	900	0.01	–	0.000	3.42	3.40
				0.292	0.118	1100	0.01	–	0.008	4.42	4.56
				0.434	0.292	1200	0.01	–	0.002	6.91	7.08
				0.292	0.042	1400	0.07	–	0.052	4.66	4.78
				0.429	0.140	1500	0.08	–	0.05	8.23	8.42

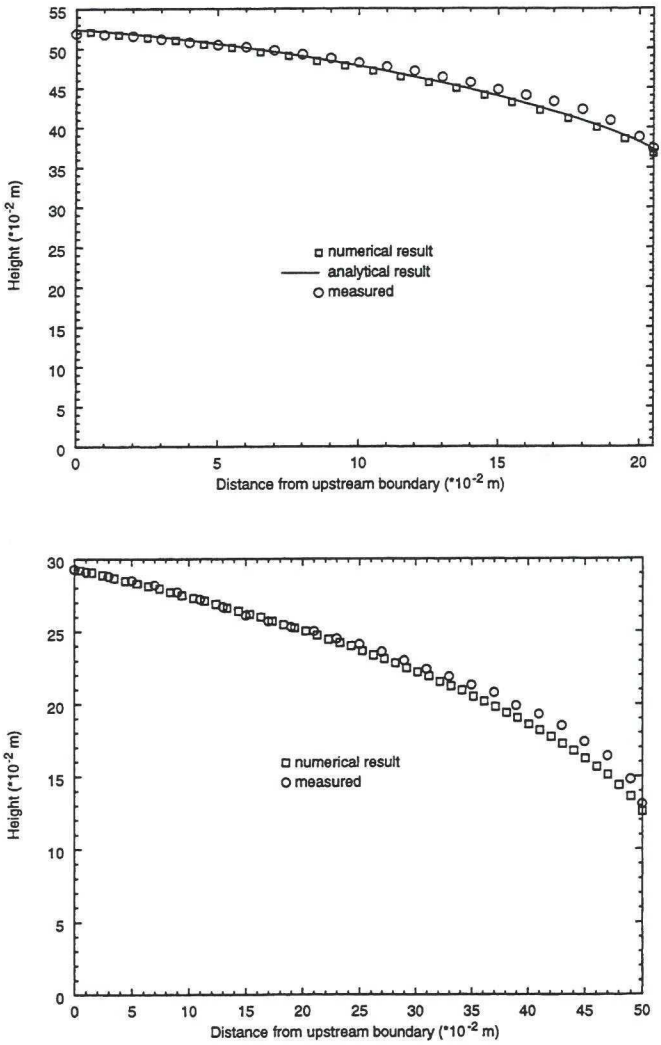

Figure 4. Water surface profiles for the porous media experiment. Top: Sphere diameter = 0.002 m, H = 0.522 m, h = 0.015 m, Re = 25. Bottom: Sphere diameter = 0.025 m, H = 0.292 m, h = 0.118 m, Re = 1100.

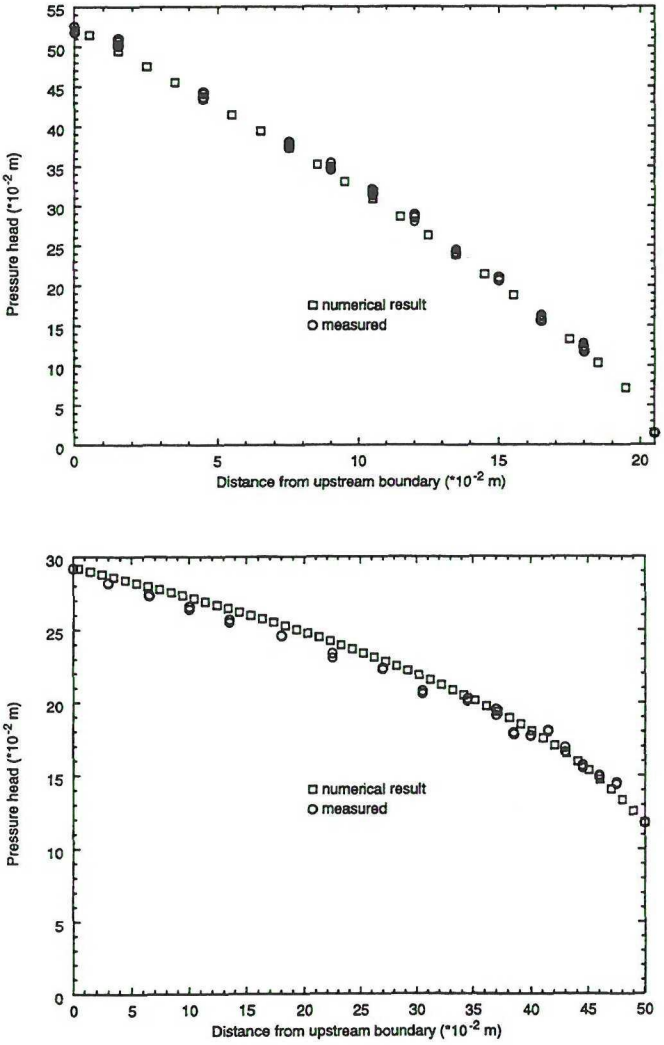

Figure 5. Pressure profiles for the porous media experiment. Top: Sphere diameter = 0.002 m, H = 0.522 m, h = 0.015 m, Re = 25. Bottom: Sphere diameter = 0.025 m, H = 0.292 m, h = 0.118 m, Re = 1100.

6. Discussion and Conclusions

The primary objective of the study was to determine whether the numerical model is in agreement with analytical solutions and experimental data. If so, the model provides a good starting point for further development (introduction of inhomogeneous conductivity fields, realistic dam shapes, three-dimensional flows etc.). The results obtained demonstrate that such an agreement has been achieved. The discrepancy in seepage level between the Hele–Shaw experiments and the calculations may be due to a nonideal outflow condition in the experimental set up. Glycerine is very adhesive

Table IV. Discharge for various values of the porosity in bed of glass beads

Diameter (m)	W (m)	H (m)	h (m)	n (%)	Q_{num} (l/s)
0.002	0.132	0.521	0.104	36	1.02
				35	0.93
				34	0.85
				33	0.77
				32	0.70
0.025	0.301	0.292	0.118	43	5.00
				42	4.77
				41	4.56
				40	4.35
				39	4.11

and it was noted in the experiment that glycerine got stuck on the walls perpendicular to the outlet (see Figure 2); this may have resulted in some additional friction at the outlet, not considered in the numerical simulations.

It should also be emphasized that the resistance formula, Equation (10), is empirical. The constants A and B were selected to 200 and 1.8, respectively, and the porosities to 0.34 for the small beads and 0.41 for the larger ones. The constants and porosities were all chosen with reference to earlier investigations, our own measurements (porosities) and the fact that these values gave a good agreement in general between numerical and experimental results. The simulations of the porous media experiment are sensitive to the porosity values as shown in Table IV. If the porosity is modified by 2% ($34 \pm 2\%$ and $41 \pm 2\%$) the discharge is changed by about $\pm 20\%$ for the small beads and $\pm 10\%$ for the large ones.

The conclusions of the paper are

- Close agreement was found between the results of the numerical model and of the analysis. Hence, the numerical model, including the HOL method, provides a solution to the basic equations.
- Comparisons of the calculated results with the data from the Hele–Shaw experiment show that the resistance was effectively linear. The agreement in these comparisons was quite good except that predictions of the seepage level were consistently 50% lower for all Reynolds numbers considered. No firm conclusion about the cause of this disagreement has been found. The conclusion from this comparison is that a creeping flow with a linear resistance term can be simulated.
- Excellent agreement is obtained for the porous media experiment, for both small and large glass beads. The calculations are however sensitive to the values of

the empirical coefficients and the porosity used in the resistance formulae. The values used correspond with those in the literature on the subject; the simulations of the flow through a porous matrix are therefore regarded as successful.

References

Batchelor, G. K.: 1967, *An Introduction to Fluid Dynamics*, Cambridge University Press, Cambridge.

Bear, J.: 1972, *Dynamics of Fluid in Porous Media*, American Elsevier Publishing Company.

Crank, J.: 1984, *Free and Moving Boundary Problems*, Oxford University Press, Oxford.

Crawford, C. W. and Plumb, O. A.: 1986, The influence of surface roughness on resistance to flow through packed beds, *J. Fluids Engng., Transactions of the ASME* **108**, 343–347.

Dudgeon, C. R.: 1967, Wall effects in permeameters, *J. Hydraul. Div., Transactions of the ASCE* **93**, 137–148.

Du Plessis, J. P.: 1994, Analytical quantification of coefficients in the Ergun equation for fluid friction in a packed bed, *Transport in Porous Media* **16**(2), 189–207.

Ergun, S.: 1952, Fluid flow through packed columns, *Chem. Engng. Progress* **48**(2), 89–94.

Fand, R. M., Kim, B. Y. K., Lam, A. C. C. and Phan, R. T.: 1987, Resistance to flow of fluids through simple and complex porous media whose matrices are composed of randomly packed spheres, *J. Fluids Engng.* **109**, 268–274.

Forchheimer, P.: 1901, Wasserbeweguing durch Boden, *Zeischrift. Verein Deutscher Ingenieure* **45**, 1782–1788.

Goodwill, I. M. and Kalliontzis, C.: 1988, Identification of non-Darcy groundwater flow parameters, *Int. J. Numer. Methods Fluids* **8**, 151–164.

Graton, L. C.: 1935, Systematic packing of spheres with particular relation to porosity and permeability, *J. Geology*, **43**, The University of Chicago Press.

Greenly, B. T. and Joy, D. M.: 1996, One-dimensional finite-element model for high flow velocities in porous media, *J. Geotech. Engng.* (October), 789–796.

Hansen, D.: 1992, The behaviour of flowthrough rockfill dams, Doctoral Thesis, University of Ottawa, Canada.

Johansson, S.: 1997, Seepage monitoring in embankment dams, Doctoral Thesis, Royal Institute of Technology, Sweden.

Kececioglu, I. and Jiang, Y.: 1994, Flow through porous media of packed spheres saturated with water, *J. Fluids Engng., Transactions of the ASME* **116**, 164–170.

Koo, M-H. and Leap, D. I.: 1998, Modeling three-dimensional groundwater flows by the Body-Fitted Coordinate (BFC) method: II. Free and moving boundary problems, *Transport in Porous Media* **30**(3), 345–362.

Kunii, D. and Levenspiel, O.: 1969, *Fluidization Engineering*, John Wiley & Sons, New York.

Macdonald, I. F., El-Sayed, M. S., Mow, K. and Dullien, F. A. L.: 1979, Flow through porous media – the Ergun's equation revisited, *Industr. Engng. Chem. Fundamentals* **18**(3), 199–208.

Mitchell, P. H. and Hunt, B.: 1985, Unsteady groundwater drawdown in embankments, *J. Hydraul. Res.* **23**(3), 241–254.

Polubarinova-Kochina, P. Ya.: 1962, *Theory of Groundwater Movement*, Princeton University Press, Princeton, NJ.

Spalding, D. B.: 1981, A general purpose computer program for multi-dimensional one- and two-phase flow, *Math. Comput. Simulations* **8**, 267–276.

Spalding, D. B. and Jun, L.: 1991, The Height-of-Liquid (HOL) method for computing flows with moving interfaces, *The PHOENICS Code Manual*, CHAM, London, England.

Triumf, C. A. and Thunehed, H.: 1996, Two years of self-potential measurements on a large dam in northern Sweden, In: *Proc. Stockholm Symposia: Repair and Upgrading of Dams*, Royal Institute of Technology, pp. 307–315.

Paper 2

Billstein M., Svensson U., and Johansson N.: 1999, Application and validation of a numerical model of flow through embankment dams with fractures - comparisons with experimental data, *Canadian Geotechnical Journal*, **36**, 651 - 659.

Application and validation of a numerical model of flow through embankment dams with fractures: comparisons with experimental data

Mats Billstein, Urban Svensson, and Nils Johansson

Abstract: The focus of this paper is on the development and validation of a numerical model of flow through simplified embankment dams with fractures. Two laboratory experiments were conducted to provide data for validation of the numerical model, one dealing with steady flow in a Hele-Shaw cell and one with steady flow through a bed of packed glass beads. A horizontal fracture, extending from the upstream boundary to a point within the embankment, was used in both experiments, and it was shown to have a significant influence on the discharge, pressure distribution, height of the seepage face, and free surface profile. Comparisons between numerically determined and experimentally measured results were carried out with respect to the discharge, pressure distribution, height of the seepage face, and free surface profile. In the experiments it is shown that a fracture increases the discharge and that the discharge increases more when a fracture is located far away from the free surface profile than when it is located close to the free surface profile. The height of the seepage face above the tailwater is strongly dependent upon the length of the fracture. The influence on the free surface profile is greater when a fracture is close to the free surface profile than when it is far away from the free surface profile. These effects are also found in the numerical simulations. It is thus concluded that the agreement is generally satisfactory between the experimental and numerical results.

Key words: numerical model, embankment dam, fracture, experimental data, discharge.

Résumé : Cet article se concentre sur le développement et la validation d'un modèle numérique du flot à travers un barrage en remblai, fissuré, simplifié. Deux expériences de laboratoire on été conduites pour fournir des données pour la validation du modèle numérique : une concernant le flot stabilisé dans une cellule de Hele-Shaw et une avec le flot stabilisé à travers un banc de billes de verre. Une fracture horizontale, s'étendant de la limite amont jusqu'au centre du barrage, a été utilisée dans les deux expériences, et elle s'est montré avoir une influence significative sur le débit, la distribution de pression, le niveau de sortie en aval et le profile de la surface libre. Les résultats numériques et expérimentaux ont été comparés pour le débit, la distribution de pression, le niveau de sortie en aval et le profile de la surface libre. Il a été montré par les expériences, que la fissure augmente le débit, et que le débit augmente plus, quand la fissure est située loin de la surface libre que lorsqu'elle en est située à proximité. La hauteur du niveau de sortie au dessus du niveau aval est largement dépendante de la longueur de la fissure. L'influence de la fissure sur le profile de la surface libre est plus grand lorsqu'elle est située près de la surface libre que lorsqu'elle en est éloignée. Ces effets sont aussi observés lors des simulations numériques. Il est donc conclu que la concordance est généralement satisfaisante entre les résultats expérimentaux et numériques.

Mots clés : modèle numérique, barrage en remblai, fissure, données expérimentales, débit.

Introduction

Internal erosion is a major problem in embankment dams. Statistics from the International Commission on Large Dams (ICOLD 1995) show that embankment dam problems and failures are often related to internal erosion in one way or another. The seepage rate depends mainly on the hydraulic conductivity of the core which is strongly dependent upon the core material and the way the material is compacted. In practice, it is impossible to construct a dam without inhomogeneities, as dams are always more or less stratified horizontally as a result of being constructed in horizontal layers. An increased seepage rate increases the rate of material transport and this may lead to erosive leakage. Most cases of erosive leakage or excessive seepage in embankment dams have been interpreted in terms of internal erosion, hydraulic fracturing, or piping (Sherard 1986; Löfquist 1992). However, these interpretations describe only what can be suspected or seen at the dam after the process has been going on for some time. The real origin of the leak is usually difficult to discover or to explain.

To obtain data for describing the condition of dams, in part for safety reasons, dams need to be inspected regularly. Dams are inspected in different ways (e.g., pore-pressure measurements, discharge measurements, temperature–resistivity measurements, radar measurements (Johansson 1997) and self-potential measurements (Triumf and Thunehed 1996)).

Received July 17, 1998. Accepted February 12, 1999.

M. Billstein. Division of Water Resources Engineering, Luleå University of Technology, Se-971 87 Luleå, Sweden.
U. Svensson. Computer-aided Fluid Engineering AB, Norrköping, Sweden.
N. Johansson. Vattenfall Utveckling AB, Älvkarleby, Sweden.

In most branches of engineering, numerical simulation models can be useful complements to more traditional techniques. In embankment engineering, a numerical model can be used to study pressure distributions, water surface profiles, heights of the seepage faces, velocity distributions, and discharges for different flow conditions, both steady and unsteady. However, before extensive use is made of a numerical model, a demonstration that the model can simulate the hydraulics of a dam in a satisfactory way is required. Billstein et al. (1999) developed a well-verified numerical model of steady flow through a simplified embankment dam. Results from the numerical model were compared with analytical solutions and experimental measurements. The experimental part included a Hele-Shaw cell and a bed of packed glass beads. However, the experiments and the numerical model were restricted to homogeneous hydraulic conductivity conditions. To numerically simulate an embankment dam in an accurate way, inhomogeneities have to be taken into account. An inhomogeneity may be a fracture or an impervious layer.

Some numerical simulations and theoretical approaches to inhomogeneities in embankment dams have already been carried out. Greenly and Joy (1996) developed a one-dimensional, finite-element model for high flow velocities in coarse porous media. The model can handle a changing cross-sectional area, which represents an improvement over previous numerical models of non-Darcy flow by McCorquodale (1970) and Hansen (1992). Askew and Thatcher (1984) discussed a method based on a stream-function calculation for a porous dam with an impermeable sheet. Rehbinder and Wörman (1994) presented a generalization of Dupuit's solution for the case of two-dimensional flow around an idealized thin sheet pile in an embankment dam. Martinet (1998) presented the approximate solution of Baiocchi et al. (1973) as a solution for a fractured dam. However, the literature survey shows that no detailed laboratory experiments with flow in inhomogeneous embankment dams are available. This finding led to the conclusion that this work should also include an experimental component. A full account of the experiments can be found in Billstein (1998).

The objective of this work is to extend the numerical model described in Billstein et al. (1999) to incorporate fracture inhomogeneities. Results from the numerical model are compared with those from two laboratory experiments with a fracture, one dealing with flow in a Hele-Shaw cell and one with flow through a bed of packed glass beads.

The study is thus concerned with numerical simulations of two experiments; no attempt will be made to simulate the hydraulics of a "real world" dam. Although this is the ultimate goal, it is believed that it should first be demonstrated that inhomogeneities can be simulated in well-controlled experiments. Applying the model to a real dam is a major undertaking with respect to the specification of the porous media. The present paper will hopefully show that the computational techniques for such an application are available.

Experimental study

Figure 1 shows the basic layout of the experiments. The experiments were designed to minimize as many uncertainties as possible regarding the embankment geometry, flow resistance, and fracture geometry. In both experiments the fluid surface levels upstream and downstream were held constant and the steady flow in the domain in between was studied. A horizontal fracture extending from the upstream boundary to a point within the embankment was used in both experiments. A range of fracture lengths, fracture locations, and boundary conditions was examined. To obtain additional information about the flow in the vicinity of the fracture, a tracer was introduced at the upstream boundary in some of the tests. In the Hele-Shaw cell, the creeping flow between two parallel plates was studied. In the other experiment a bed of packed glass beads provided the flow resistance.

The Hele-Shaw method is based on the analogy between creeping flow and flow through a porous media. This analogy is valid if inertia terms are negligible (Batchelor 1967). The advantage of the method is that it is not necessary to create a porous matrix. The establishment of creeping flow requires the use of a very small space between the parallel plates. A source of error is introduced in the experimental conditions if the space between the plates is comparable to the manufacturing accuracy. However, if glycerine is used as the test fluid (glycerine has a viscosity about 1000 times higher than that of water), the space between the plates can be rather large, i.e., several millimetres, a space which is easy to fabricate and control. Another advantage with a large space is that the capillary rise is negligible. The fracture was created by a local increase of the space between the two parallel plates at a certain level over a certain length (Fig. 1). The thickness of the fracture slot was 5 mm. In the zone with the increased space, the pressure is close to that at the upstream boundary. The tracer was a suspension of nacreous powder in glycerine. The main results from these experiments are the discharge, free surface profile, and height of the seepage face above the tailwater (h_0 in Fig. 1).

The second experiment involved a porous matrix, and water was used as the test fluid. The porous matrix consisted of glass beads of uniform diameter randomly packed between two parallel plates as shown in Fig. 1. A thin net, with negligible flow resistance, at the upstream and downstream boundaries kept the beads in place. Two quite different bead diameters, 0.002 and 0.025 m, were used to vary the Reynolds number from 4 to 1400 (i.e., Forchheimer to turbulent flow conditions; Fand et al. 1987). The Reynolds number is based on the Darcy velocity, the diameter of the spheres, and the kinematic viscosity. The fracture was made out of two parallel plates, spaced apart, and perforated to a porosity of 0.5 to allow the water to enter from all directions. The thickness of the plates was 0.002 m. A thin net kept the fracture free from the beads. The width of the fracture was equal to the width of the porous media, and the thickness of the fracture was 0.01 m. The tracer was a solution of Rhodamine dye. Once the discharge had become steady, the discharge, pressure distribution, free surface profile, and height of the seepage face were measured.

The experimental conditions are summarized in Table 1. The temperature was recorded in each experimental run because the viscosity of glycerine is strongly dependent upon temperature. In the Hele-Shaw experiment, the free surface profile and the height of the seepage face were determined

Fig. 1. Schematic view of the simplified embankment dam in the experimental setup. In both experiments the embankment walls were made of clear acrylic. (*a*) In the Hele-Shaw experiment the flow is between two parallel plates. (*b*) A bed of packed glass beads is used in the porous media experiment.

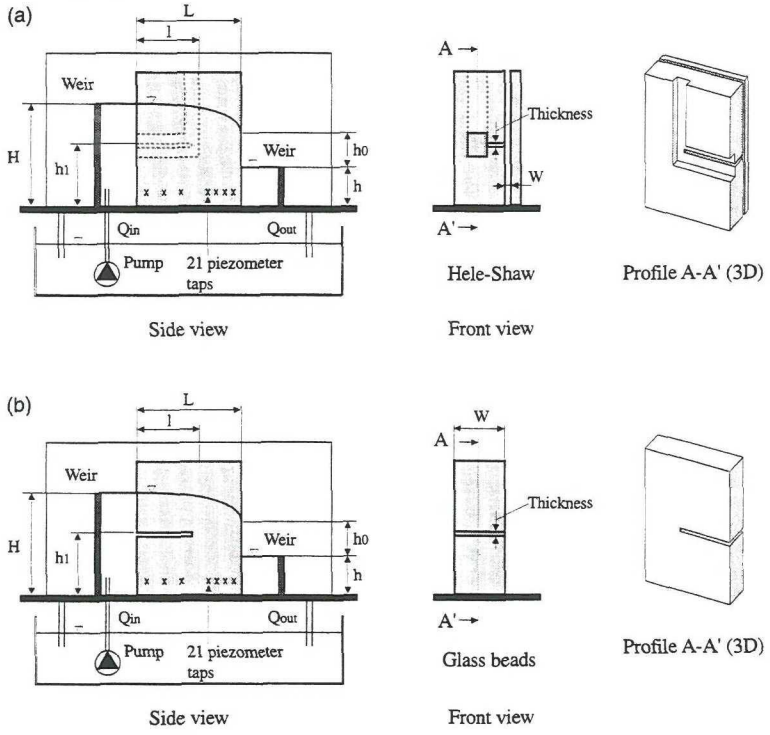

from photographs, and the discharge was measured with a container and a clock. The errors of the discharge measurements were within 2–5% of the measured values. The pressure drop in the fracture was measured by a piezometer in the slot extending to the top of the cell (Fig. 1, profile A–A′).

In the experiment with the porous matrix, the discharge was measured with a 90° triangular weir and the pressure by piezometers at 21 points, located 0.04 m above the bottom of the flume and spaced 0.015 and 0.03 m at the downstream and upstream parts of the dam, respectively. The free water surface was determined from direct observations, taking the capillary rise into account. It was estimated that the capillary rise for a bead diameter of 0.002 m was 0.01 m while it was negligible for a bead diameter of 0.025 m. The height of the seepage face was also determined from direct observations. The errors of the pressure and discharge measurements were less than 1.0% of the measured values.

Numerical simulation of free surface flow through porous media

The numerical simulation model is based on a direct solution of the conservation equations. For an incompressible fluid, these equations are given as

$$[1] \quad \nabla(\rho \boldsymbol{u}) = 0$$

Table 1. Experimental conditions.

L (m)	W (m)	l (m)	h_1 (m)	Bead diameter (m)
		Hele-Shaw cell		
0.300	0.0044	0.20	0.20	—
0.300	0.0043	0.20	0.10	—
0.300	0.0044	0.10	0.20	—
0.300	0.0045	0.10	0.10	—
		Porous media (glass beads)		
0.505	0.132	0.25	0.27	0.002
0.505	0.132	0.25	0.10	0.002
0.500	0.301	0.25	0.21	0.025
0.500	0.301	0.25	0.13	0.025

for conservation of mass, and

$$[2] \quad -\nabla p + \rho \boldsymbol{g} + \boldsymbol{F} = 0$$

for conservation of momentum, where $\boldsymbol{u}$ is the velocity vector, ρ is the density, p is the pressure, $\boldsymbol{g}$ is the gravitational vector, and $\boldsymbol{F}$ is a vector representing frictional forces. ∇ is the vector operator $\partial/\partial x$, $\partial/\partial y$.

The frictional forces in the Hele-Shaw cell are determined from the laminar velocity profile in a slot with smooth walls

(Bear 1972). The wall friction is calculated with respect to the mean velocity in the slot:

$$[3] \qquad \boldsymbol{F} = \left(-\frac{12\mu}{W^2} u, -\frac{12\mu}{W^2} v \right)$$

in which u is the x-component mean velocity, v is the y-component mean velocity, W is the width of the slot, and μ is the dynamic viscosity of the fluid. In the simulations, the kinematic viscosity of the glycerine was set to 9×10^{-4} m^2/s and the density to 1250 kg/m^3.

Billstein et al. (1999) concluded that the frictional forces in the porous medium could be determined using the Forchheimer equation (Forchheimer 1901) with the constants presented by Ergun (1952):

$$[4] \qquad \boldsymbol{F} = \left(-A\frac{(1-n)^2}{n^3}\frac{\mu}{d^2}u - B\frac{(1-n)}{n^3}\frac{\rho}{d}u^2, \; -A\frac{(1-n)^2}{n^3}\frac{\mu}{d^2}v - B\frac{(1-n)}{n^3}\frac{\rho}{d}v^2 \right)$$

in which u is the x-component Darcy velocity, v is the y-component Darcy velocity, A and B are empirical constants, n is the porosity, and d is the sphere diameter. For the empirical constants, Ergun suggested $A = 150$ and $B = 1.75$. More recently, investigators have proposed somewhat higher values. Macdonald et al. (1979) recommended $A = 180$ and $B = 1.8$ and Du Plessis (1994) recommended $A = 207$ and $B = 1.88$. Fand et al. (1987) gave $A = 182$ and $B = 1.92$ for the Forchheimer regime and $A = 225$ and $B = 1.61$ for turbulent flows. With reference to the investigations reported by these authors, the values $A = 200$ and $B = 1.8$ were chosen for the simulations. Preliminary tests also indicated that these values would ensure good agreement with the present experimental data. However, the simulations are not very sensitive to a small change of the constants. If the constants are modified by ±2%, the discharge is changed by ±1%.

To use eq. [4], one must know the value of the porosity. Spheres can be packed in various arrangements. The loosest packing is the cubic arrangement, which has a porosity of 0.4764, and the most dense is the rhombohedral packing, which has a porosity of 0.2595 (Graton and Fraser 1935). The porosity for randomly packed spheres is usually in the range 0.31–0.43 (Kunii and Levenspiel 1969). Crawford and Plumb (1986) found the porosity to be 0.356 for smooth particles, and Kececioglu and Jiang (1994) assumed a value of 0.40 as an average porosity in their experiments. Fand et al. (1987) found the porosity to be in the interval 0.357–0.360. The glass beads used in the present experiment have diameters of 0.002 and 0.025 m with a standard deviation of about 1% of the diameter. Although this variation is small, it may lead to porosities that are somewhat smaller than those for uniform spheres. With reference to the investigations cited and the fact that the spheres were not completely uniform, a porosity of 0.34 for the smaller glass beads was chosen. For the larger spheres, the wall effect must be considered because the ratio d/W (where W is defined in Fig. 1) is large, about 0.1. Hansen (1992) and Dudgeon (1967) have summarized estimates of the wall effect. From their summaries, the average porosity is estimated to be some 5–10 percentage points larger than if the wall effect is negligible. These indications lead to an estimate of 0.41 for the porosity of the larger beads. The porosities as determined from our measurements of the two bead diameters were in the ranges 0.34 ± 0.02 and 0.41 ± 0.02, values that correspond well with the estimates from the literature. However, our measurements were made in the simplest possible manner (filling a container of the same size and shape as the dam with water) and were only intended to add confidence to the estimates from the literature.

A hydrostatic pressure distribution was specified at the upstream and downstream boundaries, whereas the pressure is atmospheric above the free surface.

In the experiments with the Hele-Shaw cell the pressure drop along the fracture was measured to 10–40 Pa, the variation being due to the various experimental conditions. The fracture in the Hele-Shaw cell was simulated by specifying the upstream pressure at the fracture level with a linearly decreasing pressure drop of 10–40 Pa along the fracture.

To numerically simulate a fracture in the experiments with a bed of packed glass beads, a zone of low flow resistance was specified. At the boundary between the fracture and the surrounding porous matrix, a skin resistance was specified. The skin resistance is due to the net around the fracture and is defined as

$$[5] \qquad \Delta p = \rho c_s u$$

where c_s is the skin-resistance coefficient. Determined from resistance measurements, the skin-resistance coefficients were 4.91 and 1.96 m/s for the two nets used for bead diameters 0.002 and 0.025 m, respectively.

The system of equations is solved by the general equation solver PHOENICS (Spalding 1981). PHOENICS is based on a finite-volume formulation of the basic equations and embodies a wide range of coordinate systems (cartesian, body-fitted, cylindrical, etc.) and numerical techniques (higher order schemes, solvers, etc.). Several free surface techniques are also available in the PHOENICS system. An algorithm called the Scalar-Equation-Method (SEM) was used (Spalding and Jun 1988). The algorithm deduces the fluid interface from the solution of a conservation equation for a scalar "fluid marker" variable. To prevent numerical diffusion, the Van Leer scheme is used. SEM is a transient method and, due to an explicit formulation, the Courant criterion places a maximum limit on the time increment for the stability of the solution. To achieve a stable solution, the time increment in the simulations was 0.01 s. In the numerical simulations the grid spacing was set to 0.01 m in both the horizontal and vertical directions. This grid spacing was found to be adequate for grid-independent solutions.

Results

Results from the two experiments are compared with the corresponding numerical solutions and the numerical solution for the homogeneous case, which is called the reference case. Tables 2 and 3 contain all heights of the seepage faces and discharges for the Hele-Shaw cell and the porous media experiments, respectively. Figures 2, 3, and 4 show the free surface profiles and the pressure profiles for the Hele-Shaw cell and the porous media experiments, respectively.

Table 2. Comparison of discharges and heights of the seepage faces as given by the Hele-Shaw experiment and the numerical simulation.

					With fracture						Without fracture	
L (m)	W (m)	H (m)	h (m)	Temp. (°C)	l (m)	h_1 (m)	$h_{0\ exp}$ (m)	$h_{0\ numer}$ (m)	Q_{exp} (mL/s)	Q_{numer} (mL/s)	$h_{0\ numer}$ (m)	Q_{numer} (mL/s)
0.300	0.0044	0.304	0.000	21.7	0.20	0.20	0.179	0.181	59.7	58.2	0.103	37.0
0.300	0.0043	0.303	0.000	22.2	0.20	0.10	0.169	0.163	55.5	62.0	0.103	37.0
0.300	0.0044	0.303	0.000	22.3	0.10	0.20	0.129	0.121	38.3	42.0	0.103	37.0
0.300	0.0045	0.304	0.000	21.7	0.10	0.10	0.127	0.122	41.5	46.7	0.103	37.0
0.300	0.0044	0.304	0.152	22.5	0.20	0.20	0.042	0.042	49.0	46.2	0.012	28.0
0.300	0.0044	0.303	0.151	22.7	0.20	0.10	0.036	0.031	44.8	47.1	0.012	28.0
0.300	0.0044	0.303	0.151	22.0	0.10	0.20	0.020	0.014	29.3	31.9	0.012	28.0
0.300	0.0045	0.303	0.151	22.1	0.10	0.10	0.017	0.013	33.9	34.8	0.012	28.0

Note: Q, discharge. Subscripts: exp, experimentally; numer, numerically.

Table 3. Comparison of discharges and heights of the seepage faces as given by the porous media experiment and the numerical simulation.

							With fracture						Without fracture	
Bead diameter (m)	W (m)	n (%)	L (m)	H (m)	h (m)	Re	l (m)	h_1 (m)	$h_{0\ exp}$ (m)	$h_{0\ numer}$ (m)	Q_{exp} (L/s)	Q_{numer} (L/s)	$h_{0\ numer}$ (m)	Q_{numer} (L/s)
0.002	0.132	34	0.505	0.381	0.015	12	0.25	0.27	0.17	0.13	0.28	0.27	0.10	0.22
0.002	0.132	34	0.505	0.380	0.015	12	0.25	0.10	0.14	0.12	0.28	0.28	0.10	0.22
0.002	0.132	34	0.505	0.380	0.097	10	0.25	0.27	0.09	0.06	0.27	0.26	0.03	0.20
0.002	0.132	34	0.505	0.381	0.097	10	0.25	0.10	0.08	0.06	0.27	0.27	0.03	0.20
0.002	0.132	34	0.505	0.380	0.262	4	0.25	0.27	0.00	0.00	0.16	0.16	0.00	0.12
0.002	0.132	34	0.505	0.380	0.262	4	0.25	0.10	0.00	0.00	0.16	0.16	0.00	0.12
0.025	0.301	41	0.500	0.290	0.042	1400	0.25	0.21	0.08	0.07	5.10	5.20	0.05	4.78
0.025	0.301	41	0.500	0.290	0.042	1400	0.25	0.13	0.09	0.07	5.20	5.28	0.05	4.78
0.025	0.301	41	0.500	0.288	0.121	1100	0.25	0.21	0.02	0.01	4.85	4.90	0.01	4.56
0.025	0.301	41	0.500	0.289	0.122	1100	0.25	0.13	0.03	0.01	4.89	4.96	0.01	4.56
0.025	0.301	41	0.500	0.288	0.264	500	0.25	0.21	0.00	0.00	2.30	2.31	0.00	2.02
0.025	0.301	41	0.500	0.290	0.265	500	0.25	0.13	0.00	0.00	2.30	2.31	0.00	2.02

Note: Q, discharge. Subscripts: exp, experimentally; numer, numerically.

Table 2 and Fig. 2 show that the fracture has a significant influence on the discharge, height of the seepage face, and the free surface profile in the Hele-Shaw cell. The discharge increases 60–70% with a long fracture present but only 10–30% with a short fracture present. Based on the results from some of the tests and the numerical simulations, it is shown that the discharge increases more with a fracture located far away from the free surface profile than with a fracture located close to the free surface profile. The height of the seepage face is strongly dependent upon the length of the fracture. For example, in the case with no tailwater present, a long fracture increases the height of the seepage face approximately 70%, whereas a short fracture increases the height of the seepage face approximately 25%. With a fracture close to the free surface profile, the influence on the free surface profile is higher than with a fracture far away from the free surface profile. With H = 0.304 m and h = 0.0 m, the discharge and height of the seepage face without a fracture are 37 mL/s and 0.103 m, respectively. With a 0.2 m long fracture located at a height h_1 = 0.2 m, the discharge increases to 59.7 mL/s and the height of the seepage face to 0.179 m. The corresponding discharge and height of the seepage face calculated with the numerical model are 58.2 mL/s and 0.181 m, respectively.

Table 3 and Figs. 3 and 4 show that the fracture has a significant influence on the discharge, pressure distribution, height of the seepage face, and free surface profile in the experiment with packed glass beads. The discharge increases 7–35% with a fracture present. With a sphere diameter of 0.002 m, H = 0.381 m, and h = 0.015 m, the discharge and height of the seepage face without a fracture are 0.22 L/s and 0.10 m, respectively. With a 0.25 m long fracture located at h_1 = 0.27 m, the discharge increases to 0.28 L/s and the height of the seepage face to 0.17 m. Corresponding values calculated with the numerical model are 0.27 L/s and 0.13 m, respectively.

The numerical model captures the influence of the fracture and the results are very close to the measured data. However, some minor differences can be found. The predicted surface profiles are systematically some 1–4% higher than the experimental results in the Hele-Shaw cell, an effect enhanced with the long fracture. In the experiments with packed glass beads, the predicted surface profiles are systematically 1–7% lower than the experimental results.

Discussion

The viscosity of glycerine, used in the Hele-Shaw experi-

Fig. 2. Free surface profiles in the Hele-Shaw experiment for different fracture lengths and fracture levels: (*a*) H = 0.304 m, h = 0.0 m, and l = 0.20 m; (*b*) H = 0.304 m, h = 0.0 m, and l = 0.10 m; (*c*) H = 0.304 m, h = 0.151 m, and l = 0.20 m; (*d*) H = 0.304 m, h = 0.151 m, and l = 0.10 m.

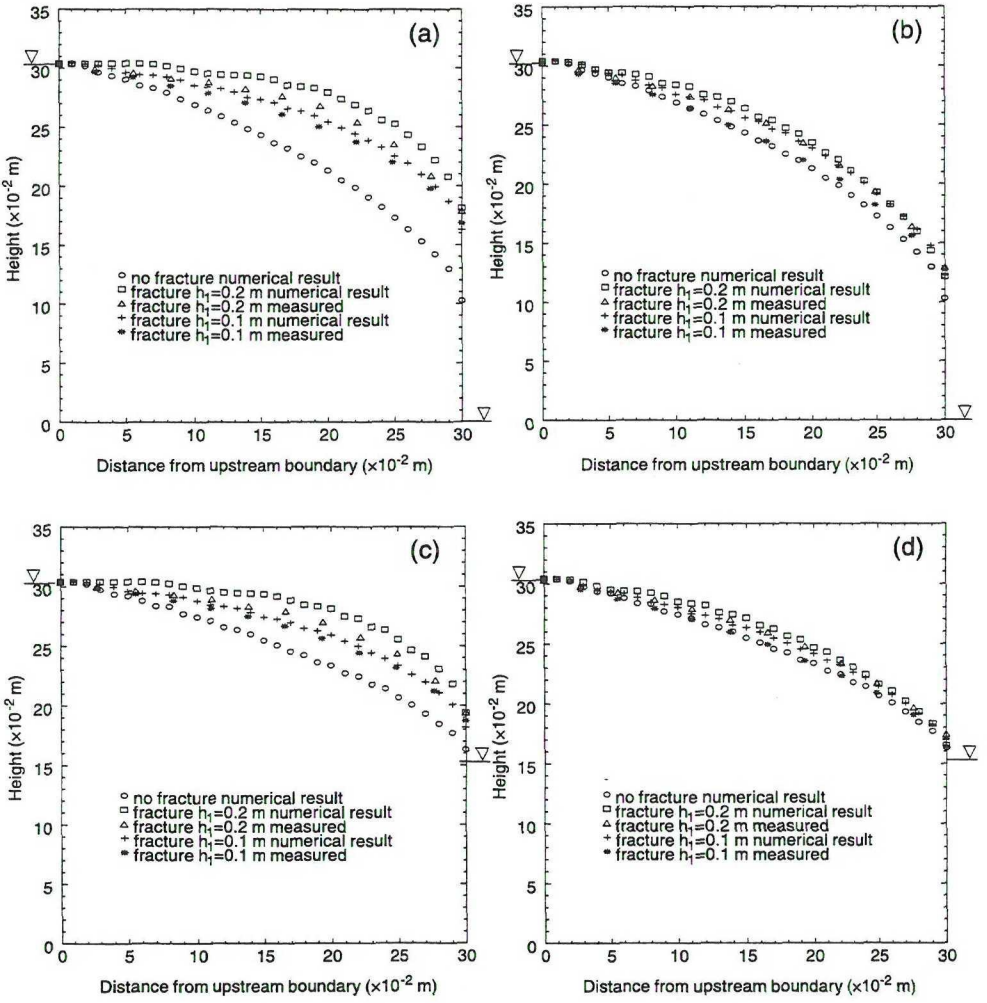

ment, is strongly dependent upon the temperature and water content. The viscosity in the current temperature interval, 21.7–22.7°C, varies between 1.0×10^{-3} and 1.1×10^{-3} m^2/s (Rehbinder 1990). A change of water content by 1% causes a change in viscosity of 100%. The glycerine was recirculated with a pump, and the heat from the pump increased the temperature of the glycerine which then resulted in a decrease in the viscosity of the glycerine. When glycerine is exposed to air it absorbs water and the water content increases, which also reduced the viscosity of the glycerine. A change in viscosity does not influence the free surface profile or the height of the seepage face but it does influence the discharge, which is linearly dependent upon the viscosity. The viscosity used in the simulations (9×10^{-4} m^2/s) was found to give good agreement with the discharges in the experiment and is also in fair agreement with the estimated value from Rehbinder (1990). In the experiments with the tracer, it was shown that the streamlines leaving the fracture did not do so at right angles to the fracture. This finding indicates that the fracture is not an equipotential line, i.e., the potential is not constant along the fracture. A pressure drop of 10–40 Pa was prescribed along the fracture in the numerical model. However, as the numerically calculated free surface profiles are systematically higher than the measured ones, it is possible that the actual pressure drop was somewhat higher than that indicated above. The uncertainty about

Fig. 3. Pressure profiles in the porous media experiment for different fracture levels: (*a*) sphere diameter 0.002 m, H = 0.380 m, h = 0.015 m, and l = 0.25 m; (*b*) sphere diameter 0.002 m, H = 0.380 m, h = 0.097 m, and l = 0.25 m; (*c*) sphere diameter 0.025 m, H = 0.290 m, h = 0.042 m, and l = 0.25 m; (*d*) sphere diameter 0.025 m, H = 0.289 m, h = 0.121 m, and l = 0.25 m.

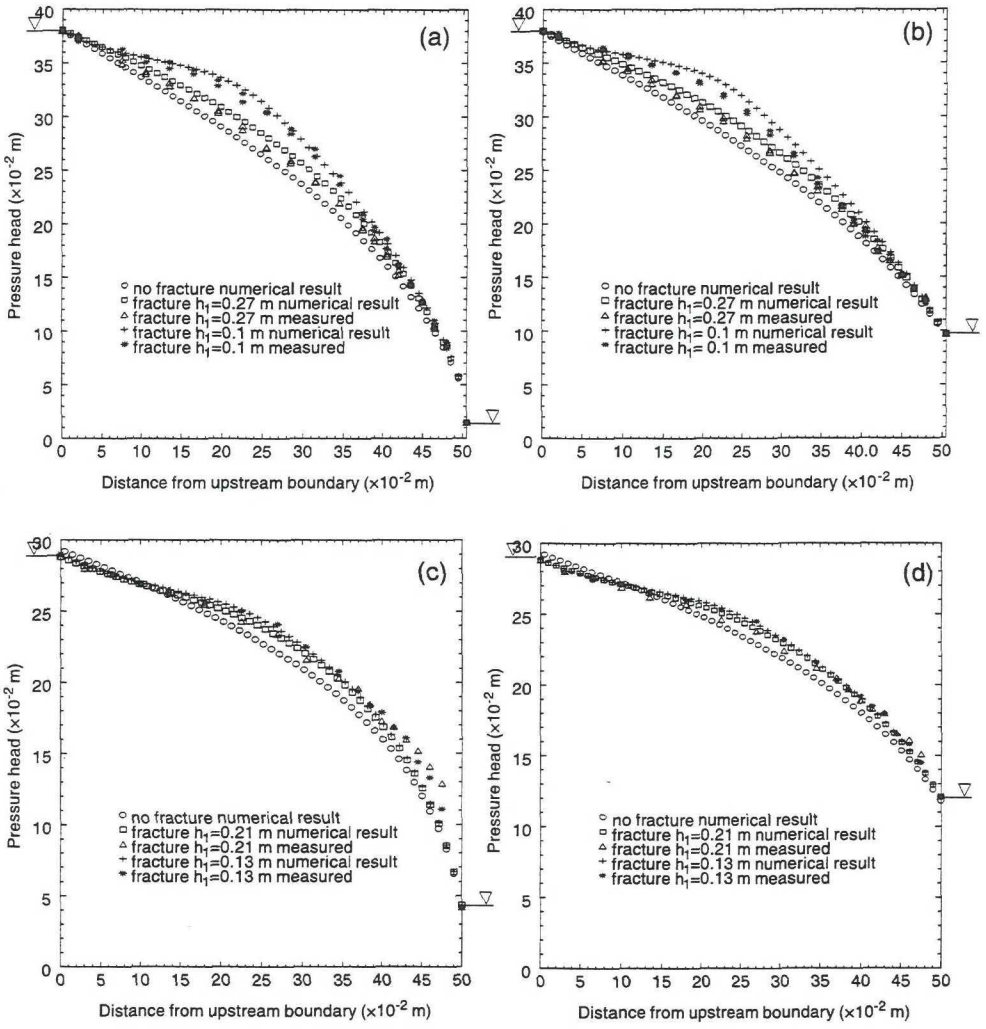

the pressure drop along the fracture may thus explain the higher calculated free surface profile.

In the experiments with the bed of packed glass beads, it is expected that the flow resistance in the fracture is of minor importance and the skin-resistance due to the net of greater importance with respect to the discharge. Small variations in the thickness of the fracture are of no importance with respect to pressure distribution and water surface profile. This finding indicates that the pressure is uniform in the fracture. A possible explanation as to why the measured water surface profiles are systematically higher than the predicted profile is that the resistance due to the net is higher than estimated. The resistance coefficient was determined in a flume experiment with no glass beads. The coefficient may be larger with the glass beads present on one side of the net.

Summary and conclusions

Two new series of experiments for analysing steady flow through simplified embankments are presented, one dealing with a Hele-Shaw cell and one dealing with a bed of packed glass beads. A horizontal fracture, extending from the upstream boundary to a point within the embankment, was used in both experiments. The fracture was shown to have a

Fig. 4. Water surface profiles in the porous media experiment for different fracture levels: (*a*) sphere diameter 0.002 m, H = 0.380 m, h = 0.015 m, and l = 0.25 m; (*b*) sphere diameter 0.002 m, H = 0.380 m, h = 0.097 m, and l = 0.25 m; (*c*) sphere diameter 0.025 m, H = 0.290 m, h = 0.042 m, and l = 0.25 m; (*d*) sphere diameter 0.025 m, H = 0.289 m, h = 0.121 m, and l = 0.25 m.

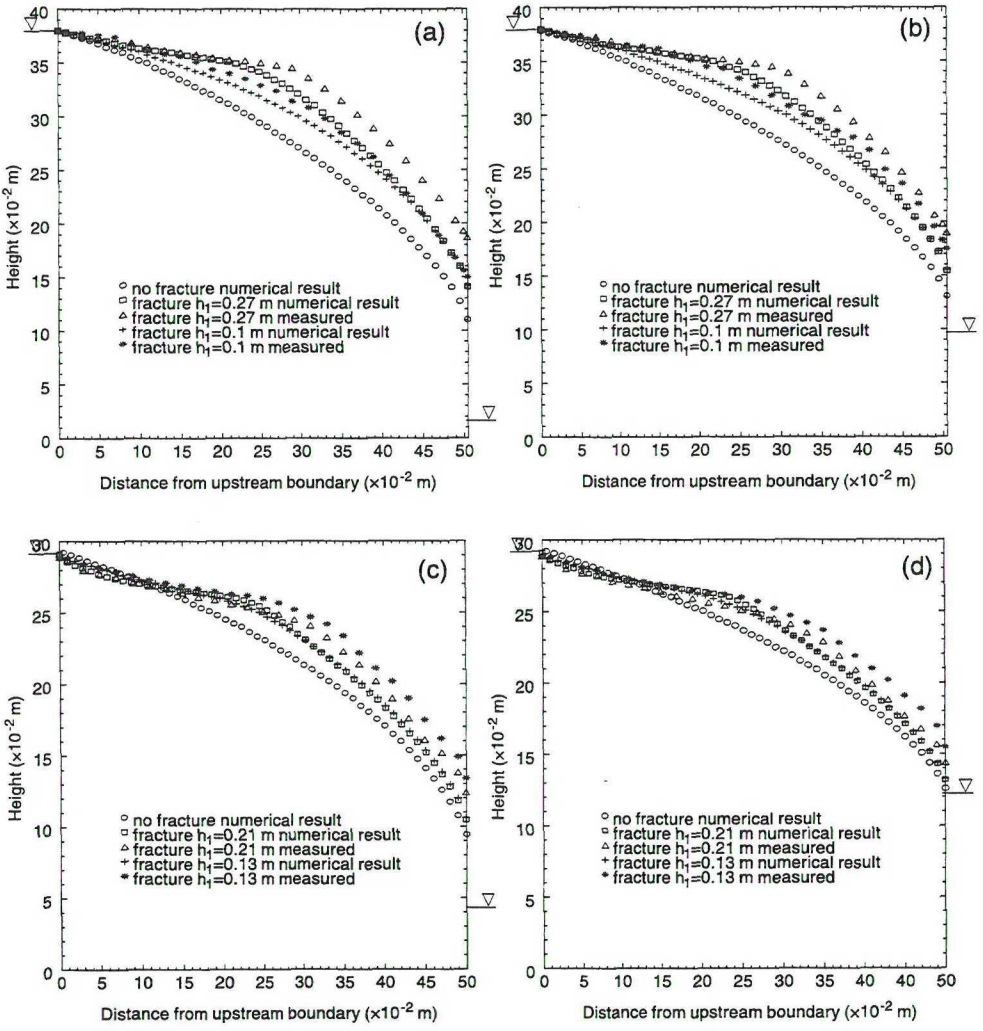

significant influence on the discharge, pressure distribution, height of the seepage face, and free surface profile.

From the experiments it can be concluded that (1) the discharge increases with a fracture present; (2) a fracture far away from the free surface profile increases the discharge more than a fracture close to the free surface profile; (3) the height of the seepage face is strongly dependent upon the length of the fracture; and (4) with a fracture close to the free surface profile, the influence on the free surface profile is higher than that with a fracture far away from the free surface profile.

All of the above listed effects of a fracture were also found in the numerical simulations; in most cases a good quantitative agreement was achieved. It is thus concluded that the numerical model described herein can predict the influence of a fracture in a simplified embankment dam.

References

Askew, S.L., and Thatcher, R.W. 1984. Calculating the discharge from a porous dam. Computers and Fluids, **12**(1): 47–53.

Baiocchi, C., Comincioli, V., Guerrei, L., and Volpi, G. 1973. Free boundary problems in the theory of fluids flow through porous media: a numerical approach. Calcolo, **10**: 1–85.

Batchelor, G.K. 1967. An introduction to fluid dynamics. Cambridge University Press, Cambridge.

Bear, J. 1972. Dynamics of fluid in porous media. American Elsevier Publishing Company, New York.

Billstein, M. 1998. Experimental study of flow through a bed of packed glass beads. *In* Proceedings of the 4th ICOLD International Symposium on New Trends and Guidelines on Dam Safety, Barcelona, Spain, pp. 833–840.

Billstein, M., Svensson, U., and Johansson, N. 1999. Development and validation of a numerical model of flow through embankment dams. Comparisons with experimental data and analytical solutions. Transport in Porous Media, **35**: 395–406.

Crawford, C.W., and Plumb, O.A. 1986. The influence of surface roughness on resistance to flow through packed beds. Journal of Fluids Engineering, **108**: 343–347.

Dudgeon, C.R. 1967. Wall effects in permeameters. Journal of the Hydraulics Division, ASCE, **93**: 137–148.

Du Plessis, J.P. 1994. Analytical quantification of coefficients in the Ergun equation for fluid friction in a packed bed. Transport in Porous Media, **16**(2): 189–207.

Ergun, S. 1952. Fluid flow through packed columns. Chemical Engineering Progress, **48**(2): 89–94.

Fand, R.M., Kim, B.Y.K., Lam, A.C.C., and Phan, R.T. 1987. Resistance to flow of fluids through simple and complex porous media whose matrices are composed of randomly packed spheres. Journal of Fluids Engineering, **109**: 268–274.

Forchheimer, P. 1901. Wasserbeweguing durch Boden. Zeischrift des Vereines Deutscher Ingenieure, **45**: 1782–1788.

Graton, L.C., and Fraser, H.J. 1935. Systematic packing of spheres with particular relation to porosity and permeability. Journal of Geology, **43**: 785–909.

Greenly, B.T., and Joy, D.M. 1996. One-dimensional finite-element model for high flow velocities in porous media. Journal of Geotechnical Engineering, ASCE, **122**: 789–796.

Hansen, D. 1992. The behaviour of flowthrough rockfill dams. Doctoral thesis, University of Ottawa, Ottawa.

ICOLD. 1995. Dam failures statistical analysis. International Commission on Large Dams, Bulletin 99.

Johansson, S. 1997. Seepage monitoring in embankment dams. Doctoral thesis, Royal Institute of Technology, Stockholm, Sweden.

Kececioglu, I., and Jiang Y. 1994. Flow through porous media of packed spheres saturated with water. Journal of Fluids Engineering, **116**: 164–170.

Kunii, D., and Levenspiel, O. 1969. Fluidization engineering. John Wiley & Sons, Inc., New York.

Löfquist, B. 1992. Hydraulic penetration in embankment dams. Ground Engineering, **6**: 40–43.

Macdonald, I.F., El-Sayed, M.S., Mow, K., and Dullien, F.A.L. 1979. Flow through porous media — the Ergun's equation revisited. Industrial & Engineering Chemistry Fundamentals, **18**(3): 199–208.

Martinet, P. 1998. Flow and clogging mechanisms in porous media with applications to dams. Doctoral thesis, Royal Institute of Technology, Stockholm, Sweden.

McCorquodale, J.A. 1970. Variational approach to non-Darcy flow. Journal of the Hydraulics Division, ASCE, **96**(11): 789–796.

Rehbinder, G. 1990. Flow through an embankment dam with a fracture. Theory and experiment, part 1. (Strömning genom en damm med läckvägar. Teori och experiment, etapp 1). Report No. 47, Royal Institute of Technology, Sweden. (In Swedish.)

Rehbinder, G., and Wörman, A. 1994. Deformation of Dupuit's parabola in a dam with sheet piling. Applied Scientific Research, **52**: 173–185.

Sherard, J.L. 1986. Hydraulic fracturing in embankment dams. Journal of Geotechnical Engineering, ASCE, **112**(10): 905–927.

Spalding, D.B. 1981. A general purpose computer program for multi-dimensional one- and two-phase flow. Mathematical Computational Simulations, **8**: 267–276.

Spalding, D.B., and Jun, L. 1988. Numerical simulation of flows with moving interfaces. PCH PhysicoChemical Hydrodynamics, **10**(5/6): 625–637.

Triumf, C.A., and Thunehed, H. 1996. Two years of self-potential measurements on a large dam in northern Sweden. *In* Proceedings of the Stockholm Symposia, Repair and Upgrading of Dams. Royal Institute of Technology, Stockholm, pp. 307–315.

Paper 3

Billstein M., and Svensson U.: A numerical evaluation of air bubbles as a potential explanation to the higher than expected pore pressures in the core of WAC Bennett Dam, (Submitted to *Journal of Hydraulic Research*).

A numerical evaluation of air bubbles as a potential explanation to the higher than expected pore pressures in the core of WAC Bennett Dam

Une évaluation numérique des bulles d'air comme possible explication aux pressions intersticielles supérieures aux prévisions dans le noyau du barrage WAC Bennett Dam

MATS BILLSTEIN, Division of Water Resources Engineering, Luleå University of Technology, Se-971 87 Luleå, Sweden

URBAN SVENSSON, Computer-aided Fluid Engineering AB, Se-602 10 Norrköping, Sweden

ABSTRACT

The objective of this study is to numerically evaluate if the Air Hypothesis is a potential explanation of the unusual pressure behaviour of the core at WAC Bennett Dam. Up to now, the pore pressures have exceeded the expected normal steady state distribution for about 25 years. The Air Hypothesis describes the influence of air bubbles on the pressure distribution in the core. An increased water pressure will compress the air bubbles and increases the amount of air that can go into solution at the upstream side of the core. At the downstream side, the situation is reversed, i.e. the air volume will increase and cause a hydraulic blockage. A one-dimensional numerical model, that is based on relevant conservation laws, physical laws (Darcy's, Boyle's, and Henry's laws), and the relationships between the relative hydraulic conductivity and water saturation level, is able to predict the pressure evolution in both a qualitative and quantitative way. The model is applied to both a hypothetical core and the core of WAC Bennett Dam. Results from a plug flow analysis on the dissolution of the air in the hypothetical core are in fair agreement with the numerical results. Comparisons with pressure measurements from WAC Bennett Dam show that the Air Hypothesis is a potential explanation to the unusual pressure distribution in the core.

RESUME

L'objectif de cette étude est d'évaluer numériquement si l'hypothèse des bulles d'air est une explication possible du comportement inhabituel de la pression dans le noyau du barrage WAC Bennett Dam. Les pressions intersticielles ont été supérieures à la distribution normalement prévisible des pressions stabilisées, depuis plus de 25 ans. L'hypothèse des bulles d'air décrit l'influence des bulles sur la distribution de la pression dans le noyau. L'augmentation de la pression hydraulique comprime les bulles d'air, augmentant la quantité d'air qui peut se dissoudre du coté amont du noyau. Du coté aval, la situation est inversée, le volume d'air augmente et est à l'origine d'un blocage hydraulique. Un modèle unidimensionel, basé sur les lois de conservation, les lois physiques appropriées (Lois de Darcy, Boyle et Henry) et les relations entre la conductivité hydraulique relative et le degré de saturation en eau, peut prédire l'évolution inhabituelle de la pression à la fois d'une manière quantitative et qualitative. Le modèle numérique est appliqué à la fois à un noyau fictif et au noyau du barrage WAC Bennett Dam. Les resultats des analyses de flot sur la dissolution de l'air dans le noyau fictif est en accord avec les résultats numériques. La comparaison avec les mesures de pression dans le barrage WAC Bennett Dam montre que l'hypothèse des bulles d'air est une explication potentielle de la distribution inhabituelle de la pression dans le noyau.

1 Introduction

The unusual behaviour of the core of WAC Bennett Dam was discussed in [1] and [2]. It refers to the condition where, following the reservoir filling, the pore pressures within the core are in excess of the expected normal steady state distribution. Piezometer pressures continued to rise for about four years after the filling, were steady for another two years, and declined after that. Some peak pressure heads were as much as 60 m higher than expected; however, 25 years later, the pressure heads within the core had dropped 55 m from their peak values. A literature search showed that a surprisingly high number of large embankment dams in Quebec (Canada) and Norway exhibit similar behaviour, suggesting that the behaviour in WAC Bennett Dam is not unique. A hypothesis was developed suggesting that a blockage had occurred in the downstream portion of the core or in the transition zone between the core and filter. Many different potential mechanisms were considered during the development of the hypothesis: (1) the influence of dissolved air in the seepage water under high pressures; (2) the influence of consolidation of the core under high vertical stresses; (3) bleeding of fines at the downstream edge of the core under high seepage gradients resulting in a filter blockage; and (4) siltation of the upstream face of the dam leading to reducing core pressures. At this time, it was concluded that the above alternatives could only explain portions of the pressure behaviour, not the whole. Therefore, it was decided to adopt a hypothesis based on generally understood soil mechanics principles as a major criterion.

Even though the phenomenon with higher than expected pore pressures have been addressed by many dam specialists, it is not yet fully understood. In [3], it is suggested that air present in the voids of the dam can be responsible for the higher than expected pore pressures; in this paper we call this the Air Hypothesis. The key feature of the Air Hypothesis is that *trapped air bubbles in the embankment cause a blockage that decreases the hydraulic conductivity and results in a pressure increase.* [4] made a one-dimensional numerical examination of the Air Hypothesis in a hypothetical dam. They concluded that the time required to get steady state conditions was approximately 30 years, which is in accordance with the experiences from WAC Bennett Dam.

Due to each embankment dam's uniqueness with respect to site, geometry, and material properties, and because the behaviour of the dam is probably due to a combination of mechanisms, it is difficult to give general explanations on particular problems. Still, there are always some conditions and processes that have to be considered: (1) initially there is always air present in the voids ([5]); (2) air is compressible (Boyle's law); and (3) the amount of air that can go into solution increases with pressure (Henry's law). These processes are considered in the Air Hypothesis. The basic idea is as follows (Figure 1):

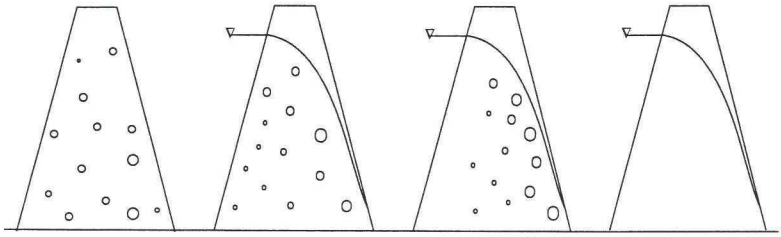

Figure 1. Schematic outline of the problem considered. (a) when the dam is completed the voids are filled with both water and air. (b) an increased pressure will compress the air and increase the amount of air that can go into solution. (c) at the downstream part of the core the pressure decreases, the air will be decompressed and air bubbles will evolve again. (d) eventually, all air bubbles will be dissolved by the water.

- When the dam is completed, the voids are filled with both water and air. The air presumably in form of air bubbles.
- As the filling of the reservoir starts, the pressure on the upstream side, as well as progressively inside the core, increases.
- Two effects can be expected as the pressure increases:
  1. The bubbles will be compressed and hence the volume reduced (a water pressure head of 100 m will cause a reduction in volume of air with a factor of 10).
  2. The air in the upstream part of the core will go into solution, be transported by the water, and evolve again in the downstream part of the core due to a lower ambient pressure.
- The air bubbles in the downstream part of the core cause a blockage for the water and, therefore, a decreasing hydraulic conductivity in the flow direction.
- Eventually, all air bubbles will be dissolved by the water and a fully saturated core will be the final steady state condition.

A full account of the Air Hypothesis can be found in [3] and [4].

The objective of this work is to numerically evaluate if the Air Hypothesis is a potential explanation to the pressure evolution measured in the core of WAC Bennett Dam.

In order to meet the objective, realistic coefficients and physical laws (Darcy's, Boyle's, and Henry's laws) have been implemented in a one-dimensional numerical model. The

model is applied to both a hypothetical core and the core of WAC Bennett Dam. The hypothetical case will be used to discuss in detail the transport mechanisms of the air and for a comparison with a plug flow analysis. Results from pore pressure measurements in the core of WAC Bennett Dam will be used for comparisons with simulated pressure development.

2 The situations considered

2.1 Hypothetical core

The hypothetical core is 100 m long with the same material properties and initial conditions as the core of WAC Bennett Dam. At the upstream boundary, the pressure head is 100 m while atmospheric pressure prevails at the downstream boundary. The upstream pressure head is applied instantaneously and held constant throughout the calculations.

Two situations are considered: one where there is no Darcian flow of air and one where there is a flow of air.

2.2 WAC Bennett Dam

All geometric data, material properties, and piezometer readings regarding WAC Bennett Dam are obtained from [1] and [2]. The geometry of the core and the impoundment are outlined in Figure 2. The reservoir was filled at a rate of 14 m/month over the first eight months; thereafter at a rate of 1.3 m/month until the reservoir was full after three years. In the numerical simulations, it is assumed that the pore pressure head at the upstream boundary of the core is equal to the reservoir level.

Piezometer EP04 is located 150 m below the reservoir level and 135 m downstream from the upstream boundary. The length of the core where EP04 is located is 168 m with a mean water saturation of about 0.64 as placed in the core. No porosity information is available. However, a core of well graded, non-plastic, silty sand and gravel is likely to have a void ratio of 0.23 to 0.35 [6], equivalent to a porosity of 0.22, a value that will be used in the simulations. The water entering the core is assumed to be saturated with air at atmospheric pressure. By considering laboratory and in-situ tests, a representative saturated water conductivity was determined to be $6*10^{-7}$ m/s. However, the approximate range was found to be between $8*10^{-8}$ and $2*10^{-6}$ m/s. The average temperature of the water was assumed to be 4 °C. The pressure condition at the downstream boundary of the core was not recorded; it was only stated that it was probably not atmospheric pressure [7]. Experiences from [8] indicate that a downstream pressure head of 10 m will give a numerically calculated pressure residual, the steady state pressure at that point, in accordance with the measured pressure residual. A pressure head of 10 m is likely when considering that there is a transition zone and a filter in front of a vertical drain where one may expect atmospheric pressure.

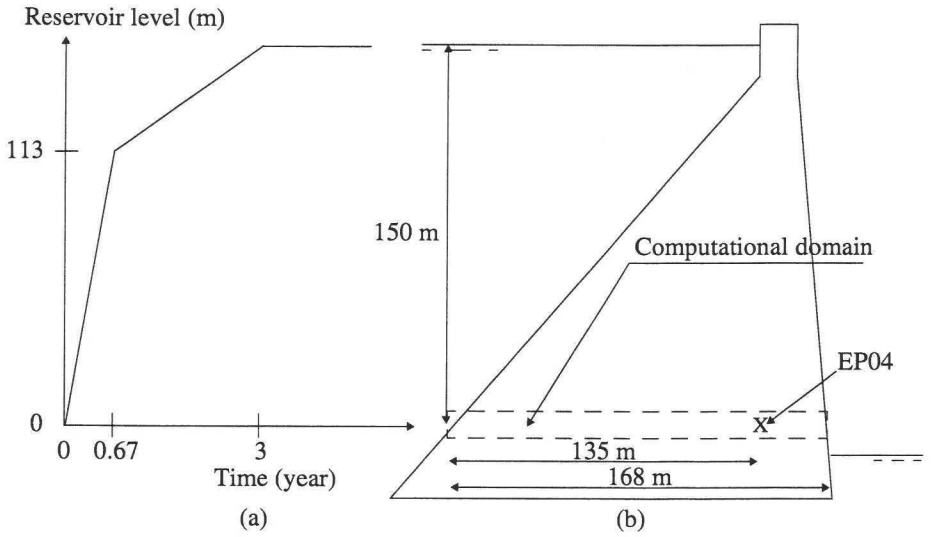

Figure 2. The core of WAC Bennett Dam: (a) reservoir level versus time with reference to the level where piezometer EP04 is located. (b) geometry of the core and the position of piezometer EP04.

3 Mathematical formulation

When the dam is completed and the impoundment starts, the flow through the dam is unsaturated whereas it is saturated when all air is dissolved. To describe fluid flow in both unsaturated and saturated soil, a relationship between the air and water conductivity and the water saturation level, S_r, is needed. A review of existing relationships is summarised in Figure 3; as can be seen all cited relationships are in fair agreement. In this study, the chosen relationship between the relative air conductivity, k_{ar}, and water saturation level is given by:

$$k_{ar} = e^{-(11.34 \cdot S_r^2)} - 1.19 \cdot 10^{-5} \tag{1}$$

The air conductivity, k_a, for $S_r = 0$, continuous air phase, can be determined as [9]:

$$k_a = \frac{k_i g}{\nu} \tag{2}$$

in which k_i is the permeability of the soil material, g gravitational constant, and ν kinematic viscosity of air.

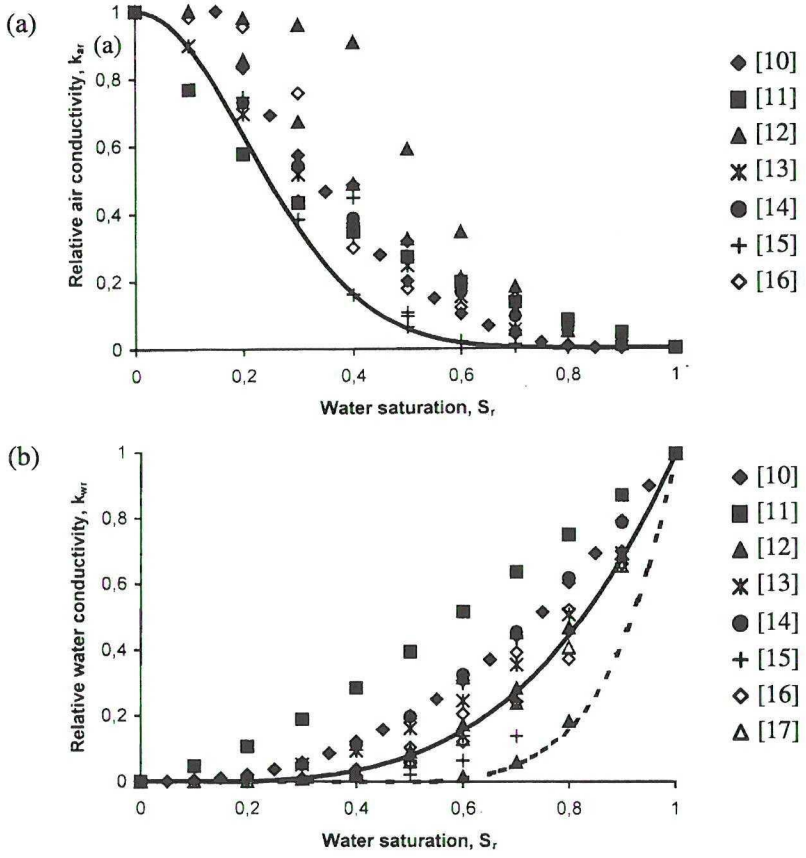

Figure 3. **(a) relationship between relative air conductivity and water saturation level. ——— is the relationship used in this work. (b) relationship between relative water conductivity and water saturation level. ——— is the best fit relationship and ▪ ▬ ▬ ▪ is an alternative relationship used in the application to WAC Bennett Dam. (10) to (17) refers to references.**

The chosen relationship between the relative water conductivity, k_{wr}, and water saturation level is determined via:

$$k_{wr} = S_r^{3.6} - 3.05 \cdot 10^{-3} \tag{3}$$

$$k_{wr} = S_r^{8} - 8.37 \cdot 10^{-3} \tag{4}$$

(3) gives the best fit relationship and (4) a relationship that will be evaluated in the comparison with data from WAC Bennett Dam.

Boyle's law describes the pressure/volume relationship for a perfect gas:

$$p_1 V_1 = p_2 V_2 \tag{5}$$

in which p is pressure in atm, V is volume, and index *1* and *2* represent two states.

Henry's law, given as

$$C_s = Hp \tag{6}$$

states the amount of air that can be dissolved at a given pressure. In (6), C_s is the saturation concentration of air in the water and H is Henry's constant. The higher the pressure, the more air will be dissolved. H is a function of temperature which, at the temperature 4 °C has a value of $34.65*10^{-6}$ kg/(kg*atm) ([18]).

The dissolution of air bubbles into water is a diffusion process:

$$\dot{m} = -K(C_s - C_l) \tag{7}$$

in which $\dot{m}$ is the rate of mass flow, K overall mass transfer coefficient, and C_l is the current concentration of air in the water. K is dependent upon the bubble size and has a value of 4.7 to 9.7 s^{-1} ([19]). The smaller the size, the bigger K; therefore, K was set to 8 s^{-1} in the simulations.

All the physical mechanisms described above are combined with relevant conservation laws expressed in a set of differential equations. In the numerical simulations, the problem is considered to be one-dimensional and transient, the air is assumed to be compressible and water is treated as incompressible. It is thus a two-phase problem.

The momentum equations given as

$$0 = -r_l \frac{\partial p}{\partial x} - r_l \rho_l \phi_l u_l \tag{8}$$

$$0 = -r_g \frac{\partial p}{\partial x} - r_g \rho_g \phi_g u_g \tag{9}$$

are a balance between a pressure gradient and a linear resistance term, i.e. Darcy's law. p is the pressure, r volume fraction, ρ density, ϕ resistance factor, and u Darcy velocity. Index l denotes liquid and g gas. The resistance factor is defined as:

$$\phi = \frac{g}{k} \tag{10}$$

in which g is the gravitational constant and k the air or water conductivity, see Figure 3.

The volume change of the two phases, water and air, are calculated with the following volume fraction equations:

$$\frac{\partial}{\partial t} r_l \rho_l + \frac{\partial}{\partial x} r_l \rho_l u_l = \dot{m} \tag{11}$$

$$\frac{\partial}{\partial t} r_g \rho_g + \frac{\partial}{\partial x} r_g \rho_g u_g = \dot{m} \tag{12}$$

An obvious constraint is that the two phases should fill the whole void space, that is $r_l + r_g = 1$.

The change of current concentration of air in the water can be determined using the liquid phase saturation equation:

$$\frac{\partial}{\partial t} c_l r_l \rho_l + \frac{\partial}{\partial x} c_l r_l \rho_l u_l = \dot{m} \tag{13}$$

The above set of equations was solved using the general equation solver PHOENICS ([20]). PHOENICS is based on a finite-volume formulation of the basic equations and serves for a wide range of coordinate systems (cartesian, body-fitted, cylindrical, etc.) and numerical techniques (high order schemes, solvers, etc.). In the simulations, the grid spacing was 2 m and the time step 72000 s, values found to be adequate for grid independent solutions.

4 Results

In Figures 4 to 8, results from the hypothetical core are given. In Figure 9, the measured and simulated pressure evolution for piezometer EP04 are shown. In all calculations, the air conductivity and hydraulic conductivity used were $6.6*10^{-8}$ and $6*10^{-7}$ m/s, respectively.

4.1 Hypothetical core

Figure 4 shows the time required to remove air from the first seven cells of the core (the core is divided into 10 cells). The computational conditions in this case are: there is no Darcian flow of air and the hydraulic conductivity is constant, i.e. not a function of saturation. These conditions have been chosen in order to be able to compare the results with a plug flow analysis.

When a pressure head of 100 m is applied at the upstream boundary, it takes about 2000 hours to obtain a linear pressure distribution within the core. After 2000 hours, all the air in cells 1 and 2 have been dissolved whereas in cells 3 to 7, 0.80, 0.82, 0.84, 0.86, and 0.88 kg of air remain. The pressure in cells 3 to 7 is 8.26, 7.29, 6.32, 5.36, and 4.39 atm. When the water enters cell 3, saturated with air at atmospheric pressure, some air is dissolved to saturate the water at 8.26 atm. When the water leaves cell 3, it is saturated. In cell 4, the pressure is 7.29 atm with some air evolving so that the water becomes

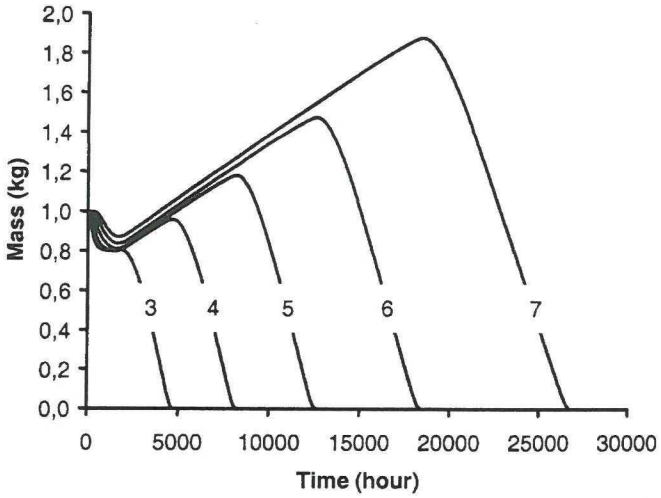

Figure 4. The distribution of air in cells 3 to 7 as function of time for the hypothetical core with no Darcian flow of air and a constant hydraulic conductivity, i.e. not a function of saturation. The upstream and downstream pressure head is 100 m and 0 m, respectively. The numbers in the figure are referring to cell numbers.

saturated at the current pressure. The process is repeated in the following cells; oversaturated water enters the cells with some air evolving so that the water becomes saturated at current pressures. The same amount of air will evolve in each cell due to the linear pressure distribution. After 4800 hours, the 0.80 kg air from cell 3 is removed and evenly distributed in cells 4 to 10 with 0.11 kg in each. Hence, after 4800 hours, the amount of air in cells 4 to 7 has increased to 0.93, 0.95, 0.97, and 0.99 kg. When there is no air left in cell 3 the same process will be repeated in cell 4 and so on. At the time when there is no air left in cell 3, the water is saturated with air at 8.26 atm. The incoming water to cell 3 is saturated with air at atmospheric pressure (1 atm); therefore, it will be a mixing with the water saturated at 8.26 atm until it is saturated at atmospheric pressure.

From a plug flow analysis, the following estimates can be made. One kg water in cell 3 can dissolve $34.65*10^{-6}(8.26 - 1.0)$ kg air, i.e. to dissolve 0.80 kg air, 3200 kg water is needed. With a hydraulic gradient of 1 and a hydraulic conductivity of $6*10^{-7}$ m/s, the mass flow of water is $6*10^{-4}$ kg/s. 3200 kg water then corresponds to a dissolution time of 1500 hours. That is, 2000 + 1500 = 3500 hours is the time required to remove the air from cell 3 if we neglect the mixing process in cell 2. An estimate of the time required to dilute the saturated water in cell 2 at current pressure to saturation at atmospheric pressure, is that the time is equal to the exchange time of water in cell 2. The exchange time is $2200/6*10^{-4}$ = 1000 hours where 2200 is the mass of water in cell 2. Thus, the total time required to remove the air from cell 3 is 4500 hours. This is in accordance with the numerical results.

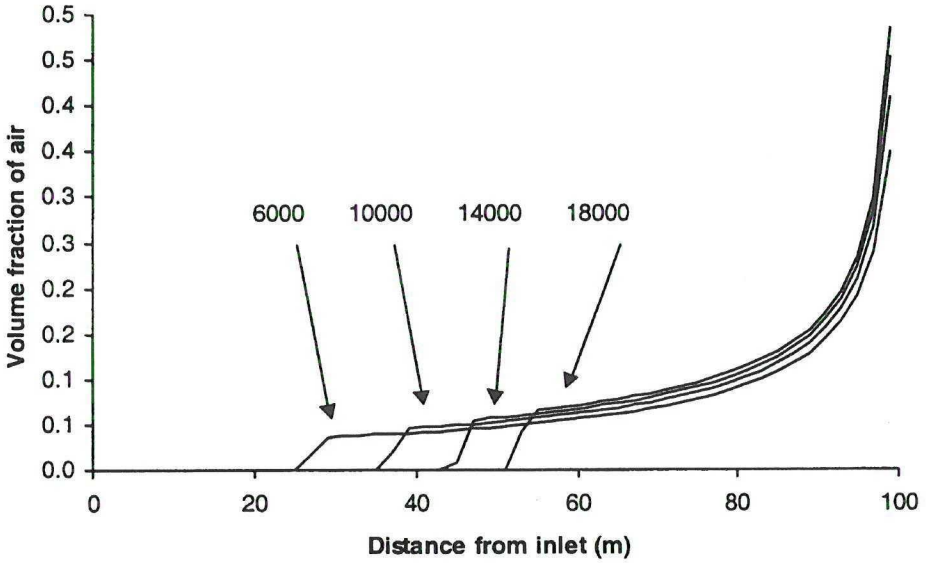

Figure 5. The change in the volume fraction of air at different distances and times for the hypothetical core. In the simulations it is assumed that there is no Darcian flow of air. The numbers in the figure give the time in hours

The computational conditions for the results in Figures 5 and 6 are: there is no Darcian flow of air, the hydraulic conductivity is a function of the water saturation level, and the core is divided into 20 cells. After 6000 hours, the air has been removed from the first 25 m of the core. By comparing the amount of air left after 6000, 10000, 14000, and 18000 hours, it is evident that there is no loss of air, but only a redistribution of air in the core. This is to be expected when the downstream boundary is at atmospheric pressure and the incoming water is saturated with air at atmospheric pressure. The increased amount of air in the downstream part of the core decreases the hydraulic conductivity in the flow direction resulting in an increased pressure in the core.

Figures 7 and 8 show the effects of adding the Darcian flow of air, with air conductivity as a function of the water saturation level. The effect of the Darcian air flow can be seen by comparing the volume fraction of air in the core at a certain distance from the inlet. After 18000 hours and 80 m from the inlet, the volume fraction of air with and without Darcian air flow is 0.14 and 0.11, respectively. When there is a Darcian flow of air, there will be no accumulation of air at the downstream boundary and, therefore, the pressure increase will be less than without flow of air.

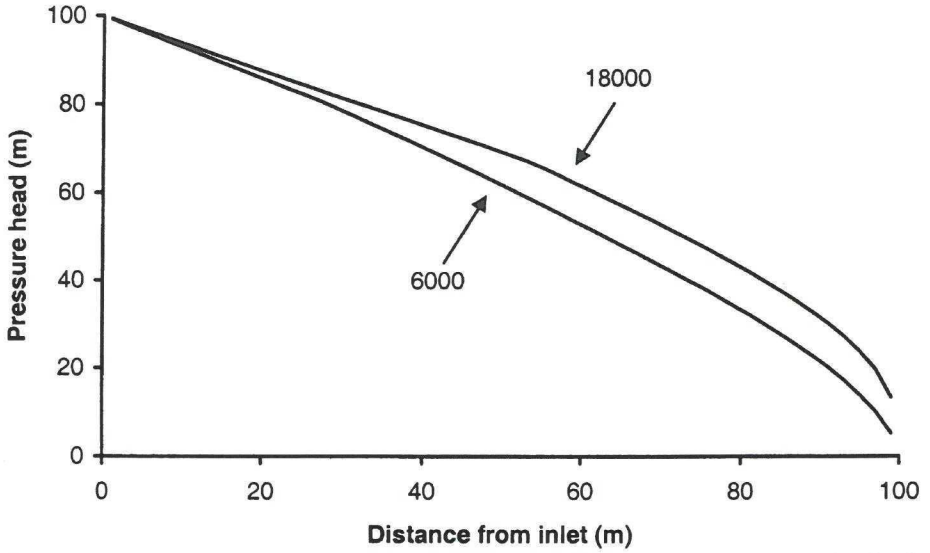

Figure 6. The change in pressure head at different distances and times for the hypothetical core. In the simulations it is assumed that there is no Darcian flow of air. The numbers in the figure give the time in hours

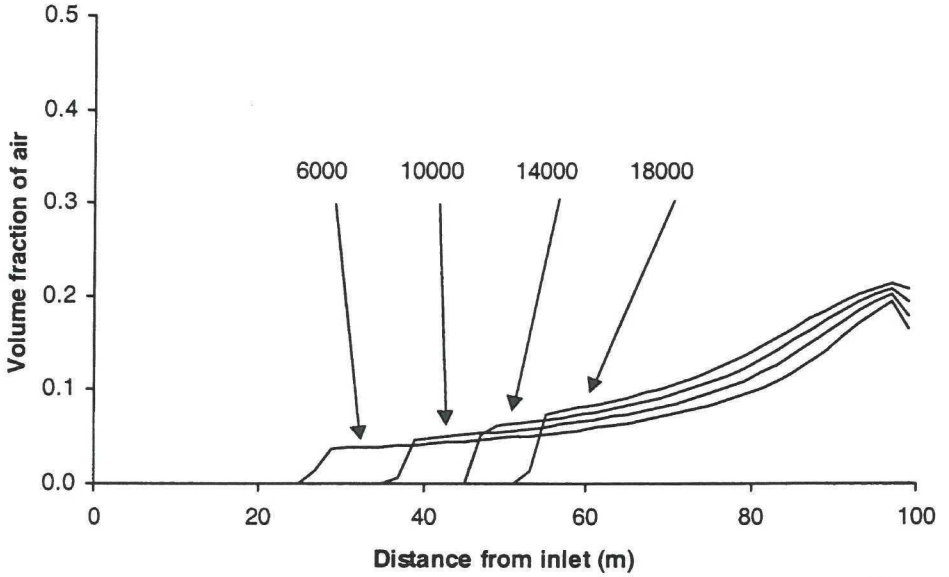

Figure 7. The change in the volume fraction of air at different distances and times for the hypothetical core. In the simulations it is assumed that there is a Darcian flow of air. The numbers in the figure give the time in hours

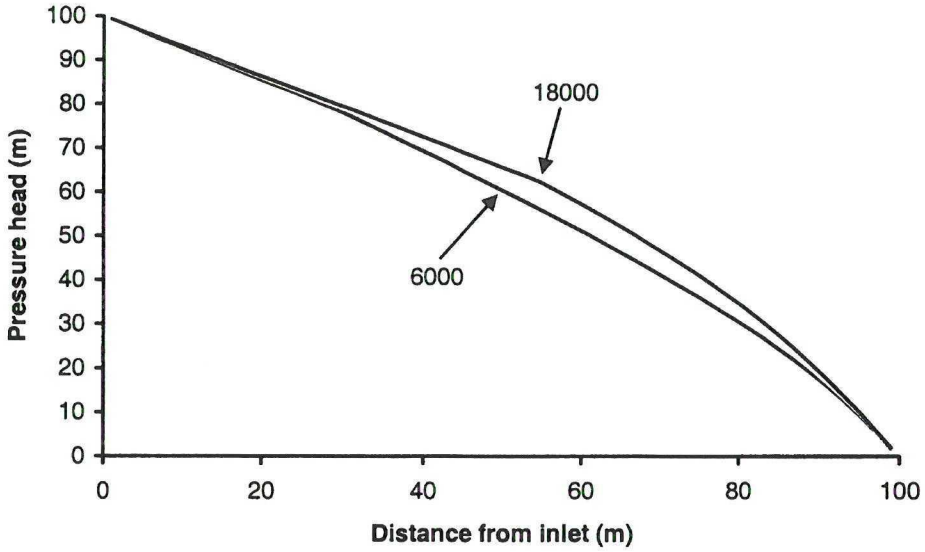

Figure 8. **The change in pressure head at different distances and times for the hypothetical core. In the simulations it is assumed that there is a Darcian flow of air. The numbers in the figure give the time in hours**

4.2 WAC Bennett Dam

Figure 9 (a) shows the measured and numerically calculated pressure evolution in the core of WAC Bennett Dam. The simulation assumes a Darcian flow of air and conductivities that are a function of saturation. The calculated pressures continue to rise for about five years after the filling and decline after that, a behaviour similar to what was found in WAC Bennett Dam. The measured peak pressure head is 98 m after nine years and the simulated is 65 m after seven years. The measurements indicate a pressure residual of 35 to 40 m after 25 to 30 years whereas the calculated pressure residual is 38 m after 12 years, i.e. when all air bubbles are dissolved and steady state conditions are approached.

The result in Figure 9 (b) is based on the same computational conditions as the simulation shown in Figure 9 (a) except for the relationship hydraulic conductivity - water saturation level. In this case, the alternative relationship, see Figure 3, is chosen. The changed relationship resulted in an increased peak pressure head, 90 m after eight years, and all air bubbles dissolved after 13 years.

Figure 9 (c) is based on the same situation as in Figure 9 (b), but with no Darcian flow of air. In this case, the peak pressure head is 104 m after 12 years and steady state conditions are obtained after 14 years. The two pressure distributions are too similar to evaluate whether Darcian flow of air is significant or not.

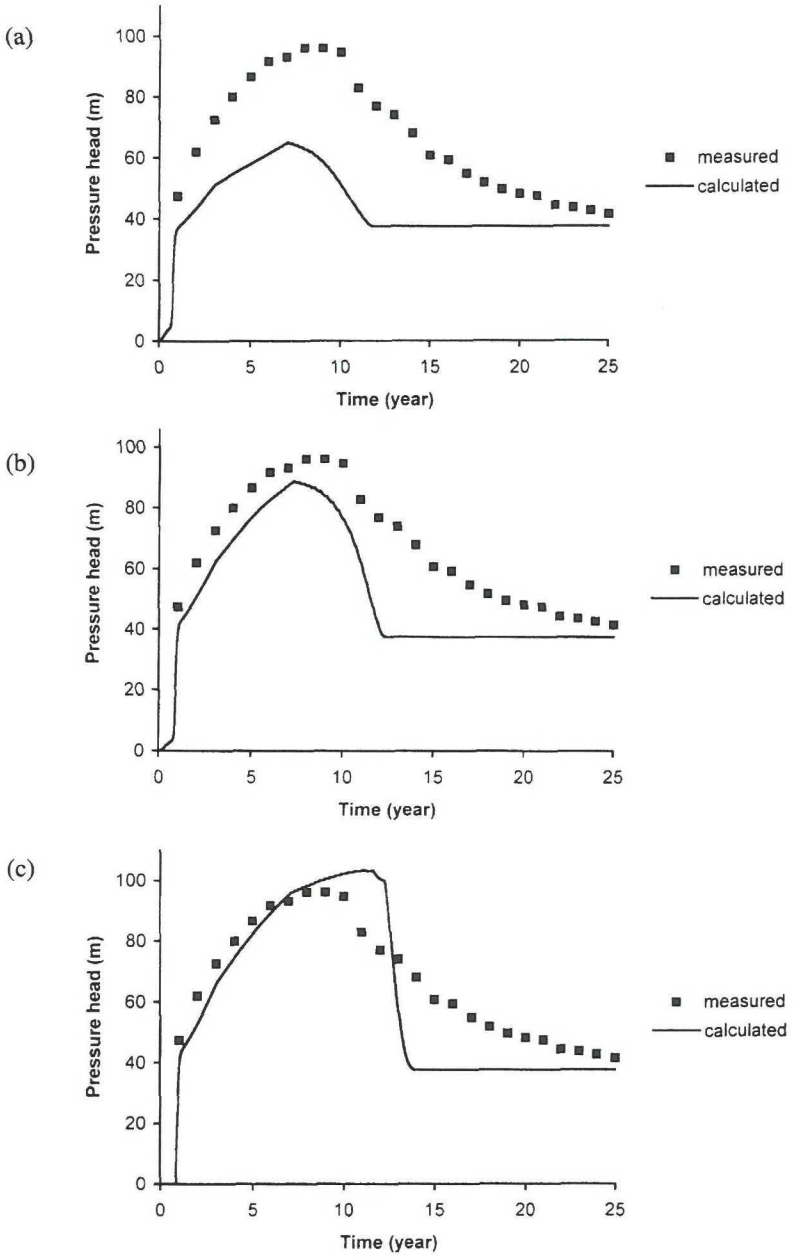

Figure 9. **Piezometer EP04: (a) measured and calculated pressure evolution; (b) measured and calculated pressure evolution where the alternative relationship hydraulic conductivity - water saturation level is used, see Figure 3; (c) measured and calculated pressure evolution where the alternative relationship hydraulic conductivity - water saturation level is used and no Darcian flow of air.**

5 Discussion

The results indicate that the mathematical model presented can simulate the effect of air bubbles on the pressure distribution in an embankment dam. The model is based on relevant conservation principles and physical laws (Darcy's, Boyle's, and Henry's law), but less fundamental assumptions are still needed. In order to put the simulation in perspective, the more important of these will now be listed and discussed.

- One-dimensional simulation:

  A vertical transport of air bubbles due to buoyancy can be expected. However, the one-dimensional assumption is reasonable because the amount of air bubbles entering and leaving the core remains the same even though the bubbles leave the core a little bit downstream from the entering point, i.e. there is no net flow of air in the vertical direction. However, to be able to consider a realistic cross section and the water surface profile, two dimensions are necessary.

- Hydraulic conductivity - water saturation level relationships:

  The relationship between the relative water conductivity and water saturation level is uncertain; the sensitivity is demonstrated in Figures 9 (a) and (b). The relationship between the relative air conductivity and water saturation level used in this work is in fair agreement with a number of experimental results. However, the relationship must still be regarded as uncertain. In the further development of the model, an increased knowledge concerning the conductivity data is certainly one of the key elements.

- The overall mass transfer coefficient, K:

  The value of K used in the simulation is somewhat uncertain, but this is not crucial as the dissolution process is fast in comparison with the time scale of the problem considered. There is hence always time for an equilibrium to be established.

It should also be pointed out that the input data for the WAC Bennett Dam simulation are incomplete. The porosity, temperature, level of air saturation of the water entering the core and the pressure conditions on the upstream and downstream boundary are not known, but only assumed.

6 Conclusions

From the comparisons between measured and simulated pressure evolution, it can be concluded that the Air Hypothesis is a potential explanation to the unexpected behaviour of the core at WAC Bennett Dam.

A one-dimensional numerical model based on basic conservation principles, relevant physical laws (Darcy's, Boyle's, and Henry's laws), and the relationships between the relative conductivity and water saturation level, is able to predict the pressure evolution in both a qualitative and quantitative way. From the simulations it cannot be stated whether Darcian flow of air is significant or not.

In the further development of the numerical model, experiments and field measurements, it is suggested that the following points are considered: (1) the saturated water conductivity of the core; (2) the pressure at the downstream boundary of the core; (3) the relationship between the relative air and water conductivity and water saturation level; (4) the amount of dissolved air in the incoming water; and (5) the two- and three-dimensional situation.

Notations

$1, 2$ indices for a state

C_s saturation concentration of air in water

C_l current concentration of air in water

g gravitational constant

g index for gas

H Henry's constant

K overall mass transfer coefficient

k conductivity

k_a air conductivity

k_{ar} relative air conductivity

k_i permeability of soil material

k_{wr} relative hydraulic conductivity

l index for liquid

$\dot{m}$ rate of mass flow

p pressure

r volume fraction

S_r water saturation level

t time

u Darcy velocity

V volume

x horizontal distance

ϕ resistance factor

ν kinematic viscosity of air

ρ density

Paper 4

Billstein M., and Svensson U.: 2000, Air bubbles - a potential explanation of the unusual pressure behaviour of the core at WAC Bennett Dam, In: *Proc. ICOLD's 20th Congress*, Beijing, Q.78-R.26, 369 - 384.

COMMISSION INTERNATIONALE
DES GRANDS BARRAGES

VINGTIÈME CONGRÈS
DES GRANDS BARRAGES
Beijing, 2000

AIR BUBBLES - A POTENTIAL EXPLANATION OF THE UNUSUAL PRESSURE BEHAVIOUR OF THE CORE AT WAC BENNETT DAM (*)

Mats BILLSTEIN
Division of Water Resources Engineering,
Luleå University of Technology,

Urban SVENSSON
Computer-Aided Fluid Engineering AB,

SWEDEN

1. INTRODUCTION

The unusual behaviour of the core at WAC Bennett Dam was discussed in [1] and [2]. It refers to the condition where, following the reservoir filling, the pore pressures within the core are in excess of expected normal steady state distribution. Piezometer pressures continued to rise for about 4 years after the filling, were steady for another 2 years and declined after that. In 1992, some of the pressure heads within the core had dropped 55 m from their peak values, nothing indicating that these pressure readings are steady state conditions. A search showed that a surprising number of large embankment dams in Quebec (Canada) and Norway exhibit similar behaviour, suggesting that the behaviour in WAC Bennett Dam is not unique. A hypothesis was developed which suggests that a blockage had occurred in the downstream portion of the core or in the transition. Many different potential mechanisms were considered during the development of the hypothesis: (1) the influence of dissolved air in the seepage water under high pressures; (2) the influence of consolidation of the core under high vertical stresses; (3) bleeding of fines at the downstream edge of the core under high seepage gradients resulting in a filter blockage and (4) siltation of the upstream face of the dam leading to reducing core pressures. It was decided to

(*) *Des bulles d'air - une explication possible de l'évolution inhabituelle des pressions dans le noyau du barrage WAC Bennett.*

adopt a hypothesis based on generally understood soil mechanics principles as a major criterion.

Even though the phenomenon with higher than expected pore pressures have been addressed by many dam specialists, it is not yet fully understood. In [3] it is suggested that air present in the voids of the dam can be responsible for the higher than expected pore pressures, in this paper we call this the Air Hypothesis. The key feature of the Air Hypothesis is : *air bubbles trapped in the embankment cause a hydraulic blockage that decreases the hydraulic conductivity, with a pressure increase as a result.* [4] made a one-dimensional numerical examination of the Air Hypothesis in a hypothetical dam. They concluded that the time required to get steady state conditions was approximately 30 years, which is in accordance with the experiences from WAC Bennett Dam.

Because each embankment dam is unique with respect to site, geometry and material properties and the behaviour of the dam is probably a combination of mechanisms, it is difficult to give general explanations on particular problems. Still, there are always some mechanisms that have to be considered: (1) initially there is always air present in the voids ([5]); (2) air is compressible (Boyle's law) and (3) the amount of air that can go into solution increases with pressure (Henry's law). These mechanisms are considered in the Air Hypothesis and the basic idea is as follows (Fig. 1) :

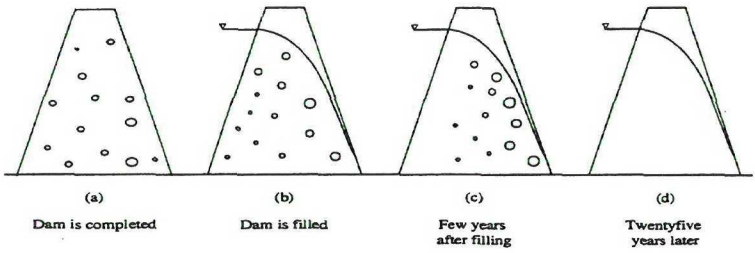

Fig. 1
Schematic outline of the problem considered
Description schématique du problème considéré

(a) When the dam is completed, the voids are filled with both water and air

(a) *Quand le barrage est terminé, le volume des vides est rempli à la fois d'eau et d'air*

(b) An increased pressure will compress the air and increase the amount of air that can go into solution

(b) *Une augmentation de la pression comprime l'air et augmente la quantité d'air qui peut se dissoudre*

(c) The small bubbles may move through the pores but, as they approach the downstream part, the pressure decreases, the air will be decompressed and air bubbles will evolve again

(c) *Les petites bulles peuvent être transportées à travers les pores mais, quand elles s'approchent de l'aval, la pression diminue, l'air est décomprimé et les bulles d'air se reforment*

(d) Eventually all air will be dissolved by the water

(d) *Éventuellement, tout l'air se dissout dans l'eau*

* When the dam is completed, the voids are filled with both water and air. The air presumably in form of air bubbles.

* As the filling of the reservoir starts, the pressure on the upstream side, and progressively also inside the core, increases.

* Two effects can be expected to move the air downstream as the pressure increases :

    1. The bubbles will be compressed and the volume will be reduced (a water pressure head of 100 m will cause a reduction in volume with a factor 10). The small bubbles may then move through the pores. However, as they approach the downstream part of the core, with atmospheric pressure, the size of the bubbles increases and they get trapped again.

    2. The air in the upstream part of the core will go into solution, be transported by the water and evolve again in the downstream part of the core due to a lower ambient pressure.

* The air bubbles in the downstream part of the core cause a blockage for the water and hence a decreasing hydraulic conductivity in the flow direction.

* Eventually all air bubbles will be dissolved by the water and a fully saturated core will be the final steady state condition.

A full account of the Air Hypothesis can be found in [3, 4 and 6].

The objective of this work is to numerically evaluate if the Air Hypothesis is a potential explanation to the pressure evolution measured in the core at WAC Bennett Dam.

In order to meet the objective, realistic coefficients and physical laws (Darcy's, Boyle's and Henry's laws) have been implemented in a one-dimensional numerical model. Dimensions and material properties from the core at WAC Bennett Dam have been used. Measurements of the pressure evolution in two points at different levels will be used for comparison with results from the simulations.

2. THE SITUATION CONSIDERED

When the dam is completed and the impoundment starts, the flow through the dam is unsaturated whereas it is saturated when all air is dissolved. To describe fluid flow in both unsaturated and saturated soil, a relationship between the air and water conductivity and the water saturation level, S_r, is needed. A

review of existing relationships is summarised in Fig. 2 and 3. All relationships are in fair agreement and the chosen relationships for this study are taken as an average of cited studies.

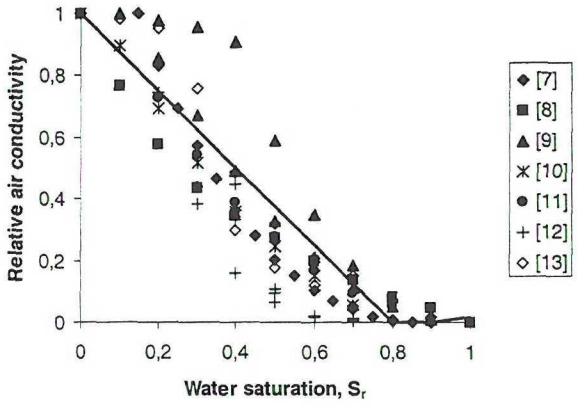

Fig. 2
Relationships between relative air conductivity and water saturation level
[7] to [13] refer to the references. —— is the relationship used in this work
Relations entre la conductibilité relative pour l'air et le degré de saturation en eau
[7] à [13] correspondent aux références. —— est la relation utilisée dans cette étude

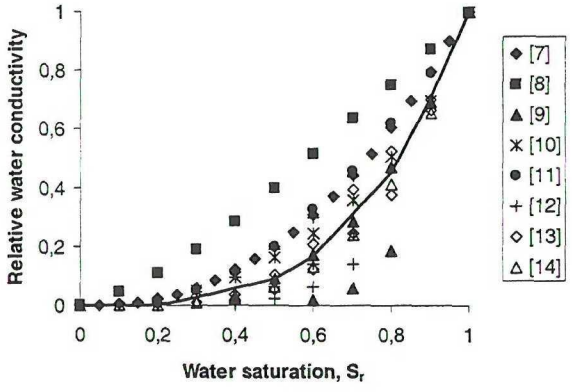

Fig. 3
Relationships between relative water conductivity and water saturation level
[7] to [14] refer to the references. —— is the relationship used in this work
Relations entre la conductibilité relative pour l'eau et le degré de saturation en eau
[7] à [14] correspondent aux références. —— est la relation utilisée dans cette étude

The air conductivity, k_a, for $S_r = 0$, continuous air phase, can be determined via Equation (1) :

$$k_a = \frac{k_i g}{\nu}, \tag{1}$$

in which k_i is the permeability of the soil material, g gravitational constant and ν kinematic viscosity of air. For S_r greater than 0.99, it is assumed that only very small bubbles are present and that the air bubbles and water have the same velocity.

Boyle's law given as Equation (2) describes the pressure/size relationship for a perfect gas :

$$p_1 V_1 = p_2 V_2, \tag{2}$$

in which p is pressure, V is volume and index *1* and *2* represent two states, respectively.

Henry's law, given as

$$C_s = Hp, \tag{3}$$

states the amount of air that can be dissolved at a given pressure, where C_s is the saturation concentration of air in the water and H is Henry's constant. H is a function of temperature which, at the temperature 4 °C, imply $H = 34.65*10^{-6}$ kg/(kg*atm) ([15]). The temperature, as an average, is assumed to be 4 °C.

The dissolution of air bubbles into the water is a diffusion process, Equation (4) :

$$\dot{m} = -K(C_s - C_l), \tag{4}$$

in which $\dot{m}$ is the rate of mass flow, K overall mass transfer coefficient and C_l current concentration of air in the water. K is dependent upon the bubble size and is in the range 4.7 to 9.7 s^{-1} ([16]), the smaller size the bigger K. K was set to 8 s^{-1} in the simulations.

All geometric data, material properties and piezometer readings are obtained from [1] and [2]. The geometry of the core and the impoundment is outlined in Fig. 4. The reservoir was filled at a rate of 14 m/month over the first 8 months, thereafter at a rate of 1.3 m/month until the reservoir was full after 3 years. In the numerical simulations it is assumed that the pore pressure at

the upstream boundary of the core is equal to the reservoir level, which is held constant throughout the calculations.

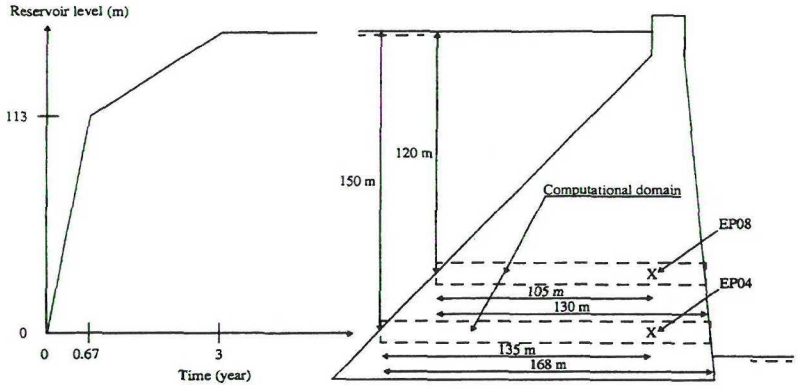

Fig. 4
The geometry of WAC Bennett Dam and the location of EP04 and EP08 (right) - The reservoir filling with reference to EP04 (left)
Géométrie du barrage WAC Bennett et emplacement de EP04 et EP08 (à droite) - Remplissage du réservoir avec la référence à EP04 (à gauche)

Piezometers EP04 and EP08 are located 150 m and 120 m below the reservoir level, and 135 m and 105 m downstream the upstream boundary, respectively. The length of the core where EP04 and EP08 are located is 168 m and 130 m, respectively. The core had a mean water saturation of about 0.64 as placed. There is no information about the porosity available, therefore the porosity is assumed to be 0.22 throughout the core. By considering laboratory and in-situ tests, a representative saturated water conductivity was determined to $6*10^{-7}$ m/s. However, the approximate range was found to be $8*10^{-8}$ to $2*10^{-6}$ m/s. The downstream boundary of the core is assumed to be at atmospheric pressure.

3. MATHEMATICAL FORMULATION

All the physical mechanisms described above can be summarised in a set of differential equations. In the numerical simulations the problem is considered as one-dimensional and transient, air will be assumed compressible while water will be treated as incompressible. It is thus a two phase problem.

The momentum equations given as :

$$0 = -r_l \frac{\partial p}{\partial x} - r_l \rho_l \phi_l u_l , \qquad (5)$$

$$0 = -r_g \frac{\partial p}{\partial x} - r_g \rho_g \phi_g u_g , \tag{6}$$

are a balance between a pressure gradient and a linear resistance term, i.e. Darcy's law. p is the pressure, r volume fraction, ρ density, ϕ resistance factor and u Darcy velocity. Index l denote liquid and g gas. The soil fraction is not included in Darcy's law, though it is incorporated in the resistance factor defined as :

$$\phi = \frac{g}{k} , \tag{7}$$

in which g is the gravitational constant and k the air or water conductivity, see Fig. 2 and 3.

The volume change of the two phases, water and air, are calculated with the volume fraction equations :

$$\frac{\partial}{\partial t} r_l \rho_l + \frac{\partial}{\partial x} r_l \rho_l u_l = \dot{m}_{lg} , \tag{8}$$

$$\frac{\partial}{\partial t} r_g \rho_g + \frac{\partial}{\partial x} r_g \rho_g u_g = \dot{m}_{gl} , \tag{9}$$

in which $\dot{m}$ is the mass exchange between the phases. An obvious constraint is that the two phases should fill the whole space, that is $r_l + r_g = 1$.

The change of current concentration of air in the water can be determined using the liquid phase saturation equation :

$$\frac{\partial}{\partial t} c_l r_l \rho_l + \frac{\partial}{\partial x} c_l r_l \rho_l u_l = \dot{m}_{c_l} , \tag{10}$$

in which $\dot{m}_{c_l}$ is the transfer rate through the liquid/gas interface.

In Equations (8) to (10) the first term represents the change over time, the second convection and the third is the production (source) or consumption (sink) rate. The sink/source equation given as :

$$\dot{m}_{c_l} = \dot{m}_{gl} = -K(C_s - C_l) , \tag{11}$$

must be similar in Equations (8) to (10) because it is the same physical process, Equation (4), which is responsible for the mass exchange between the two phases.

The equation of state given as :

$$\rho_g(p) = \rho_{g,atm}(1 + \frac{p - p_0}{p_0}), \qquad (12)$$

is a linear increase of density with pressure, Boyle's law, in which index *atm* denotes atmospheric conditions, p_0 is $1.01325*10^5$ Pa and p is current pressure given in Pa.

The above set of equations is solved using the general equation solver PHOENICS ([17]). PHOENICS is based on a finite-volume formulation of the basic equations and serves for a wide range of coordinate systems (cartesian, body-fitted, cylindrical, etc.) and numerical techniques (high order schemes, solvers, etc.). In the simulations the grid spacing was 2 m and the time spacing 30 000 s, values found to be adequate for grid independent solutions.

4. RESULTS

In Fig. 5 to 12 the measured and simulated pressure evolution for the two piezometers EP04 and EP08 are plotted. Firstly, a comparison between measured and simulated pressures, with all relationships, parameters and coefficients chosen "as good as possible" with respect to the available information about the core material, is shown. Secondly, some parameters in the simulation will be tuned, within given ranges, to fit the measurements. In all simulations the upstream pressure head for EP04 is 150 m and for EP08 120 m.

In Fig. 5 and 6 the water conductivity is $6*10^{-7}$ m/s and the air conductivity is $6.6*10^{-8}$ m/s. For EP04 the measured pressure head drop is 55 m while the computed pressure head drop is 25 m. The measured peak pressure head is 98 m and the simulated is 55 m. The measurements indicate a pressure head residual at 35 to 40 m while the calculated pressure head residual is 30 m. EP08 exhibits similar behaviour. At both levels the simulated pressures continue to rise for about 2 years after the filling, are steady for one year and decline after that. All air bubbles will be dissolved by the water and steady state conditions will be obtained within 7 to 8 years, compared with 25 to 35 years in the measurements.

Fig. 7 and 8 show the results when the water and air conductivity have been changed to $1.7*10^{-7}$ m/s and $1.87*10^{-8}$ m/s, respectively. A change in the conductivities does not effect the range of the pressure drop or the peak pressure, only the time scale involved. Steady state conditions are obtained within 22 to 26 years.

The effect of a pressure head of 10 m at the downstream boundary is shown in Fig. 9. By comparing with Fig. 5, it can be seen that the back pressure does not change the pressure drop but the peak pressure head is increased with 7 m. With a back pressure head of 10 m, the calculated pressure head residual, 38 m, is in better agreement with the measured ones.

The same situation as in Fig. 5, but with the relationship between the water conductivity and water saturation level changed to slow down the water velocity for a given saturation, is shown in Fig. 10. The relationship between the water conductivity and water saturation level is in the lower part of the range in Fig. 3. The pressure head drop is increased from 25 to 38 m and the peak pressure head is increased with 13 m.

In Fig. 11 the same situation as in Fig. 10 is considered but with a back pressure head of 10 m applied. The peak pressure head is increased with 20 m compared with Fig. 10 and with 33 m compared with Fig. 5. The pressure head drop is increased to 50 m and steady state conditions are obtained within 10 years.

Fig. 12 considers the same situation as Fig. 11 but the water conductivity and the air conductivity have been changed to $3*10^{-7}$ m/s and $3.3*10^{-8}$ m/s, respectively. The calculated pressure head drop is 50 m and the measured is 55 m, the calculated peak pressure head is 88 m while the measured is 98 m and the time to get steady state conditions is 18 years compared with 25 to 35 years in the measurements.

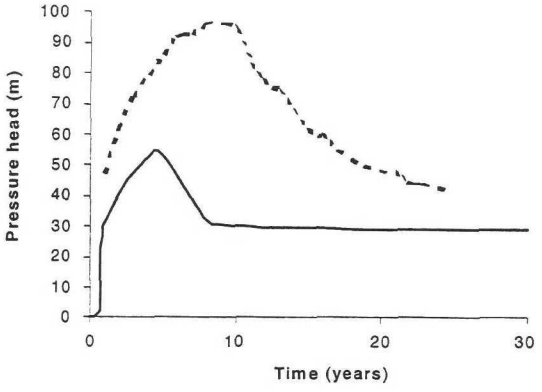

Fig. 5
Measured and calculated pressure evolution for EP04.
Water conductivity $6*10^{-7}$ m/s and air conductivity $6.6*10^{-8}$ m/s. No pressure head at the downstream boundary (- - - - - measured, —— calculated)
Évolution de la pression, mesurée et calculée, pour EP04.
Conductibilité hydraulique $6*10^{-7}$ m/s et conductibilité pour l'air $6,6*10^{-8}$ m/s. Pas de pression à la limite aval (- - - - - mesurée, —— calculée)

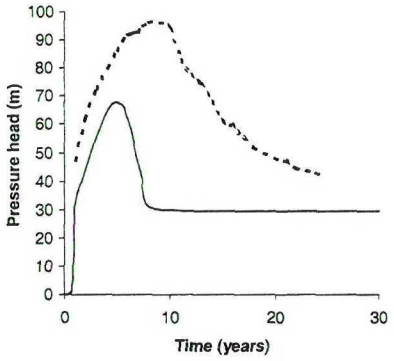

Fig.10
Measured and calculated pressure evolution for EP04.
Water conductivity $6*10^{-7}$ m/s and air conductivity $6.6*10^{-8}$ m/s. No pressure head at the downstream boundary. The relationship between water conductivity and water saturation level is changed to slow down the water velocity for a given saturation
(- - - - - measured, —— calculated)
Évolution de la pression, mesurée et calculée, pour EP04.
Conductibilité hydraulique $6*10^{-7}$ m/s et conductibilité pour l'air $6,6*10^{-8}$ m/s. Pas de pression à la limite aval. La relation entre la conductibilité hydraulique et la saturation en eau est changée pour ralentir la vitesse de l'eau pour une saturation donnée
(- - - - - mesurée, —— calculée)

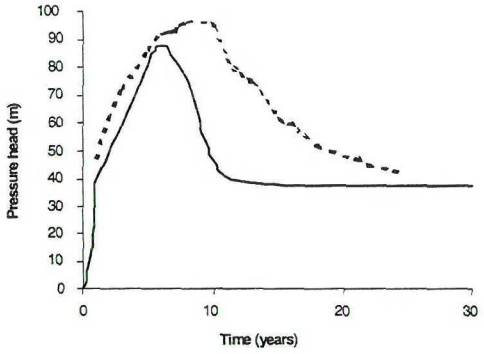

Fig. 11
Measured and calculated pressure evolution for EP04.
Water conductivity $6*10^{-7}$ m/s and air conductivity $6.6*10^{-8}$ m/s. The pressure head at the downstream boundary is 10 m. The relationship between water conductivity and water saturation level is changed to slow down the water velocity for a given saturation
(- - - - - measured, —— calculated)
Évolution de la pression, mesurée et calculée, pour EP04.
Conductibilité hydraulique $6*10^{-7}$ m/s et conductibilité pour l'air $6,6*10^{-8}$ m/s. La pression à la limite aval est de 10 m. La relation entre la conductibilité hydraulique et la saturation en eau est changée pour ralentir la vitesse de l'eau pour une saturation donnée
(- - - - - mesurée, —— calculée)

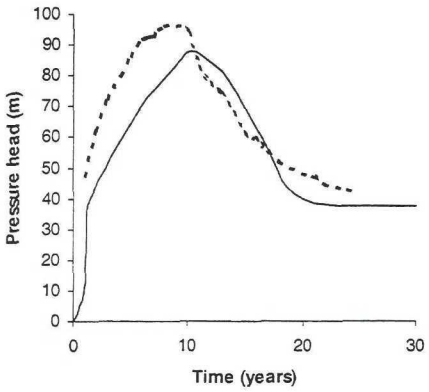

Fig. 12
Measured and calculated pressure evolution for EP04.
Water conductivity $3*10^{-7}$ m/s and air conductivity $3.3*10^{-8}$ m/s. The pressure head at the downstream boundary is 10 m. The relationship between water conductivity and water saturation level is changed to slow down the water velocity for a given saturation
(- - - - - measured, —— calculated)
Évolution de la pression, mesurée et calculée, pour EP04.
Conductibilité hydraulique $3*10^{-7}$ m/s et conductibilité pour l'air $3,3*10^{-8}$ m/s. La pression à la limite aval est de 10 m. La relation entre la conductibilité hydraulique et la saturation en eau est changée pour ralentir la vitesse de l'eau pour une saturation donnée
(- - - - - mesurée, —— calculée)

5. DISCUSSION

A qualitative agreement between the numerically simulated and measured pressure evolution is obvious from Fig. 5 and 6 when all relationships, parameters and coefficients were chosen 'as good as possible' with respect to the available information about the core material. The same kind of pressure increase and decrease is identified even though the time scale involved is wrong. However, there are uncertainties about some conditions. The water conductivity was only specified within the range $2*10^{-6}$ to $8*10^{-8}$ m/s, with a representative conductivity of $6*10^{-7}$ m/s. This range is wide enough to obtain a steady state solutions within 5 to 35 years.

Further, the pressure at the downstream boundary of the core could not be determined, it was only pointed out [18] that it was probably not atmospheric pressure. The tail water is situated below EP04. Behind the core there is a transition zone and a filter in front of a vertical drain. Atmospheric pressure can be expected in the drain and a pressure head drop in the order of 10 m is likely over the transition zone and the filter. Hence, a back pressure head of 10 m is likely at the downstream boundary of the core.

By combining the effects of changing the air and water conductivity, applying a back pressure head and changing the relationship between the water conductivity and water saturation level, within given ranges of uncertainties, a qualitative and quantitative agreement between the numerically calculated and measured pressure evolution for EP04 is achieved, Fig. 12. By applying a back pressure head there is no change in the pressure head drop but the peak pressure head increases with 7 m. By changing the relationship between the water conductivity and water saturation level the pressure head drop increases with 13 m and the peak pressure head increases with 13 m. By combining the effects of applying a back pressure head and changing the relationship between the water conductivity and water saturation level the pressure head drop increases with 25 m and the peak pressure head increases with 33 m. That is, there is a non-linear effect in the combination of a back pressure head and changing the relationship between the water conductivity and water saturation level.

Even though the agreement between the measurements and simulations in Fig. 12 is striking, it should be emphasised that it is a one-dimensional model with all the conditions idealised. No variation of the material properties within the computational domain is considered. In a real dam the air bubbles may disappear in other directions than in the flow direction.

6. CONCLUSIONS

From the comparisons between measured and simulated pressure evolution, it can be concluded that the Air Hypothesis is a potential explanation to the unusual behaviour of the core at WAC Bennett Dam.

A one-dimensional numerical model based on relevant physical laws (Darcy's, Boyle's and Henry's laws) and relationships between the relative conductivity and water saturation level is able to predict the pressure evolution in both a qualitative and quantitative way. It is indicated from the simulations that there is a non-linear effect in the combination of a back pressure head and changing the relationship between the water conductivity and water saturation level.

In the further development of the numerical model, the following points ought to be considered: (1) the saturated water conductivity of the core; (2) the pressure at the downstream boundary of the core; (3) the relationship between the relative conductivity and water saturation level and (4) the two-dimensional situation.

REFERENCES

[1] STEWART, R.A., IMRIE, A.S. and HAWSON, H.H., 1990, Unusual behaviour of the core at WAC Bennett Dam, In: *Proc. 43rd Canadian Geotechnical Conference*, Quebec, 2, 549-558.

[2] STEWART, R.A. and IMRIE, A.S., 1993, A new perspective based on the 25 year performance of WAC Bennett Dam, In: *Proc. International Workshop on Dam Safety Evaluation*, Grindelwald, 53-69.

[3] ST-ARNAUD, G., 1995, The high pore pressures within embankment dams: an unsaturated soil approach, *Canadian Geotechnical Journal* 32(5), 892-898.

[4] LEBIHAN, J.P. and LEROUEIL, S., 1999, Transient water flow through unsaturated soils: implications for earth dams, In: *Proc. 52nd Canadian Geotechnical Conference*, Regina.

[5] SHERARD,J.L., WOODWARD, R.J., GIZIENSKI, S.F., and CLEVENGER, W.A., 1963, *Earth and Earth-Rock Dams*, John Wiley & Sons, New York.

[6] BILLSTEIN, M., and SVENSSON, U. 1999, In preparation.

[7] DONG, M., and DULLIEN, F.A.L., 1997, A new model for immiscible displacement in porous media, *Transport in Porous Media* 27, 185-204.

[8] DE PARSEVAL, Y., PILLAI, K.M., and ADVANI, S.G., 1997, A simple model for the variation of permeability due to partial saturation in dual scale porous media, *Transport in Porous Media* 27, 243-264.

[9] BOTSET, H.G., 1940, Flow of gas-liquid mixtures through consolidated sand, *Trans. AIME* 186, 91-108.

[10] BEAR, J., and VERRUIJT, A., 1987, *Modeling Groundwater Flow and Pollution*, D. Reidel Publishing company, Dordrecht.

[11] DE MARSILY, G., 1986, *Quantitative Hydrogeology - Groundwater Hydrology for Engineers*, Academic Press, San Diego.

[12] DULLIEN, F.A.L., 1992, *Porous Media - Fluid Transport and Pore Structure*, Academic Press, San Diego.

[13] WYCKOFF, R.D., and BOTSET, H.G., 1936, The flow of gas-liquid mixtures through unconsolidated sands, *Physics* 7, 325-345.

[14] BRAS, R.L., 1990, *Hydrology - An Introduction to Hydrologic Science*, Addison-Wesley Publishing Company, Massachusetts.

[15] FREDLUND, D.G. and RAHARDJO, H., 1993, *Soil Mechanics for Unsaturated Soils*, John Wiley & Sons, New York.

[16] AMERICAN WATER WORKS ASSOCIATION, 1990, *Water Quality and Treatment: A Handbook of Community Water Supplies/American Water Works Association*, McGraw-Hill, New York.

[17] SPALDING, D.B., 1981, A general purpose computer program for multi-dimensional one- and two-phase flow, *Math. Comput. Simulations* 8, 267-276.

[18] PECK, R.B., 1990, Interface between core and downstream filter In: *Proc. H Bolton Seed Memorial Symposium*, San Francisco, 2, 237-251.

SUMMARY

The objective of this study is to numerically evaluate if the Air Hypothesis is a potential explanation of the unusual pressure behaviour of the core at WAC Bennett Dam. The pore pressures have been in excess of the expected normal steady state distribution for about 25 years now. The Air Hypothesis describes the influence of air bubbles on the pressure distribution in the core. An increased water pressure will compress the air bubbles and make them mobile, and increases the amount of air that can go into solution at the upstream side of the core. At the downstream side the situation is reversed, i.e. the air volume will increase, and that will cause a hydraulic blockage. A one-dimensional numerical model based on relevant physical laws (Darcy's, Boyle's and Henry's laws) and relationships between the relative conductivity and water saturation level is able to predict the pressure evolution in both a qualitative and quantitative way. A non-linear effect in the combination of a back pressure head and changing the relationship between the water conductivity and water saturation level is found. Comparisons with pressure measurements from WAC Bennett Dam show that the Air Hypothesis is a potential explanation to the unusual pressure distribution in the core.

RÉSUMÉ

L'objectif de cette étude est d'évaluer numériquement si l'hypothèse des bulles d'air est une explication possible de l'évolution inhabituelle des pressions dans le noyau du barrage WAC Bennett. Depuis plus de 25 ans, les pressions interstitielles ont été supérieures à la distribution normalement prévisible des pressions stabilisées. L' hypothèse des bulles d'air décrit l'influence des bulles sur la distribution des pressions dans le noyau. L'augmentation de la pression hydraulique comprime les bulles d'air et les rend mobiles, augmentant la quantité d'air qui peut se dissoudre du côté amont du noyau. Du côté aval, la situation est inversée, le volume d'air augmente et est à l'origine d'un blocage hydraulique. Un modèle unidimensionel, basé sur les lois physiques appropriées (Lois de Darcy, Boyle et Henry) et les relations entre la conductibilité relative et le degré de saturation en eau, peut prédire l'évolution de la pression à la fois d'une manière qualitative et quantitative. Un effet non linéaire est observé dans la combinaison d'une pression en amont et d'un changement de relation entre la conductibilité hydraulique et le degré de saturation en eau. La comparaison avec les pressions mesurées dans le barrage WAC Bennett montre que l'hypothèse des bulles d'air est une explication possible de la distribution inhabituelle des pressions dans le noyau.

Paper 5

Billstein M.: 1998, Experimental study of flow through a bed of packed glass beads, In: *Proc. International symposium on new trends and guidelines on dam safety*, Barcelona, **2**, 833 - 840.

Dam Safety, Berga (ed.) © 1998 Balkema, Rotterdam, ISBN 90 5410 974 2

Experimental study of flow through a bed of packed glass beads

M. Billstein
Department of Environmental Engineering, Luleå University of Technology, Sweden

ABSTRACT: Spherical glass beads of uniform diameter were randomly packed between two parallel plates in order to create a small scale core of an embankment dam. A thin net, with negligible flow resistance, at the upstream and downstream boundaries kept the beads in place. Two quite different bead diameters, 0.002 m and 0.025 m, were used so as to vary the Reynolds number from 4 to 1500. In some of the experiments a fracture was implemented at different levels, i.e. close or far away from the free surface. The fracture extended from the upstream boundary to the centre of the core.

The water levels upstream and downstream were held constant and the steady flow in the domain in between was studied. Once the discharge had become steady, the pressure distribution, free surface profile and seepage level were measured.

The influence of a fracture is shown by comparing results from experiments with the same upstream and downstream levels with or without a fracture.

1 Introduction

At Luleå University of Technology a numerical simulation model of flow in embankment dams is under development. This model can be a useful complement to existing techniques, e.g. measuring: pore pressure, discharge, temperature, resistivity, self-potential etc., for dam inspections. With a numerical model it is possible to analyse pressure distributions, discharges, seepage levels and velocity distributions for different flow conditions - both transient and stationary. The model can be used in an inverse mode, e.g. with known boundary conditions, seepage level and pressure distribution, different alternatives of porous media and fractures can be studied to see what combination that best fits the measurements. However, before an extensive use of the numerical model, a demonstration that the model can simulate the hydraulics of a dam in a satisfactory way is required. In order to provide data for validation, it is important to use a well defined porous media with known flow resistance properties. Therefore a small scale core of an embankment dam was created out of spherical glass beads of uniform diameter randomly packed between two parallel plates. In some of the experiments a fracture extended from the upstream boundary to the centre of the core.

A lot of work have been carried out in order to describe the flow resistance of a porous media. The general practise is to use the Forchheimer equation (Forchheimer, 1901) which involves porosity as a parameter and two empirical constants, A and B. Over the years, different suggestions have been proposed by different investigators, A varies between 150 and 225 and B varies between 1.61 and 1.92. The resulting flow resistance is a strong function of the porosity assumed. The porosity for randomly packed spheres is usually in the range 31 - 43% (Kunii and Levenspiel, 1969).

The objective of the work is to create sets of data for validation of the numerical model and to

investigate if the influence of a fracture is significant. The data sets include boundary conditions, discharges, seepage levels and pressure distributions.

2 Experimental setup

At the upstream and downstream part of the two parallel plates a thin net, with negligible flow resistance, kept the beads in place. Two quite different bead diameters, 0.002 m and 0.025 m with a standard deviation of 1% of the diameter, were used so as to vary the Reynolds number significantly, from 4 to 1500. Water at constant temperature, 10 °C, was pumped into the flume. The water levels upstream and downstream were held constant by adjustable weirs. The experimental setup is shown in Figure 1 and the experimental conditions are summarised in Table 1.

In some of the experiments a fracture was extended from the upstream boundary to the centre of the core. The fracture was made out of two parallel plates, spaced 0.010 m apart, and perforated to allow the water to enter from all directions. The width of the fracture was equal to the width of the core. A thin net kept the fracture free form beads. The thin net together with the perforated plate had lower flow resistance than the beads to make sure that the water could leave the fracture over its whole length.

Once the discharge had become steady, the pressure distribution, free surface profile and seepage level were measured. The pressure distribution was measured by using pressure gauges at points located 0.04 m above the bottom of the flume. The discharge was measured by using a triangular weir. The two plates were transparent to make it possible to measure the water surface profile from direct observations, taking the capillary rise into account. Also the seepage level was measured form direct observations. The porosity was determined from measurements to be in the range 34 ± 2% and 41 ± 2% for diameter 0.002 and 0.025 m respectively.

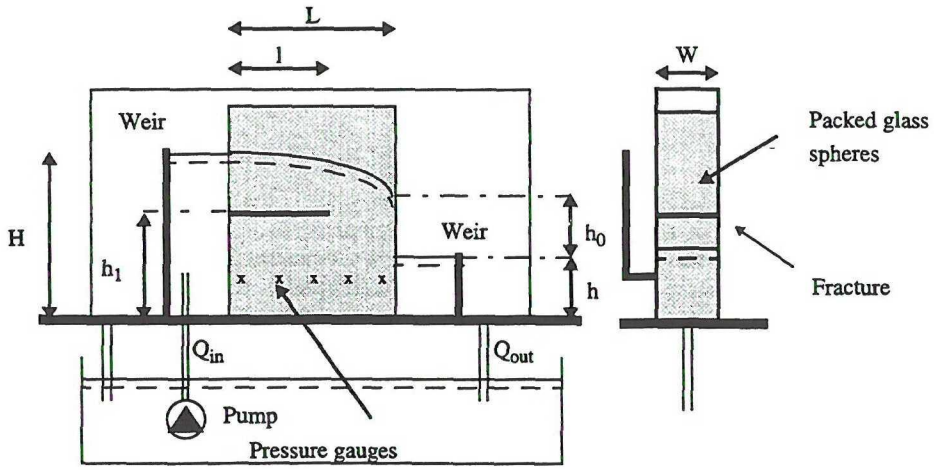

Figure 1. Experimental setup. Small scale dam core built out of glass beads.

3 Result

All the results are summarised in Table 2. Figures 2 - 5 show some of the results with respect to pressure distributions and water surface profiles.

Small beads: The presence of a fracture increases the discharge with 33 - 45% and the location does not influence the discharge. When the fracture is close to the pressure points, the influence

of the pressure distribution is higher than if the fracture is close to the water surface.The opposite is true for the water surface profile. At the downstream end of the fracture, the pressure increases with 15 - 19% and 5 - 6% with the fracture located close to the pressure points and close to the water surface, respectively.

Large beads: The presence of a fracture increases the discharge with 9 - 12% but the location does not influence the discharge, the pressure distribution or the water surface profile. At the downstream end of the fracture, the pressure and water surface level increase with 9 - 11% and 6 - 7% respectively.

Table 1. Experimental conditions.

			With fracture	
Bead diameter (m)	L (m)	W (m)	l (m)	h_1 (m)
0.002	0.505	0.132	0.25	0.27
				0.11
0.025	0.500	0.301	0.25	0.20
				0.12

Table 2. Comparison between a homogeneous and an inhomogeneous dam core with respect to discharge and seepage levels.

						Without fracture		With fracture			
diameter (m)	W (m)	n (%)	L (m)	H (m)	h (m)	$h_{0\,expr}$ (m)	Q_{expr} (l/s)	l (m)	h_1 (m)	$h_{0\,exp}$ (m)	Q_{exp} (l/s)
0.002	0.132	34	0.505	0.381	0.015	0.12	0.21	0.25	0.27	0.17	0.28
				0.380	0.015				0.10	0.14	0.28
				0.380	0.097	0.06	0.19	0.25	0.27	0.09	0.27
				0.381	0.097				0.10	0.08	0.27
				0.380	0.262	0.00	0.11	0.25	0.27	0.00	0.16
				0.380	0.262				0.10	0.00	0.16
0.025	0.301	41	0.500	0.290	0.042	0.07	4.66	0.25	0.21	0.08	5.10
				0.290	0.042				0.13	0.09	5.20
				0.288	0.121	0.01	4.42	0.25	0.21	0.02	4.85
				0.289	0.122				0.13	0.03	4.89
				0.288	0.264	0.00	2.05	0.25	0.21	0.00	2.30
				0.290	0.265				0.13	0.00	2.30

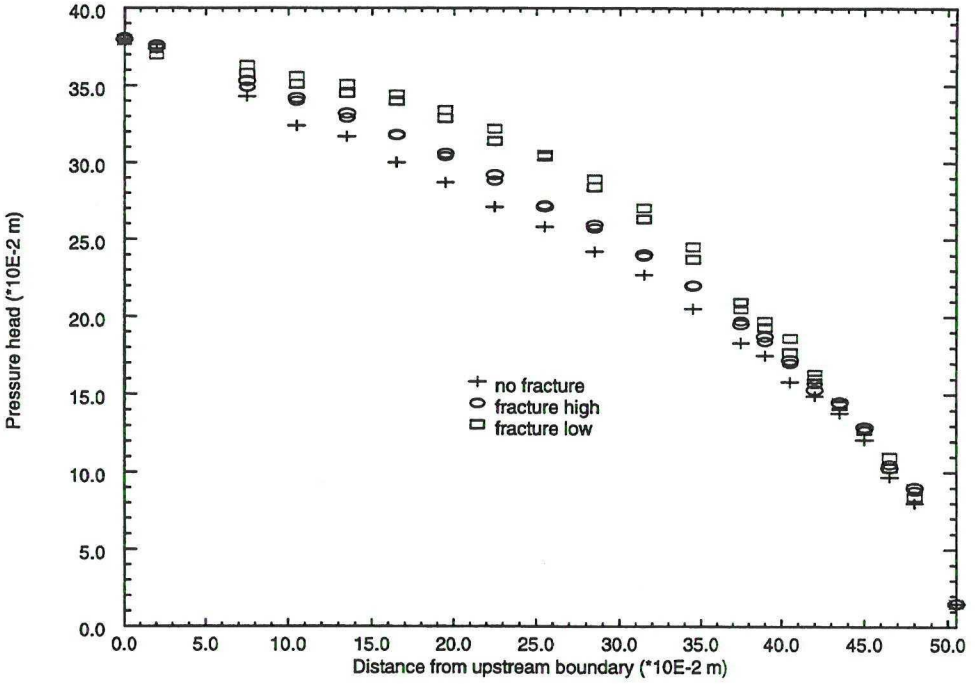

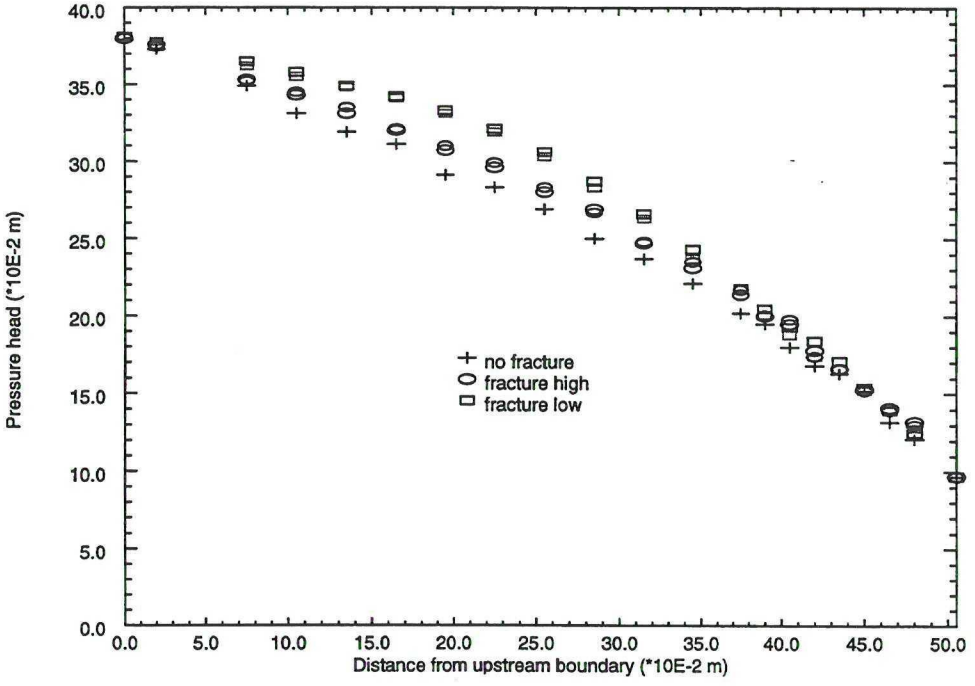

Figure 2. Pressure profiles.
Top: Sphere diameter 0.002 m, H=0.381 m, h=0.015 m.
Bottom: Sphere diameter 0.002 m, H=0.380 m, h=0.097 m.

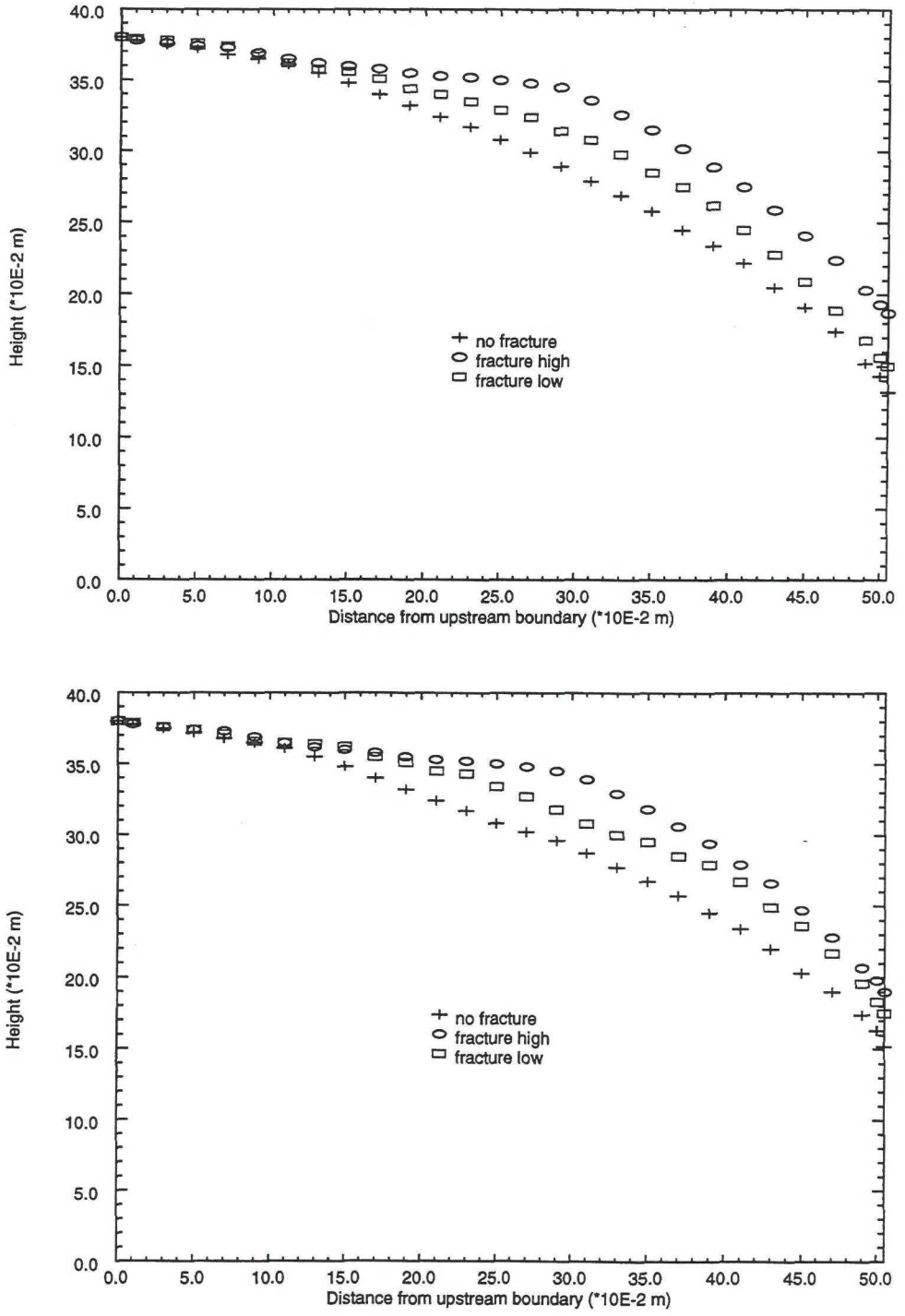

Figure 3. Water surface profiles.
Top: Sphere diameter 0.002 m, H=0.381 m, h=0.015 m.
Bottom: Sphere diameter 0.002 m, H=0.380 m, h=0.097 m.

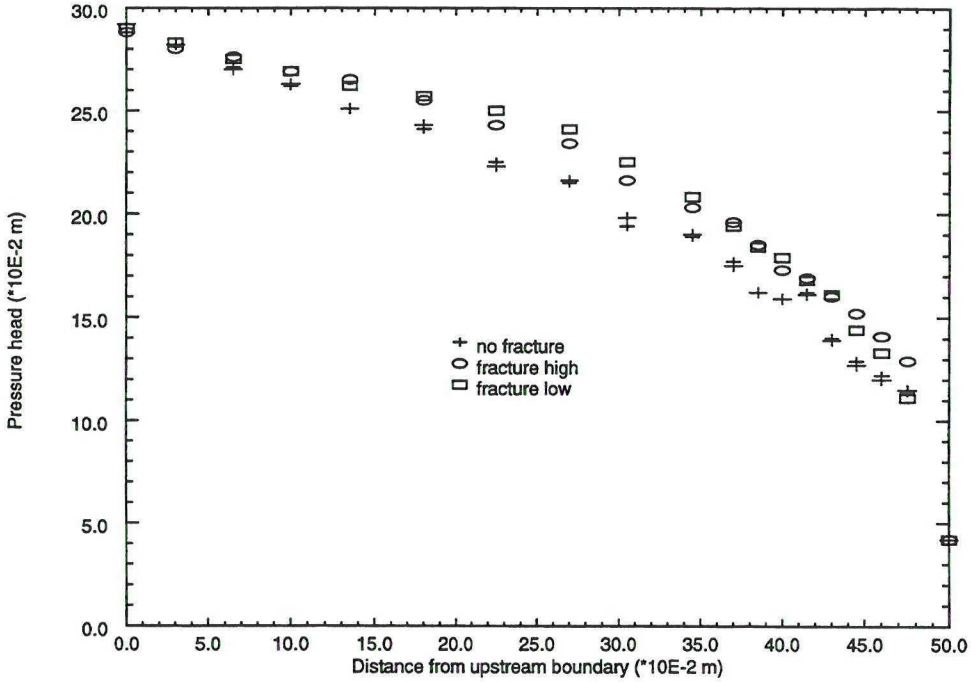

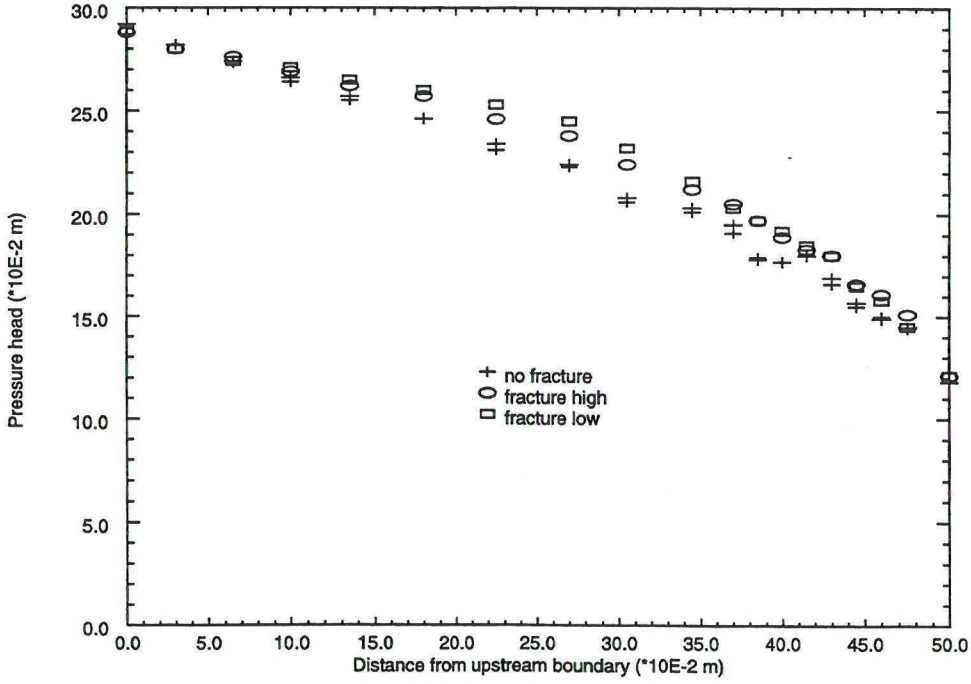

Figure 4. Pressure profiles.
Top: Sphere diameter 0.025 m, H=0.290 m, h=0.042 m.
Bottom: Sphere diameter 0.025 m, H=0.289 m, h=0.122 m.

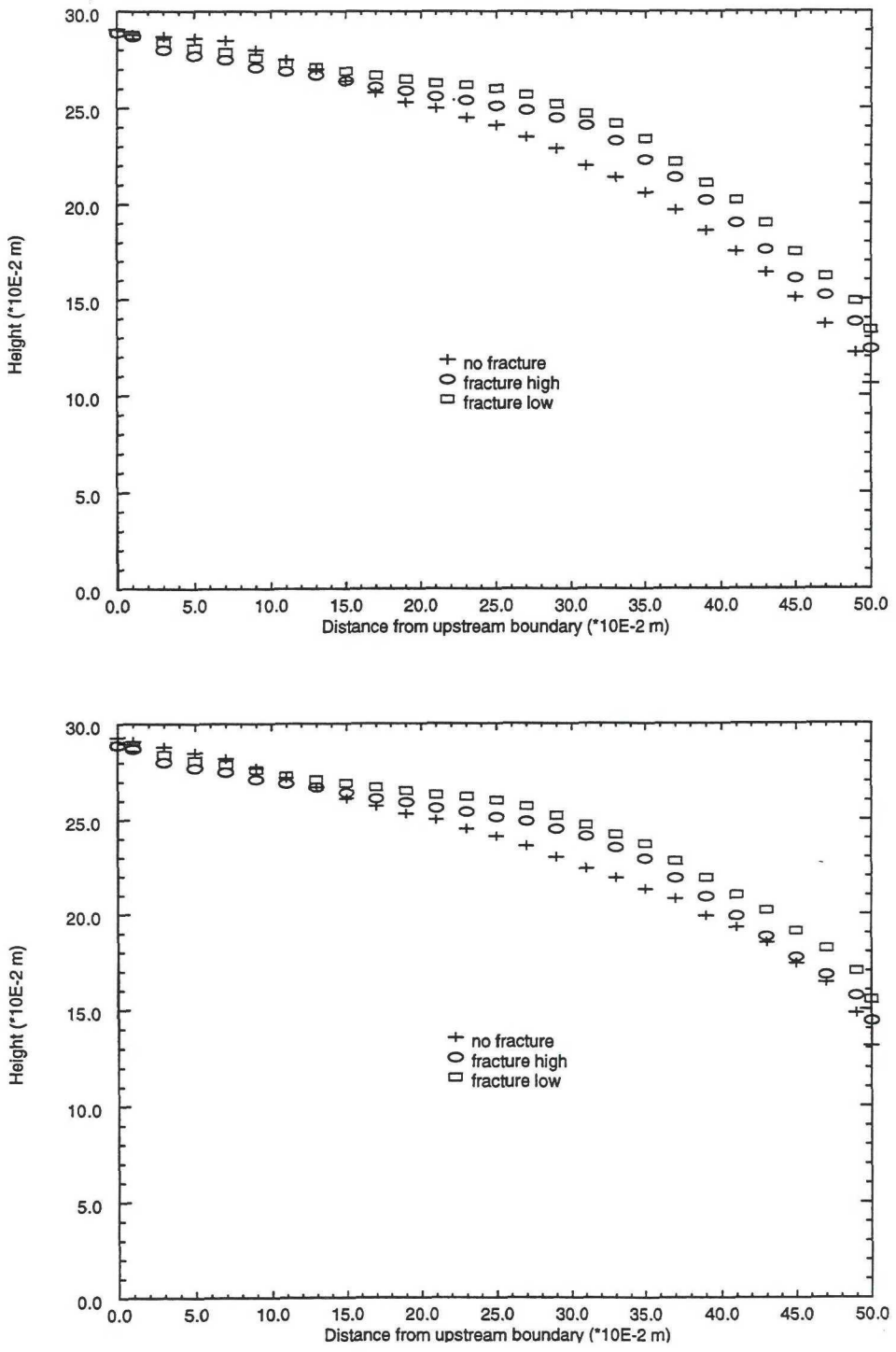

Figure 5. Water surface profiles.
Top: Sphere diameter 0.025 m, H=0.290 m, h=0.042 m.
Bottom: Sphere diameter 0.025 m, H=0.289 m, h=0.122 m.

4 Discussion and conclusions

The difference in porosity between the two bead diameters is due to the wall effects. In order to neglect the wall effect, the ratio between the width of the core and the sphere diameter has to be greater than 40 (Hansen, 1992). In the present experiment the ratio for the small beads is 66 and for the large beads 12. The thickness of the fracture is of no importance with respect to pressure distribution and water surface profile. This indicate that the pressure distribution is uniform in the fracture.

To conclude this work:

* a number of experimental sets, containing boundary conditions, discharges, pressure distributions, water surface profiles and seepage levels are presented.
* the influence of a fracture is significant; the discharge is increased with approximately 40% for the small beads and 10% for the large beads, if the fracture is close to the pressure points, the pressure distribution is most influenced and if the fracture is close to the water surface, the water surface is most influenced.
* it should be possible to use a numerical model in an inverse mode and predict the porous media.

5 References

Forchheimer, P. 1901. Wasserbeweguing durch Boden. *Zeischrift. Verein Deutscher Ingenieure, Vol. 45*, pp. 1782-1788.

Hansen, D. 1992. *The behaviour of flowthrough rockfill dams*. Doctoral thesis, University of Ottawa, Canada.

Kunii, D., and Levenspiel, O., 1969. *Fluidization engineering. ISBN 0-88275-542-0,* John Whiley & sons, Inc.

LULEÅ TEKNISKA UNIVERSITET

NR: 2000:21
ISSN: 1402-1544
ISRN: LTU-DT--00/21--SE

Institution
Samhällsbyggnadsteknik

Upplaga
400

Avdelning
Vattenteknik

Datum
2000-04-28

Titel
Influence of Fractures and Air Bubbles on the Pressure Distribution in Embankment Dams

Författare
Mats Billstein

Språk
Engelska

Sammanfattning
In some large embankment dams unexpected pore pressure distributions within the core have been observed. As an example, the piezometer pressures in WAC Bennett Dam, Canada, which rose for about four years after the reservoir was filled, were steady for two years and subsequently declined. One peak pressure head was as much as 60 m higher than the expected steady state pressure head of 40 m. However, the pressure head had dropped 55 m from the peak value 25 years later. Four hypotheses have already been proposed to explain the anomalous pore pressures within embankment dams. The objective of this study is to examine two of them, inhomogenities (e.g. fractures) in the core and trapped air bubbles, which can both be examined from a fluid mechanical point of view. The other two mechanisms, settlements and bleeding of fine material, must also be examined from a geotechnical aspect.

This examination, based on results from two numerical models, is mainly theoretical. Results from numerical simulations of simplified homogeneous and inhomogeneous embankment dams are compared with analytical solutions and basic experiments. Results from numerical simulations, including the influence of air bubbles, are evaluated using a plug flow analysis and field measurements.

A Hele-Shaw cell and a bed of packed glass beads, both a homogeneous and an inhomogeneous experimental set up, were used in the examination of how inhomogenities influence the pressure distribution. In the inhomogeneous.....(cont.)

Typ
Doctoral thesis

Fakultet
Teknisk

Nyckelord
embankment dam, pressure distribution, high pore pressure,inhomogeneity, fracture, experiment, analytical solution,numerical simulation, hele-shaw, packed glass beads, airbubbles, relative conductivity, unsaturated soil, hydraulicblockage, wac bennett dam, dam safety

Granskare/handledare
Prof. Urban Svensson

URL: http://epubl.luth.se/1402-1544/2000/21

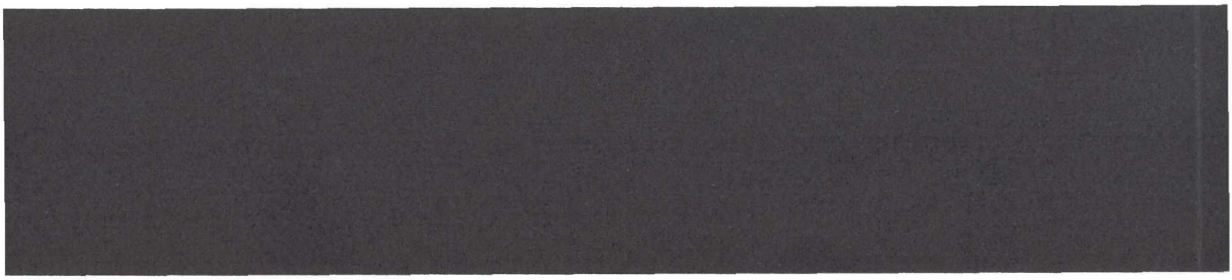

Universitetstryckeriet, Luleå